# The surface of helium crystals

Sébastien Balibar*

*Laboratoire de Physique Statistique de l'Ecole Normale Supérieure, associé au CNRS et aux Universités Paris 6 et 7, 24 rue Lhomond, 75231 Paris Cedex 05, France*

Harry Alles†

*Low Temperature Laboratory, P.O.Box 2200, FIN-02015 HUT, Espoo, Finland*

Alexander Ya. Parshin‡

*P.L. Kapitza Institute for Physical Problems Kosygina ul. 2, 119334, Moscow, Russia*

Helium crystals show facets as any usual crystal but no other crystal can grow and melt fast enough to make the propagation of crystallization waves possible at its surface. After nearly two decades of controversies, it is now generally accepted that helium crystals are model systems for the general study of crystal surfaces, but also exceptional systems with unique quantum properties. All along this review, which summarizes twenty five years of research on helium crystals, what is general to all crystals is distinguished from what is particular to helium. A central issue among the general properties is the "roughening transition", i.e., the phase transition from a smooth facetted state of the crystal surface at low temperature to a rough fluctuating state at high temperature. This review describes the series of experiments which have significantly improved the understanding of this transition and the related critical phenomena. A particular emphasis is given to the renormalization theory of roughening by Nozières which has been carefully compared with experimental measurements. Other general properties of crystal surfaces have also been studied in helium, such as the energy of steps on the facets and their mutual interactions, and several instabilities. The relevant experiments are presented together with their theoretical interpretation. The quantum mechanisms which control the growth dynamics of helium crystals are also reviewed. Here too, theories are compared with experiments, not only on crystallization waves, but more generally on the mass and heat flows in non-equilibrium situations. This concerns both stable helium isotopes, $^4$He and $^3$He, which behave in quite different ways. At the beginning of this review, experimental techniques are described, which are rather unusual in many cases. Finally, a series of open questions is presented for future research.
(draft: March 15, 2004)

PACS numbers: 67.80.-s,81.10.Aj

## Contents



*Electronic address: balibar@lps.ens.fr
†Electronic address: harry@boojum.hut.fi
‡Electronic address: parshin@kapitza.ras.ru

## I. INTRODUCTION

It is paradoxical. Helium crystals are ordinary crystals in a sense, but exceptional crystals in another sense. Their study has brought crucial information on the very general properties of all crystal surfaces. It has also shown that some of their other properties are surprising, as is often the case when quantum mechanics plays a major role (Balibar and Nozières, 1994).

Why exceptional? At low enough temperature, for example below 0.5 K, $^4$He crystals grow and melt so easily that "crystallization waves" can propagate at their surface. Imagine that you have a cryostat with optical access, and that the experimental cell inside contains a $^4$He crystal in equilibrium with its liquid phase. Now, shake the cryostat. You will see waves propagating at the liquid-solid interface just as if you looked at the free surface of water (see Fig. 1). These waves propagate because $^4$He crystals grow and melt very fast. They were predicted in 1978 (Andreev and Parshin, 1978) and discovered a year later (Keshishev *et al.*, 1979). Moreover, the lower the temperature, the faster $^4$He crystals grow. No classical crystal behaves in this manner.

As we shall see in this review, the crystallization waves and the unusual growth dynamics are spectacular phenomena which are linked to quantum properties of liquid and solid helium at low temperature. When crystal growth takes place from a superfluid, there are situations where no dissipation at all takes place at the moving interface; this would be impossible in a classical fluid where the sticking of individual atoms necessarily dissipates energy because of a momentum exchange at the moving crystal surface.

At 0.1 K, the growth of $^3$He crystals is slower than the growth of $^4$He crystals by 11 orders of magnitude (Graner *et al.*, 1989)! If one compared classical crystals made of different isotopes of the same element, one would find that they have very similar properties. On the contrary, $^3$He atoms being Fermi particles while $^4$He ones are Bose particles, the growth dynamics of $^3$He crystals is very different from that of $^4$He crystals.

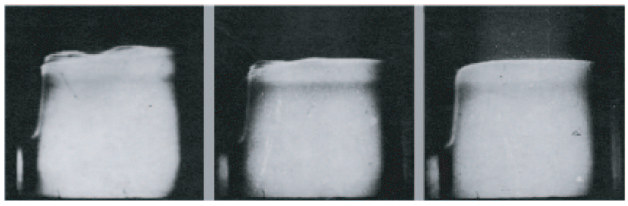

FIG. 1 . Keshishev *et al.* discovered crystallization waves in 1979 by shaking their cryostat: the interface between a $^4$He crystal and superfluid $^4$He moves so easily by growth and melting that it looks like a free liquid surface.

Given all this, how can it be that helium crystals are ideal for the study of universal properties of crystal surfaces? As temperature goes down, and as happens with any other crystal, the surface of these crystals in equilibrium is covered with more and more facets, which are smooth and flat states of the surface (see Fig. 2). Of course, in helium everything happens at lower temperature than anywhere else because the interaction energy between atoms is much smaller, but the physical mechanism for the existence of facets is the same as in other systems. Furthermore, the fast dynamics allows the use of unusual experimental methods for the measurement of quantities which are difficult to access with usual crystals. This is particularly true for the surface tensions and step energies, which are the quantities controlling facetting and roughening, i.e., the appearance and disappearance of facets at the surface of crystals.

Suppose that you pour some liquid into a glass. The liquid occupies the bottom part and its free surface reaches quickly an equilibrium shape minimizing the sum of the surface and gravitational energies. Suppose now that you pressurize a cell which contains superfluid $^4$He at low temperature. At 25.3 bar, a crystal appears. Now stop the pressurization. The helium in the cell relaxes to its thermodynamic equilibrium within a very short time. This equilibrium means that the shape of the liquid-solid interface also minimizes the effects of gravity and surface tension: the crystal occupies the bottom part of the cell, with a horizontal surface in the middle and with some capillary effects at the edges, just as if it was a liquid. This relaxation is fast because the thermal conductivities of both the liquid and solid $^4$He are large and also because the latent heat of crystallization is small, so that the crystal shape is not perturbed by any temperature inhomogeneity as in classical systems. Furthermore, since the mass transport is very easy in a superfluid, the crystal evolves very quickly by melting in one place and freezing in another place (except in the facetted areas). Its shape evolution does *not* include any deformation of the lattice inside, all the mass transport takes place in liquid. In Section IV we shall see more precisely how this dynamics proceeds but the result is there: capillary

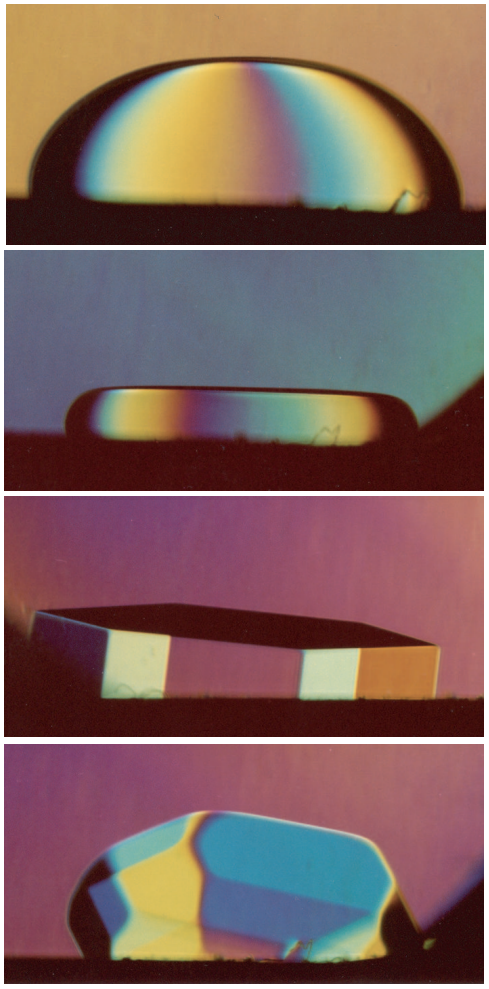

FIG. 2 . As temperature goes down, more and more facets appear at the surface of $^4$He crystals. From top to bottom, the temperature is successively 1.4 K, 1 K, 0.4 K and 0.1 K. The size of facets is enlarged by a slow growth from the surrounding superfluid. The colors are real, obtained with a prism, a lens and a small mask; more details on the visualization technique are given in Section II (photographs by S. Balibar, C. Guthmann, and E. Rolley, ENS-Paris, 1994).

phenomena show up with helium crystals as if they were liquids, although they are among the very best quality crystals one can find in nature.

In fact, the crystallization waves are manifestations of the same capillarity phenomena and an evidence has been found that they propagate from zero up to thermal frequencies ($10^{11}$ Hz). Of course this would never happen with classical crystals where heat and mass diffuse too slowly. Usually, the surface phenomena are hidden by bulk diffusion, but not in helium. This is what has allowed important comparisons of experimental results with theoretical predictions, and it is particularly true for the renormalization group (RG) theory of roughening which has been improved thanks to a comparison with experiments in helium (Balibar and Nozières, 1994).

From the theoretical point of view, the problem of the existence of facets at crystal surfaces has been a long standing problem in Statistical Physics. Already in 1949, Landau was interested in this problem and he predicted that, at $T = 0$, the crystal surface should be covered with facets in all crystalline directions having rational Miller indices (Landau, 1965). In 1949-51, Burton, Cabrera and Frank then predicted that all facets should disappear at successive "roughening temperatures", which they calculated in the frame of an approximate theory (Burton and Cabrera, 1949; Burton *et al.*, 1951). One thus realized that, as temperature increased, crystal surfaces were more and more rounded, with "smooth" facets only in a decreasing number of high-symmetry directions and "rough" surfaces in all other directions.

The modern theory of roughening came only after Wilson had introduced the renormalization group theory (Wilson, 1971). Van Beijeren, and Chui and Weeks solved the first models (van Beijeren, 1975, 1977; Chui and Weeks, 1976, 1978) and their work was soon extended by many other authors [for a review, see (Weeks, 1980)]. Some predictions of the RG theory of roughening have been tested with metallic crystals such as copper (Lapujoulade, 1994; Mochrie, 1987) and nickel (Conrad and Engel, 1994), but it seems to us that the most complete and quantitative check of this theory, one should probably say this class of theories, has been done with the hexagonal facets of $^4$He crystals. These experiments triggered later developments of the theory itself (Nozières, 1992; Nozières and Gallet, 1987). The RG theory of roughening is now well established and can be universally applied to predict the existence of facets at the surface of crystals, as shown by the recent case of some liquid crystals (Nozières *et al.*, 2001).

As we shall see, a smooth facet becomes a rough surface at its roughening temperature $T_R$ when the energy of steps between successive crystal planes decreases to zero. The long range order of facets is destroyed by the proliferation of steps. But at low temperature, facets are well-ordered surfaces whose size and growth rate are controlled by steps with non-zero energies. For a complete understanding of the properties of facets, it is important to know not only the energy of steps at this surface, but also their width, fluctuations and mutual interactions. Here again, helium crystals have allowed precise measurements of all the above properties of steps, while with ordinary crystals it is usually rather difficult.

Helium crystals have thus appeared as an interesting model system for the general study of crystal growth and shapes. Not less interesting are the quantum mechanisms underlying many aspects of their dynamics. A classical crystal grows or melts slowlier as its temperature decreases. This is because the microscopic processes are thermally activated so that, as temperature decreases, they become exponentially slow. With helium at low temperature, it seems that atoms go through energy barriers by quantum tunnelling (Andreev and Parshin, 1978). As a result, the growth dynamics of crystals is

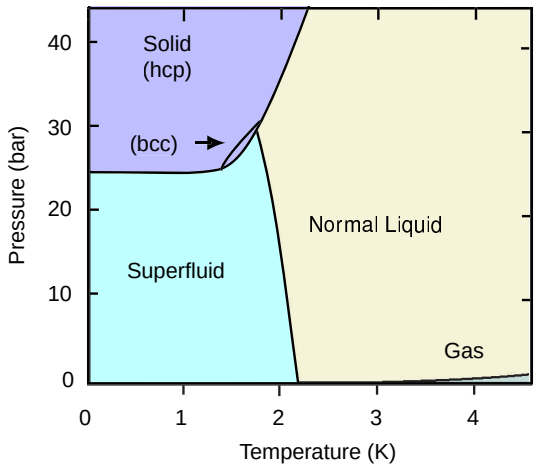


FIG. 3 . The phase diagram of $^4$He has no triple point where the solid and the liquid would coexist with the gaseous phase. At low temperature, the solid $^4$He has an hcp structure; there is a small region between 1.46 and 1.76 K, where the crystal structure is bcc.

limited only by the scattering of the moving crystal surface with thermal excitations in the liquid and solid, on both sides of the interface (Andreev and Knizhnik, 1982; Andreev and Parshin, 1978; Bowley and Edwards, 1983). At low temperature, where the dominant thermal excitations are phonons, the growth resistance of $^4$He crystals has been predicted to vanish proportionally to $T^4$ (Andreev and Knizhnik, 1982; Andreev and Parshin, 1978; Bowley and Edwards, 1983). This behavior was also observed experimentally by Keshishev *et al.* (1979, 1981). It is reminiscent of the electrical resistivity of a metallic crystal at low temperature. Electrons tunnel through the lattice of positive ions and, in a certain temperature range, their mobility is limited by collisions with phonons. As a consequence, the metallic resistivity decreases with temperature.

It was also predicted (Andreev and Parshin, 1978; Puech *et al.*, 1986a), and observed later (Graner *et al.*, 1989) that, in $^3$He, the scattering of Fermi quasiparticles leads to a much higher growth resistance than in $^4$He. One thus understands that the study of the growth dynamics of helium crystals has illustrated another general problem, namely the motion of surfaces in quantum systems. In the sub-millikelvin range, where liquid $^3$He is superfluid and solid $^3$He is a nuclear antiferromagnet, new original properties are currently under investigation.

For most of these studies, it has appeared very useful to be able to vary the temperature within a substantial range. This is possible in helium because of particular features of its phase diagram. As shown in Figs. 3 and 4, there is no triple point in helium where the liquid, solid, and gas phases would coexist. Instead, the liquid exists down to absolute zero and the solid is stable only above a pressure of the order of 25 bar in $^4$He and 30 to 35 bar in $^3$He. As a consequence, the crystal surface which we consider in this review, is a liquid-solid interface. Experiments have been performed in a temperature domain which extends over nearly four decades, from $5 \times 10^{-4}$ K to 2 K, without much change in pressure or density. Liquid $^4$He is superfluid below about 2.17 K while liquid $^3$He becomes superfluid at temperatures which are thousand times smaller. There is a transition from the hexagonal close packed (hcp) structure to the body-centered cubic one (bcc) in $^4$He at 1.46 K. At low temperature, $^3$He crystals have a bcc structure, with a nuclear antiferromagnetic phase below $T_N = 0.93$ mK (see Fig. 4).

This review article is organized as follows. In Section II, we describe the experimental techniques which have been specifically developed for the study of helium crystals over the past twenty five years. Section III is devoted to the roughening transitions, starting with $^4$He crystals. We present the successive theories with a special emphasis on the Nozières' RG theory. We then describe various experimental measurements of quantities such as the surface tension, crystal curvature, step energy and surface mobility, and we compare the experimental results with theoretical predictions. We continue with other aspects of crystal shapes, in particular with the effect of the step-step interactions. This section ends with $^3$He crystals where the study of roughening is more difficult than in $^4$He, but where additional information on the step-step interactions has been found, thanks to the discovery of a large number of different facets. In this section, as in all others in fact, we describe not only well-understood properties but we also mention the open questions which deserve further study.

Section IV describes the dynamics of rough surfaces, i.e., the growth and melting of crystal surfaces which are rough. We start with a description of crystallization waves on the rough surfaces and explain how their study has led to precise measurements of the surface tension (more precisely the surface stiffness), step energies and mutual interactions between steps. In the same section, we consider the damping of crystallization waves as a function of temperature. We analyze it as one aspect of a more general problem of non-equilibrium thermodynamics. We also describe sound transmission and heat flow through the liquid-solid interface, as well as crossed effects of temperature and chemical potential differences in the frame of the relevant Onsager matrix. After considering $^4$He, we present the dynamic properties of $^3$He crystals, which are quite different as already mentioned.

Section V is devoted to the dynamics of smooth facetted surfaces, which is much slower than of rough ones and related to the motion of steps. Here again, the observed mechanisms such as the spiral growth are common to all crystalline surfaces, while some others are particular to helium, for example the existence of critical velocities for the motion of steps.

In Section VI, we finally review various instabilities which have been studied in helium and further illustrate

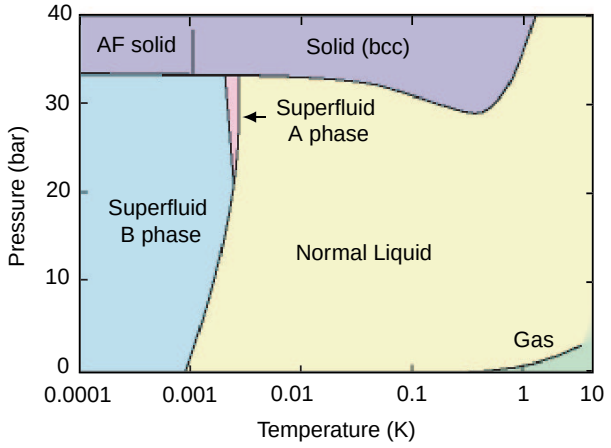


FIG. 4 . As for $^4$He, the phase diagram of $^3$He has no liquid-solid-gas triple point. There are two distinct superfluid phases below $T_c = 2.5$ mK, and the bcc crystal is antiferromagnetic below $T_N = 0.93$ mK.

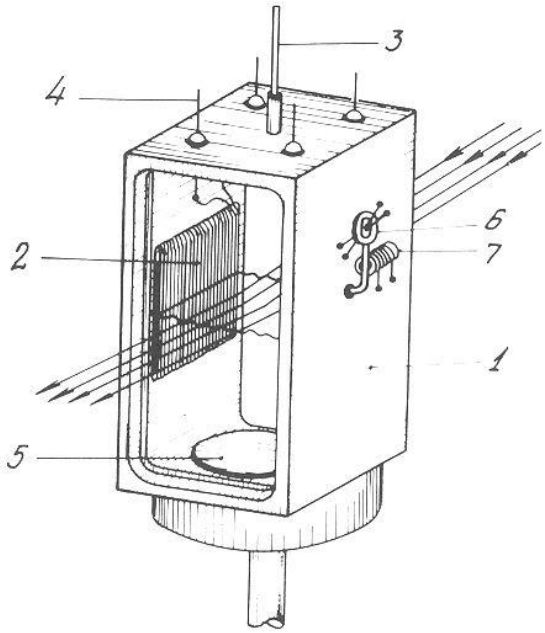


FIG. 5 . The experimental cell used by Keshishev *et al.* (1979, 1981). 1: ferrochrome cell body; 2: bifilar capacitor for the wave excitation; 3: $^4$He fill line; 4: electrical feedthrough; 5: thermal contact to the $^3$He refrigerator; 6: thermometer; 7: cadmium temperature reference.

the role of helium as a model system for other crystal surfaces. One example is the "Asaro-Tiller-Grinfeld" instability. This is an instability of the shape of crystal surfaces when a non-hydrostatic stress is applied: corrugations appear above some threshold value, a phenomenon which has been related to the spontaneous pattern formation in heteroepitaxy. We describe its theory and the experiments with $^4$He crystals which have brought the first experimental evidence for its existence. We then consider the dendritic instability and describe mainly the original case of $^3$He crystals. We shortly mention also a few other instabilities which would be interesting to study in helium.

Our conclusion contains a list of open questions for future work with these remarkable crystals.

## II. EXPERIMENTAL TECHNIQUES

### A. Optical cryostats

When Keesom discovered solid helium ($^4$He) in 1926, he tried to visualize the liquid-solid interface, but he failed. Through the walls of his glass dewar, "...there was nothing peculiar to be seen ..." (Keesom, 1926). Thirty five years later, Shal'nikov was able to grow good quality helium crystals and he also took the first pictures of the liquid-solid interface down to 1.2 K, for both $^4$He and $^3$He (Shal'nikov, 1961, 1964). However, the quantitative study of the surfaces of helium crystals really started near the end of 1970s with the work of three different groups, respectively in Haifa (Landau *et al.*, 1980), Moscow (Keshishev *et al.*, 1979) and Paris (Balibar *et al.*, 1979). Although many experiments could be done with blind cells, for example in Paris (Balibar *et al.*, 1979; Castaing *et al.*, 1980), at Brown University (Graf *et al.*, 1984; Huber and Maris, 1981), in Texas (Wang and Agnolet, 1992a), in Grenoble (Amrit and Bossy, 1990; Puech and Castaing, 1982), and in Kyoto (Kawaguchi *et al.*, 2002; Nomura *et al.*, 1994), the use of cryostats with good quality optical access proved to be very useful in these studies because the direct observation of the crystal shape allows to determine the crystal orientation, its surface state and the quality of the surface, before performing measurements.

One has to avoid looking through liquid nitrogen which usually boils, preferably also through a 4 K bath of the ordinary liquid helium, where convection takes place and snow-flakes of frozen air often move around. Conventional optical cryostats have windows attached to the low temperature screens in vacuum and optics outside (see Fig. 6 as an example). They allow easy adjustments or even complete changes of the optical setup in the course of experimental runs, but their lowest temperature is limited by the heat leak due to thermal radiation from the outside world at 300 K through the windows.

Keshishev *et al.* (1979, 1981) modified Shal'nikov's apparatus and observed crystals through five pairs of windows, respectively at 300 K, on the 77 K shield, on the two sides of a 4.2 K liquid helium bath, and on the experimental chamber which was cooled down by a $^3$He refrigerator. These windows were sealed with epoxy glue (Stycast 1266). In order to minimize the risk of leaks, the cell was built out of ferrochrome, so that the differential thermal contraction was not too large between the

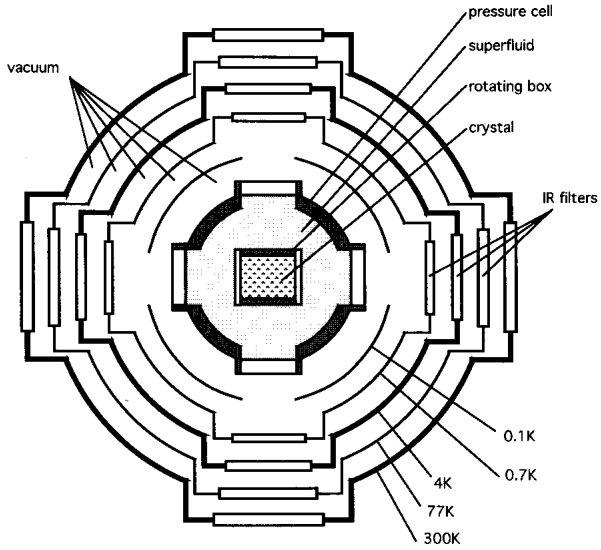


FIG. 6 . Optical setup of the Paris group (Rolley *et al.*, 1995b).

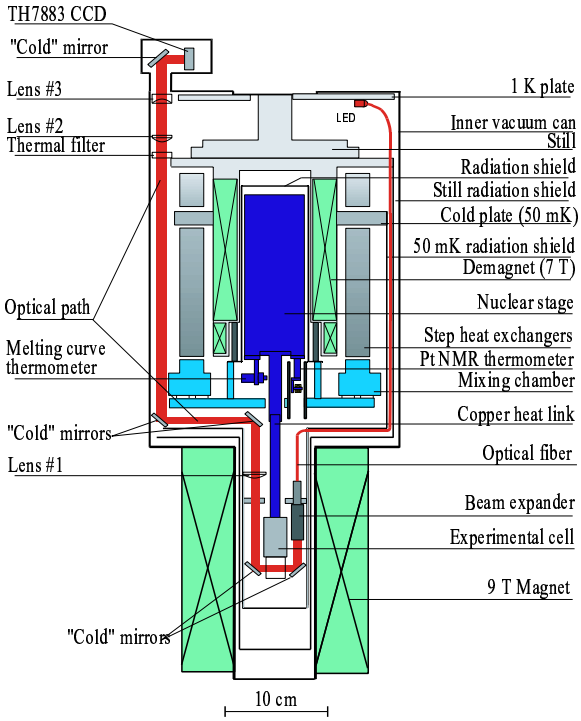


FIG. 7 . The Leiden optical setup for studies of $^3$He crystals in a high magnetic field (van Rooijen *et al.*, 2001).

cell body and the large chemical glass windows (12 mm × 28 mm) which were glued on it (see Fig. 5). For their later experiments in Paris, Wolf *et al.* (1985) and Rolley *et al.* (1995b) preferred sealing their windows with indium rings on stainless steel or copper pieces, a technique which appeared reliable and was also used in Mainz (Savignac and Leiderer, 1982), Konstanz (Thiel *et al.*, 1992), Helsinki (Babkin *et al.*, 1995; Manninen *et al.*, 1992; Ruutu *et al.*, 1998; Tsepelin *et al.*, 2002b), Tokyo (Nomura *et al.*, 1994), etc. The Leiden group successfully glued fused silica windows with Stycast 1266 on a cell made out of Araldite (Marchenkov *et al.*, 1999; van Rooijen *et al.*, 2001; Wagner *et al.*, 1994).

In conventional optical cryostats, low temperatures could not be reached without filtering the incoming infrared radiation. This is particularly important when the cell sees the room temperature environment. Radiation with wavelengths larger than 0.8 $\mu$m can be efficiently filtered with suitable coatings of windows. In order to improve this, the Paris group used pyrex glass for the windows' material (except on their cell where the use of sapphire, which is stronger, allowed the windows to be thinner). In their latest cryostat, the total absorbtion of radiation by the cell was about 10 $\mu$W with four sets of large windows from 34 mm diameter on the cell to 70 mm at 300 K (see Fig. 6). By using one set of windows only, reducing the size of windows, and improving the infrared filtering, this radiation power could probably be lowered down to 1 $\mu$W, and this would be compatible with temperatures of a few mK.

Above its superfluid transition temperature $T_c$ (2.5 mK on the melting curve), liquid $^3$He is a Fermi liquid with poor thermal conductivity and the latent heat of crystallization is large. As a consequence, $^3$He crystals behave in a way similar to classical crystals at such temperatures. However, the superfluid-solid interface below $T_c$ is expected to behave differently, and the effect of the magnetic ordering transition in the solid, at $T_N = 0.93$ mK, is also expected to be interesting. Thus, different groups built special cryostats for optical studies in the sub-millikelvin range (Manninen *et al.*, 1992; Tsepelin *et al.*, 2002b; Wagner *et al.*, 1994).

The Helsinki group was able to see the free surface of superfluid $^3$He down to about 0.7 mK by using optical fibers to communicate between room temperature and the low temperature part of their cryostat (Manninen *et al.*, 1992). The Leiden group designed and constructed a new type of optical cryostat with a CCD-camera sensor inside its vacuum can (Wagner *et al.*, 1994), their latest setup is presented in Fig. 7. This sensor works at low temperature (about 60 K) and with slow scanning (1 image every 4 s) in order to improve the sensitivity and allow the use of less light. The illumination is provided by a led which is also located inside the cryostat. In their latest cryostat, the Helsinki researchers have also adopted a low temperature CCD-camera because the resolution (576 × 384 pixels) was better than with a bundle of 30 000 fibers (Babkin *et al.*, 1995; Ruutu *et al.*, 1998). For laser light illumination a single-mode optical fiber is used as before. After filtering the thermal radiation from the CCD-sensor with two filters of $CaF_2$ and sapphire (see Fig. 9), the radiation power into the experimental cell was reduced down to a few nW.

## B. Imaging techniques

### 1. Black and white or color imaging

The polarizability of helium is weak and the density difference between the liquid and solid helium is small, so that the difference of the refractive indices is also small. However, the incidence angle for total reflection is 85 degrees from the solid side in $^4$He, so that the liquid-solid interfaces are visible at grazing incidence. A $^4$He crystal in its liquid is a transparent object in a transparent medium; when looking at it with a naked eye, it looks like an ice cube in water: one sees its profile but not its 3D shape. Growth shapes may have facet edges which are sharp enough so that light diffraction takes place and that makes these edges visible (see Fig. 37). In practice, infrared (IR) filters on the windows usually absorb some red light so that images look greenish, especially if taken with ordinary cameras whose films are sensitive to IR radiation and thus not supposed to give real colors if IR is suppressed. Video or digital cameras are not so sensitive to these IR problems.

Simple imaging techniques can be used to improve the observations of the crystal shape. If the crystal is observed in transmission with white light, a dark background can be obtained by stopping the light with a little mask at the focal point of the imaging lens. Due to the difference of the indices, the light is deviated when passing through the crystal and it converges in the focal plane but not through the focal point; thus the crystal looks bright on a dark background. A spectacular improvement of this dark background technique can be obtained by using a glass prism which disperses the white light before it reaches the helium crystal (see Fig. 8). In this case, each couple of facets forms a helium prism which refracts light at an angle which depends on the opening of the helium prism. As a result, each couple of facets appears with its own uniform color, which is different from the background color, except of course if the two facets are parallel (see Fig. 2). All these colors can be easily changed by moving the mask, which in practice was a 2 mm black rod in the Paris experiment, in the focal plane.

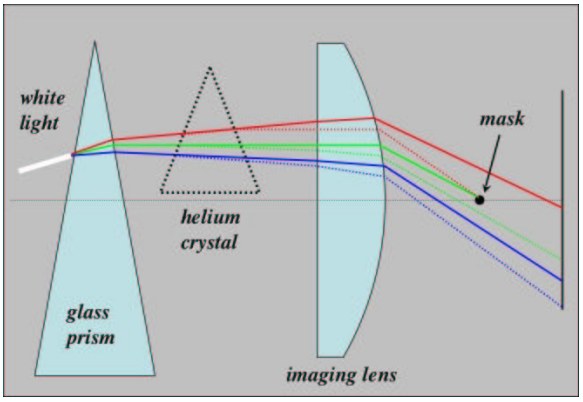


FIG. 8 . The principle of the color imaging technique used by Balibar, Rolley and Guthmann in Paris (not on scale). In practice, the "mask" was a small black cylinder with a diameter of 2 mm. By moving this mask in the focal plane of the imaging lens, the color of the background could be changed. Each couple of facets forms a helium prism whose angle determines the refraction and thus the color.

### 2. Interferometry

Conventional imaging techniques can be used for the demonstration of qualitative properties of crystal surfaces. Quantitative studies require interferometry. The refractive indices are given by the Clausius-Mossotti relation:

$$n^2 = \frac{1+2\eta}{1-\eta}\,, \qquad (1)$$

where

$$\eta = \frac{4\pi\rho\alpha_M}{3M}\,, \qquad (2)$$

and where $M$ is the molar mass (4.0026 g/mole for $^4$He and 3.0160 g/mole for $^3$He), $\rho$ is the density, and the polarizability $\alpha_M$ slightly depends on frequency. From the work of (Cuthbertson and Cuthbertson, 1932; Donnelly and Barenghi, 1998; Edwards, 1958; Harris-Lowe and Smee, 1970), it is found to be 0.1233 at zero frequency, 0.1241 for red light (632.8 nm) and 0.1245 for green light (515 nm) (Chavanne *et al.*, 2001). As a result, in $^4$He on the melting curve at low temperature, where $\rho_L = 0.17245$ g/cm$^3$ and $\rho_C = 0.19076$ g/cm$^3$, one has $n_L = 1.0338$ and $n_C = 1.0374$ for red light (respectively 1.0339 and 1.0375 for green light). The index difference $\delta n = n_C - n_L$ equals $3.6 \times 10^{-3}$. As for $^3$He in the very low temperature limit, one finds $\delta n$ = 1.0324 - 1.0307 = $1.7 \times 10^{-3}$ for red light.

(Landau *et al.*, 1980; Pipman *et al.*, 1978) applied a differential holographic technique which soon appeared too complicated to use. All other groups have installed an interferometric cavity inside their cryostat. For example, Bodensohn *et al.* (1986) and Gallet *et al.* (1987) were able to measure height changes of about 1 $\mu$m of a liquid-solid interface. This was made possible by analyzing the fringe pattern with an accuracy of one hundredth of a fringe. In such cavities, the fringe structure depends on the reflection coefficient of the walls. For small coefficients one has two-beam interferometry and sinusoidal fringes which is suitable for studies of large size surfaces. Small surface areas, such as facets, need sharper fringes for analysis, and this can be obtained using surfaces with larger reflection coefficients (in the limit of a Fabry-Pérot interferometer, the fringes are delta functions).

It is also possible to use the helium interface itself as one of the walls of the optical cavity. In this case, one gains a factor $(n/\delta n) \approx 10^3$ in sensitivity but, since the reflection coefficient of the crystal surface is very small $(10^{-6} \ldots 10^{-7})$, the other cavity wall, which is a

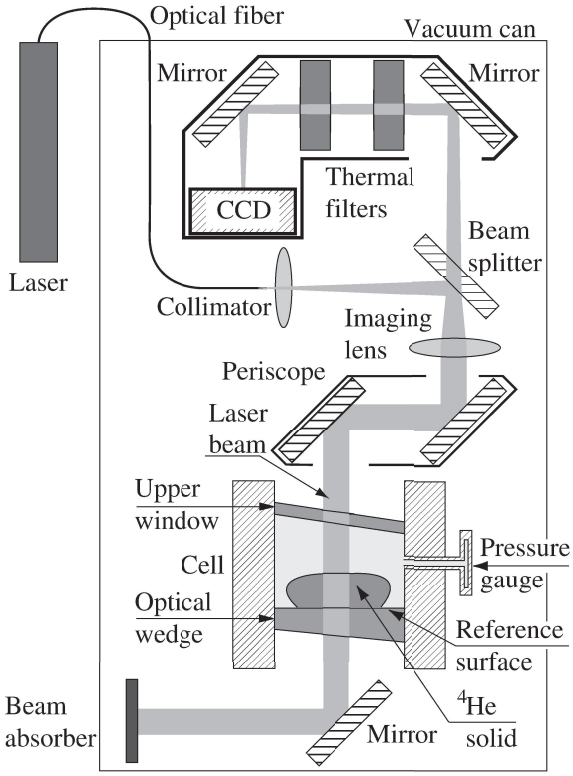


FIG. 9 . Interferometric setup for the studies of $^4$He crystals built inside the 4 K vacuum can of the nuclear demagnetization cryostat (Ruutu *et al.*, 1998).

glass plate, has to be covered with antireflection coatings in order to obtain a reasonable contrast. With the best available coatings, which have a reflection coefficient of about $10^{-4}$, the contrast between bright and dark fringes is about 1.5, i.e., quite sufficient for good measurements (Hakonen *et al.*, 1995). However, this technique can only be used if the crystal surface is nearly parallel to the glass plate.

For their studies of $^4$He crystals, the Helsinki group used the optical setup shown in Fig. 9. A He-Ne laser light ($\lambda = 632.8$ nm) enters the cryostat through a single mode optical fiber (leak-tight feedthroughs are made with Stycast 1266 epoxy glue). From the end of the fiber, the beam is expanded with two lenses, and a parallel beam with an 8 mm diameter illuminates the experimental cell. Most of the illumination is transmitted through the cell and absorbed by a black surface which is thermally anchored to the 0.7 K still of the dilution refrigerator. Only about one ppm of light is reflected back from the liquid-solid interface and about 100 ppm from the reference plane which is the antireflection coated upper surface of the lower window of the cell. These two reflected beams form the interference pattern which is focused to a cooled

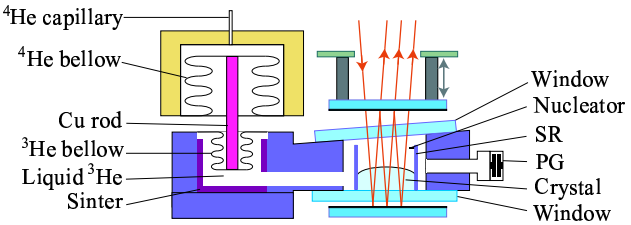


FIG. 10 . The compressional cell and a Fabry-Pérot multiple-beam interferometer for the studies of $^3$He crystals (Tsepelin *et al.* (2002b).

CCD-sensor inside the vacuum can.

The optical cell of Ruutu *et al.* is a cylindrical copper volume with an inner diameter of 17 mm. The upper window is tilted and the lower window wedged by about two degrees with respect to the cylinder axis in order to prevent the reflections from the corresponding surfaces to reach the CCD-sensor. The optical volume is connected to the silver heat exchanger at the top of the nuclear stage (not shown in Fig. 9). The pressure in the cell is measured using a sensitive capacitive gauge (Straty and Adams, 1969). With that setup the $^4$He crystals have been imaged down to about 2 mK (Ruutu *et al.*, 1998).

Later on, the Helsinki group concentrated on the studies of $^3$He crystals and, for that purpose, they modified the setup by Ruutu *et al.* and built a multiple-beam interferometer inside their nuclear demagnetization cryostat (see Fig. 10). The multiple-beam interferometry was chosen because it was necessary to determine the orientation of small facets from fringe spacings in a small area.

The volume of the experimental cell of Tsepelin *et al.* is about 13 cm$^3$. In its optical part there is a ring made of Stycast (SR) with a diameter of 18 mm. This ring stops direct flow of the liquid to the optical part of the cell and also serves as a holder for the tungsten-tip nucleator.

The interferometer consists of two nearly parallel mirrors with 50% and 70% reflectivities placed above and below the optical part of the cell and these mirrors are thermally anchored to the mixing chamber. The vertical resolution of the interferometer is a few $\mu$m while the horizontal resolution of about 15 $\mu$m is limited by the pixel size of the CCD-sensor. Crystal surfaces with a slope up to 70 degrees with respect to the bottom mirror of the interferometer could be resolved.

A typical interferogram taken with that multiple-beam interferometer is shown in Fig. 38, where a growing $^3$He crystal has been imaged at 0.55 mK. The adjacent fringes correspond to multiples of $\lambda/2(\delta n)$ in the optical path length which corresponds to 190 $\mu$m in $^3$He crystal thickness. The facets show up on the interferograms as sets of equidistant parallel straight lines, the background pattern is due to the liquid wedge and the non-perfect alignment of mirrors.

### C. Nucleation and orientation of crystals

The liquid-solid transition being of first order, there exists an energy barrier against the nucleation of crystals. In most experiments in helium, an overpressure of a few mbar is enough to overcome it. Crystals usually nucleate on local defects which are favorable to the solid phase and might be graphite dust particles attached to walls (Balibar *et al.*, 2000). Once nucleated, the crystals grow and fall down to the bottom of the cell as soon as they feel the effect of gravity, i.e., when they are larger than the capillary length $l_c \approx 1$ mm. After melting a given crystal by reducing the cell pressure, it often happens that a new nucleation leads to a crystal with the same orientation as the previous one. This is usually attributed to the possibility that wall defects keep crystal seeds even at pressures below the melting pressure $P_m$. These seeds could be killed by reducing the pressure further, sometimes very far below $P_m$, or by warming up the cell.

Keshishev *et al.* invented a clever method to obtain oriented crystals: they noticed that nucleation can be forced to occur at a particular place in the cell by using an electric field (Keshishev *et al.*, 1979). For that purpose, they made a double winding of 30 $\mu$m diameter insulated wires and applied a high voltage, typically 800 V, between the two wires. They obtained a region of high electric field in this manner; due to electrostriction, the solid density being larger than the liquid one, crystals preferably nucleated on the coil when the pressure inside the cell was increased. By locating this coil on top of the cell, they then forced the crystals to fall down to the bottom through superfluid helium. At a fraction of a Kelvin, the shape of $^4$He crystals is often flat with large c-facets, so that crystals land on a nearly horizontal c-facet (see Fig. 11). This method has been successfully used by other groups (Rolley *et al.*, 1995b; Ruutu *et al.*, 1998); the double winding could be replaced by an interdigital evaporated layer or by a sharp needle (Tsymbalenko, 1995). Eventually, since $^4$He crystals were shown to grow by epitaxy on graphite substrates (Balibar *et al.*, 1980; Eckstein *et al.*, 1980; Ramesh and Maynard, 1982; Wang and Agnolet, 1992a), it is also possible to obtain oriented crystals by placing a small piece of clean graphite in the cell. Balibar *et al.* (1980) showed that this graphite piece has to be properly degassed to work.

In order to study crystals with different orientations, it is possible to repeat the nucleation procedure several times, so that a random distribution of orientations is obtained. However, a better control could be achieved by first obtaining a crystal with known orientation and then rotating the cell. With ordinary crystals, one usually gets surfaces with different orientations by cutting new crystals at different angles. With $^4$He crystals, it was shown possible to do this in a completely different way (Andreeva and Keshishev, 1987; Rolley *et al.*, 1995b). If crystals are larger than the capillary length, their upper surface is forced by gravity to be horizontal. As a result, when a crystal is rotated together with the cell, it melts on one side and grows on the other side. This change in shape occurs within much less than a second at temperatures well below 1 K. As a consequence, the crystal surface keeps horizontal but it changes crystalline orientation because the lattice orientation rotates with the cell walls. Thanks to this method, very precise studies on the angular variation could be done with a single $^4$He crystal. Andreeva and Keshishev (1987) could rotate their cell by as much as $\pm$ 60 degrees around one axis. Rolley *et al.* (1995b) could rotate their cell by $\pm$ 6 degrees around two perpendicular axes (see Fig. 12).

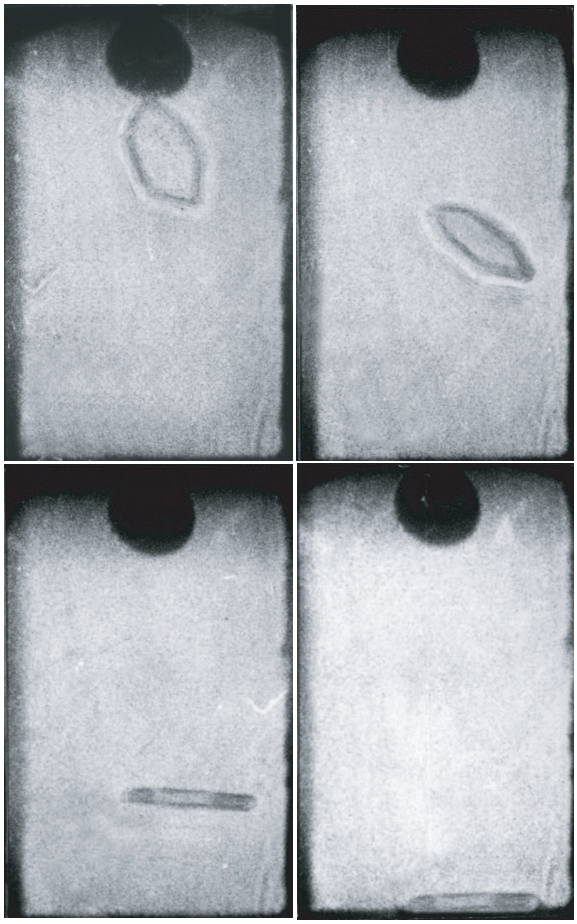

FIG. 11 . Sequence of photographs showing a $^4$He crystal falling from the top, where it nucleates, to the bottom of the cell. If its shape is a flat prism, the crystal flies like a paper sheet and lands horizontal (Babkin *et al.*, 1985).

What about crystal quality? At low temperature, the melting pressure $P_m$ of solid helium is nearly independent of temperature, so that helium crystals can be grown only by applying a small overpressure. Furthermore, Shal'nikov had shown that the quality of helium crystals was not good when they were grown by cooling down the cell which had first been filled at high temperature and then closed to follow an isochore. This is presumably because, above 1.2 K or so, the melting pressure of $^4$He increases significantly with temperature so that

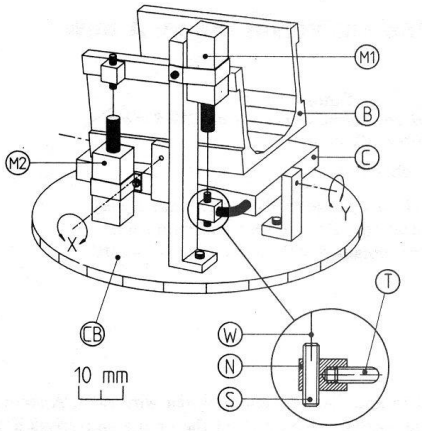


FIG. 12 . The rotating box in the Paris setup (Guthmann *et al.*, 1994). Two micromotors (M1 and M2) allow rotation by ± 6 degrees around the axes $X$ and $Y$. The motors are coupled to the box (B) and to the plate (C) thanks to flexible metallic wires (W) attached to screws (S).

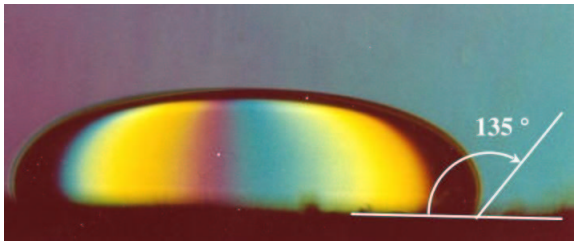


FIG. 13 . As shown by this photograph, the contact angle of the liquid-solid interface of $^4$He is about 135 degrees; the walls are preferably wet by the liquid phase (Balibar *et al.*, 1979). $^3$He crystals show a similar property (see Fig. 34).

varying the temperature leads to stresses in the crystal. These stresses lead to an instability of the crystal surface which has been carefully studied in $^4$He by the Konstanz group (Bodensohn *et al.*, 1986; Thiel *et al.*, 1992) (see Section VI.A).

In order to obtain good quality helium crystals, one has to grow them from a small seed as is done with any other crystal. For that, the crystal is first nucleated, and then melted to the smallest possible size in order to eliminate as many defects as possible. These defects can be dislocations which are important for the growth of facetted surfaces (see Section V). They can also be stacking faults, in which case the crystal surface shows macroscopic grooves as on the skin of an orange. This is because stacking faults have a surface energy comparable to the liquid-solid interfacial energy so that they create cusps with finite angles when they emerge at the liquid-solid interface. Rolley *et al.* (1995b) showed that, by growing $^4$He crystals around 0.1 K, from a 1 mm seed and not faster than 0.1 $\mu$m/s, it was possible to obtain liquid-solid interfaces without defects. Ruutu *et al.* (1996) obtained dislocation-free crystals by nucleating them spontaneously and growing them at 20 mK without special care. It thus seems that growing crystals by applying a small overpressure (a few mbar) at the lowest possible temperature leads to the best quality.

This overpressure is usually applied through the fill line of the cell, from the outside of the cryostat. The Moscow group used a buffer volume outside the cryostat, whose temperature was regulated around 300 K, sometimes modulated in order to produce successive growth and melting (Keshishev *et al.*, 1979, 1981). The Paris group used a high pressure cylinder containing high purity helium gas and an electronic flow regulation (Rolley *et al.*, 1995b). It should be noticed here that this fill line does not usually block (except if the helium is not pure enough), although the melting curve of $^4$He has a shallow minimum near 0.8 K, so that the melting pressure in a low temperature cell is higher than in some part of the fill line. Liquid $^4$He has thus to be in a metastable state in this fill line somewhere. This looks marginally possible since experiments have shown that the metastability can extend about 10 mbar above $P_m$ in the presence of ordinary walls, while the depth of the melting curve minimum is 8 mbar. However, in the case of $^3$He, where the depth of the minimum in the melting curve is about 6 bar, crystals cannot be grown/melted at low temperature by varying the pressure from the outside and deformable cells (either with bellows or with diaphragms) have to be used (Nomura *et al.*, 1994; Osheroff *et al.*, 1972; Sydoriak *et al.*, 1960; Tsepelin *et al.*, 2002b; Wagner *et al.*, 1994).

Since in $^3$He the negative slope of the melting curve is large, it is possible to nucleate crystals by applying a small heat pulse (Osheroff *et al.*, 1991). In the submillikelvin range, they first cooled down the liquid to about 0.4 mK while keeping the cell pressure at least 200 mbar below the liquid-solid equilibrium pressure $P_m$. After that, the $^3$He pressure was slowly increased up to 1.2 mbar above $P_m$ and a 1 ms heat pulse applied with an energy of 2 erg. In the experiments by Tsepelin *et al.* (2002b) the $^3$He crystals were nucleated with an electrical field like in $^4$He. By growing their crystals in a narrow tube, Osheroff *et al.* (1991) could keep only one magnetic domain of the antiferromagnetic structure. The correlation between magnetic domains and crystal growth was later studied in Kyoto (Kawaguchi *et al.*, 2002).

### D. Surface tension measurements

The surface tension of ordinary crystals is rarely accurately known. On the contrary, in the case of helium crystals, the fast growth dynamics allows simple measurements of capillary effects to be done, as if these crystals were liquids. Three different methods have been used to measure either a capillary rise, the capillary length (from the shape of large crystals), or the dispersion relation of crystallization waves.

In their early experiments, Balibar *et al.* (1979) mea-

sured a capillary rise between the two electrodes of a cylindrical capacitor, inside a blind cell. In fact, this rise was negative, it was a capillary depression because the copper wall was preferentially wet by the liquid. They found a contact angle of typically 135 degrees between the cell wall and the liquid-solid interface (see Fig. 13). This was attributed by (Dash, 1982) to the existence of large stresses in solid $^4$He near the wall, especially if this wall was rough, and later observed with most other types of solid walls, also with $^3$He (see Fig. 34). Graphite is exceptional since some matching of the crystal lattice leads to epitaxial growth of hcp $^4$He on it, i.e., complete wetting by solid $^4$He. A similar matching has been reported by (Eckstein *et al.*, 1980) for bcc $^3$He crystals on cubic MgO substrates. It is not yet clear if there exist other substrates which are completely wet by He crystals, i.e., on which they could grow by epitaxy. Balibar *et al.* (1979) also measured the minimum overpressure which was necessary for the liquid-solid interface of $^4$He to pop through a circular hole. (Balibar and Castaing, 1980) later understood that, if facets were well developed on the crystal surface, the rather high measured overpressure was not directly related to the surface tension of the crystal. This was an indirect indication that $^4$He crystals are facetted below 1 K.

The surface tension could also be measured by studying the equilibrium shape of crystals which are larger than the capillary length $l_c \approx 1$ mm. This was first done by Landau *et al.* (1980) with $^4$He crystals, and later by Rolley *et al.* (1989) with $^3$He crystals (see Fig. 34). The most precise method uses the dispersion relation of the crystallization waves, as described below.

### E. Excitation and detection of crystallization waves in $^4$He

Crystallization waves were discovered in 1979 by Keshishev *et al.* who first saw the effect of shaking their cryostat on the crystal surface. However, for an accurate measurement of crystallization wave properties, it is necessary to excite plane waves at known frequencies. For that purpose, Keshishev *et al.* used an electrostatic method: they made a small flat capacitor by winding two 30 $\mu$m diameter copper wires around a Fiberglass plate. This capacitor was placed on one side of the cell (see Fig. 5) and they applied to it a dc voltage in the range from 400 to 800 V plus an ac voltage (20 to 200 V).

A similar method was used by Wang and Agnolet (1992a) and by Rolley *et al.* (1995b), except that the double winding was replaced by an inter-digital structure evaporated on a borosilicate glass plate, so that smaller voltages could be used. Rolley *et al.* (1995b) found that the dissipation was about 30 $\mu$W at 1 kHz with 100 V peak-to-peak for the wave excitation. They attributed it to dielectric losses in the glass and this was a serious limitation for the lowest temperature at which they could study these waves. In Moscow as well as in Paris, the dc voltage was used to adjust the contact angle of the liquid-solid interface to the glass plate. Figure 14 shows a standing wave which was excited near 30 Hz and had a macroscopic amplitude. At higher frequency, or close to facetted directions as in Fig. 15, the damping is higher so that the reflection of waves from the opposite wall is negligible, except at very low temperature.

In order to detect the waves, more precisely to measure

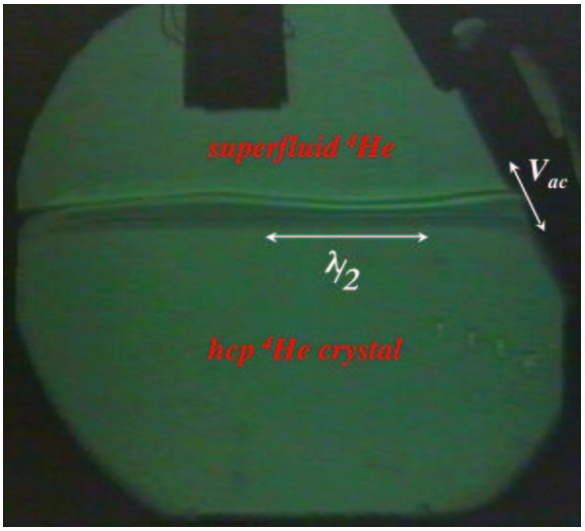


FIG. 14 . Standing crystallization waves in $^4$He as seen by Rolley *et al.* (1995b). The photograph shows the experimental cell with the oscillating interface between the crystal in the lower part and the superfluid above it. The wave was excited with an interdigital capacitor on the tilted plate on the right and it resonated in the width of the cell. The excitation frequency was about 30 Hz, so that the wavelength was close to 2/3 of the cell width (24 mm).

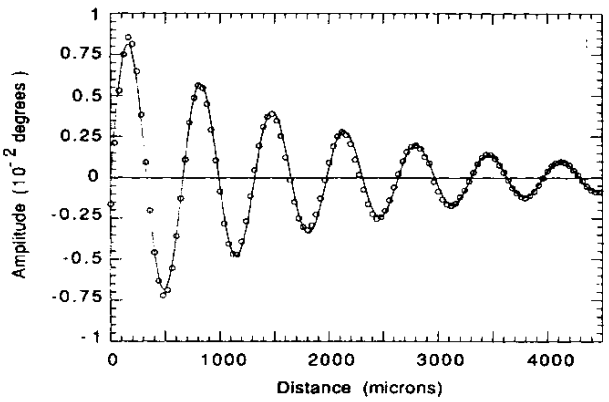


FIG. 15 . The profile of a crystallization wave propagating at the surface of a $^4$He crystal, as measured by Rolley *et al.* (1994b). In this particular case, $T = 280$ mK, the surface was oriented 3 degrees away from the (0001) plane, and the frequency was 1946 Hz, so that the wavelength was 0.660 mm. The recorded quantity is the local tilt angle of the crystal surface with respect to the horizontal.

FIG. 16 . Interference pattern of a charged liquid-solid $^4$He interface (Bodensohn *et al.*, 1986). The field of vision is about 2 cm in diameter. Here the electrons are concentrated in the central region to enhance the visibility of the deformation. The parallel fringe pattern outside the center results from a small angle between the two interferometer plates.

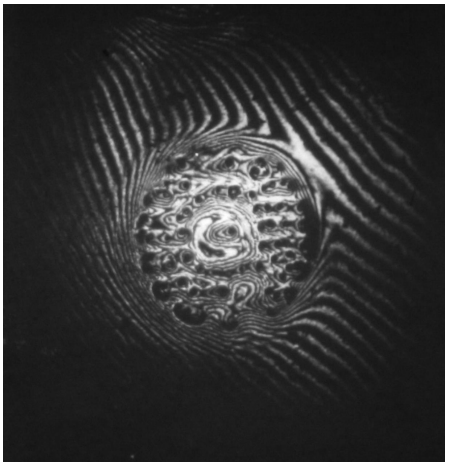

FIG. 17 . Charge-induced instability of a superfluid-hcp $^4$He interface, as observed by Savignac *et al.* (1983) above the critical electric field. The instability develops in the form of a lattice of dimples where electrons accumulate (dark spots on the image). The diameter of this pattern is about 1.5 cm.

their amplitude as a function of time or distance, Keshishev *et al.* (1979) first used the diffraction of light, but this method was not very sensitive, due to the large mechanical vibrations of their apparatus. They improved the detection sensitivity by using a light transmission technique and a lock-in amplifier. An 1 Å resolution in height was achieved by Rolley *et al.* (1995b) who measured the deflection of a laser beam on the oscillating surface (see Fig. 15), as was previously done by (Boldarev and Peshkov, 1973) and (Leiderer *et al.*, 1977) to measure the surface tension of liquid helium mixtures. Of course, none of these experiments worked if the surface had facets or surface defects on the path of the waves, so that special care had to be taken with the quality and orientation of crystals. Wang and Agnolet (1992b) used the same inter-digital capacitor for the emission and detection of the waves in a resonant cavity.

### F. Electrons at the liquid-solid interface

Leiderer and his group used electrons to study the liquid-solid interface of $^4$He (Bodensohn *et al.*, 1986; Leiderer, 1995). The principle of the method is the following. Electrons are first injected to the liquid with a field emission tip or with a radioactive source. Once they have slowed down, they form a bubble with a radius of the order of 17 Å. In the solid, the electron bubble energy is higher by about 200 K, so that there is a large energy barrier against the penetration of electrons from the liquid into the solid. Thanks to a properly oriented electric field $E_z$, the electrons can thus be pressed against the crystal surface. If the electrons are confined horizontally in some region of the crystal surface, for example in the center as shown in Fig. 16, and if the electron charge density there is $\sigma_{el}$, this part of the crystal melts down by an amount $h = \sigma_{el} E_z / g(\rho_C - \rho_L)$. Any change in the applied electric field produces a local change in height, which can be accurately measured with conventional interferometric techniques. From the relaxation time of this height change, Leiderer and his group measured the growth dynamics of rough crystal surfaces (see Fig. 44) in a temperature region where crystallization waves are too heavily damped to be used (Bodensohn *et al.*, 1986; Leiderer, 1995). Eventually, they found the same instability of the surface shape as in the case of the free surface of liquid $^4$He: beyond some critical electric field, a lattice of dimples appears [see Fig. 17 and (Savignac *et al.*, 1983)].

## III. ROUGHENING TRANSITIONS

### A. Historical observations of facets on helium crystals

Facets were first seen at the surface of slowly growing $^4$He crystals by Landau *et al.* (1980) in Haifa and by Keshishev *et al.* (1979) in Moscow. Balibar and Castaing (1980) then proposed the existence of a roughening transition around 1 K in order to understand the apparent discrepancy between the measurements of the surface tension of $^4$He crystals by Balibar *et al.* (1979) in Paris and the measurements by Landau *et al.* (1980) and by Keshishev *et al.* (1979) below this temperature. These three groups had studied different capillary effects. Balibar *et al.* had measured the minimum pressure which was necessary for a $^4$He crystal to grow through a small hole. Landau *et al.* had measured the shape of a large liquid-solid interface which was governed by both gravity and surface tension. As for Keshishev *et al.*, they had measured the dispersion relation of crystallization waves.

It was soon confirmed by Keshishev *et al.* (1981) that

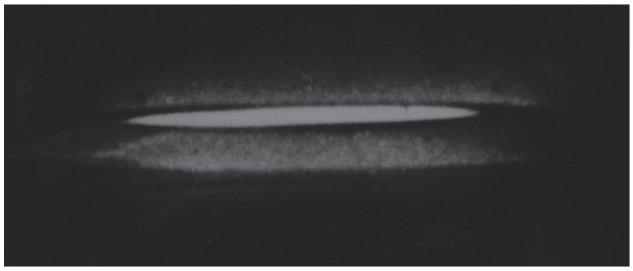

FIG. 18 . Horizontal c-facet at the surface of a $^4$He crystal as seen by Keshishev *et al.* (1981).

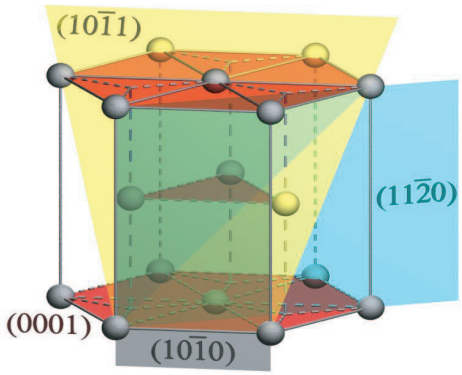


FIG. 19 . The unit cell of hcp $^4$He crystals. The plane containing three atoms in the center of the unit cell has the same energy as the bottom and top (0001) planes, so that the step height is half the lattice period in the [0001] direction.

facets existed not only on growth shapes but also on the equilibrium shapes (see Fig. 18). Furthermore, both Landau *et al.* (1980) and Keshishev *et al.* (1981) had seen that facets existed in the "c" or [0001] direction, on the basal planes of the hexagonal structure (see Fig. 19), and in the "a" direction perpendicular to "c", which was later identified as the [10$\bar{1}$0] direction (Andreeva and Keshishev, 1990; Wolf *et al.*, 1983a).[1] A third type of facets was discovered by Wolf *et al.* (1983a) below about 0.36 K; it was identified as the [10$\bar{1}$1] direction which is tilted by 58.5 degrees with respect to the [0001] direction by Andreeva and Keshishev (1990). Figure 2 shows all these three different types of facets in $^4$He.

As for the maximum temperatures at which facets could be observed, they increased with time. It is now understood that the roughening transition is very continuous, so that the facets are very small and fragile in a definite temperature domain below the roughening temperature $T_R$. As a consequence, improved measurement techniques revealed the existence of facets at higher and higher temperatures.

[1] Note that, for the hcp crystal structures, one uses sets of four Miller indices where the last index refers to the six-fold symmetry axis. The projection in the basal planes is decomposed over three equivalent vectors of the hexagons, so that the notation is symmetric and the sum of the first three indices has to be zero; the notation $\bar{1}$ means "$-1$".

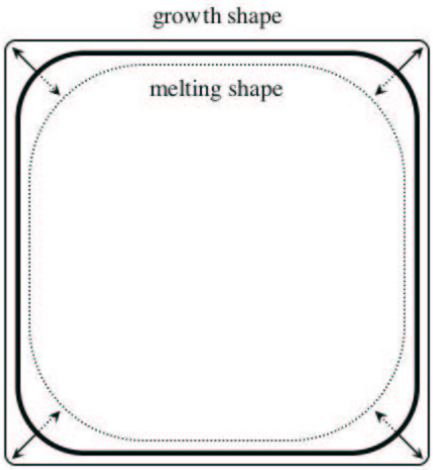


FIG. 20 . Facets grow and melt more slowly than rough corners; as a consequence, facets are larger on growth shapes than on melting shapes.

Some of the first measurements were done on the equilibrium crystal shapes. However, it was soon realized that, close to $T_R$, the facets were too small to be detected. This is because the equilibrium facet size is proportional to the step energy [see (Landau, 1965; Nozières, 1992)], which was found to vanish exponentially [see Eq. (13) and Fig. 23 below]. Actually, when the surface state of a crystal changes from rough to smooth, its mobility drops by several orders of magnitude, so that the growth shapes are highly anisotropic below the roughening temperature and reveal the slowly-growing parts of the surface. On the contrary, the melting shapes tend to be more rounded, and this can be understood from a simple geometric construction (see Fig. 20). In fact, most facets have been seen during growth in helium, both in $^4$He and in $^3$He. Note, however, that the growth has to be slow enough to avoid "dynamic roughening" as explained below.

The first measurements of facet sizes (Avron *et al.*, 1980) led to a roughening temperature $T_{R1} = 1.08$ K in the [0001] direction, but the analysis by Wolf *et al.* (1985), Gallet *et al.* (1987) and Balibar *et al.* (1993) progressively concluded that $T_{R1} = 1.30$ K. Wolf *et al.* (1985) found that, for the (10$\bar{1}$0) facets, $T_{R2}$ may be as high as 1.07 K, and Andreeva and Keshishev (1990) claimed that, for the (10$\bar{1}$1) facets, $T_{R3}$ is higher than 0.43 K. Although some indication has been found for the existence of a fourth type of facets at 0.21 K (Puech *et al.*, 1983), there is not yet a clear proof for the existence of more than three types of facets in $^4$He.

As for the bcc $^3$He crystals, the measurements by Rolley *et al.* (1986, 1989) in Paris showed that the (110) facets exist up to 100 mK. Some years later, the (100) and (211) facets were found by the Leiden group (Wagner *et al.*, 1996) and many other ones [(310), (111), (321), (411), (210), (510), (431) and (311)] by the Helsinki group (Alles *et al.*, 2001; Tsepelin *et al.*, 2001).

Among all these facets, only the (0001) facet in $^4$He has been studied with enough accuracy to check that the precise value of its roughening temperature $T_{R1}$ is correctly predicted by the theory, as well as the critical behaviors near the roughening transition. The first purpose of the next section is to present this theory and its comparison with the experiment. For the other roughening temperatures, although the measurements have been much less precise and somewhat incomplete, we shall also compare experimental observations with theoretical predictions.

### B. Main theoretical predictions

#### 1. Static properties of simple surfaces

Why are there roughening transitions at the surface of crystals? As we shall see, this has been the subject of an intense theoretical activity during the recent decades. At zero temperature, the crystal energy is the lowest if all atoms minimize their interaction energy with neighbors. This implies that the surface is smooth in all directions as predicted by Landau in 1949 [see Landau (1965)]. As temperature increases, the thermal fluctuations create defects such as terraces bounded by steps. At high enough temperature, the crystal surface will be invaded by steps and loose reference to the crystal lattice. This is illustrated in Fig. 21 (Leamy *et al.*, 1975). In fact, it is not only the density of steps which increases, it is also their average length and the size of thermally activated terraces. This is because the free energy of these steps tends to zero at a critical temperature, as can be expected for the following reason.

Consider a simple cubic crystal with a lattice spacing $a$, as in Leamy's simulations. Now, let us estimate the free energy $\beta$ of a step with a length $Na$. The step is like a random walk with three possibilities at each site. The step entropy is thus $k_B \ln(3^N)$ and the step free energy writes as

$$\beta = N[a\beta_0 - k_B T \ln(3)] , \qquad (3)$$

where $\beta_0$ is the internal energy per unit length of the step ($a\beta_0$ is approximately one half of the bond energy $J$ between two neighboring atoms). The above equation predicts that the step free energy vanishes at the critical temperature $T_R = a\beta_0/k_B \ln(3) \approx 0.45\, J$, at which both the density of steps and the typical size of terraces should diverge.

In fact, the existence of a roughening transition was first predicted by Burton, Cabrera and Frank (BCF) within a model which was nearly as simple (Burton and Cabrera, 1949; Burton *et al.*, 1951). BCF considered the surface of a cubic crystal as the last lattice plane where sites are either occupied or empty. They introduced an interaction only between the nearest neighbors, so that their surface was strictly analogous to a two-dimensional (2D) Ising model of spins. BCF then used Onsager's solution of the 2D Ising model to predict a transition to take place at $T_R = 0.57\, J$, where $J$ was the bond energy. However, BCF had realized that the crystal surface was not confined in only one atomic layer. Terraces can pile up on top of each other (see Fig. 21). As a consequence, later calculations showed that the above formulae are only rough approximations and the critical behaviors near $T_R$ different from those found with the Ising model.

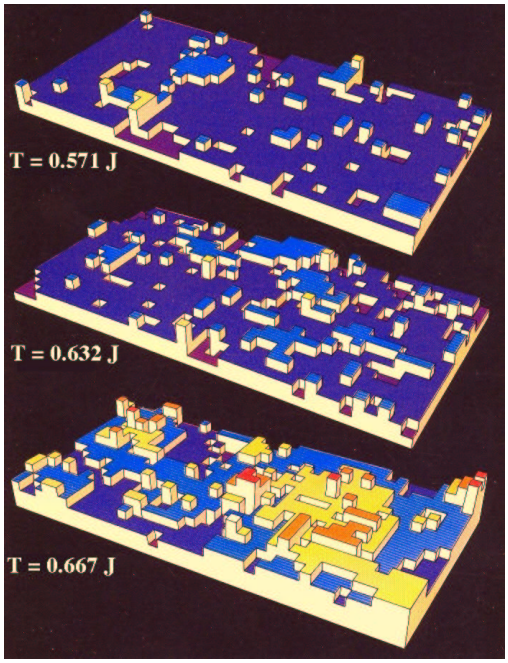


FIG. 21 . Numerical simulations by Leamy *et al.* (1975) show the basic physics of the roughening transition. The crystal has a simple cubic lattice and each atom is represented by a cube. At low temperature, there are very few defects such as adatoms, surface vacancies, steps and terraces. As temperature increases, steps proliferate and the crystal surface looses reference to the lattice. The temperature is expressed as a function of the bond energy $J$. The roughening transition occurs at $T_R = 0.632\, J$.

Further progress was obtained from the exact solutions of various models through an equivalence to other 2D systems whose transition was known. In particular, Chui and Weeks (1976) found a transition in the "discrete gaussian solid-on-solid model" (DGSOS) which was equivalent to the one found in the "2D Coulomb gas". "Gaussian" refers to the quadratic variation of the energy of local columns of atoms with their height, and SOS means that the atoms pile up without overhangs. The 2D Coulomb gas is a layer of positive and negative charges; it has an insulating phase at low temperature, where charges bind as neutral molecules, and a

conducting phase at high temperature where molecules are ionized. It is known to belong to the "Kosterlitz-Thouless" class of transitions which are of "infinite order". This means that critical behaviors are exponential with no discontinuity in any of the temperature derivatives of the free energy. Chui and Weeks thus predicted that the roughening transition was even more continuous than the second order phase transition of the Ising model. At the same time, van Beijeren (1977) demonstrated that the "body-centered solid-on-solid model" was equivalent to the "six-vertex model", another member of the Kosterlitz-Thouless class. Many 2D systems were soon found to be of the Kosterlitz-Thouless type like the superfluid transition of films, the "XY"-model of spins, some liquid-solid transitions, etc.

When it appeared possible to compare theories with experiments in helium, another theoretical progress was necessary. Indeed, it was needed to include a few adjustable parameters in the theory, so that a real crystal surface could be described. This is what Nozières and Gallet (1987) achieved. For an extensive presentation of this theory, we refer to Nozières' lecture notes at the Beg-Rohu summer school (Nozières, 1992). Here we only summarize its principle, starting point, approximations and main results, so that one can understand how it could be compared with experimental results.

Nozières starts by writing an effective hamiltonian to describe the energy of a surface deformation:

$$H = \int d^2r \left[ \frac{1}{2}\gamma \, (\nabla z)^2 \; + \; V \cos \frac{2\pi z}{d} \right] \; . \qquad (4)$$

In this expression, $z(r)$ is the height of the crystal surface at a position $r$ and the cosine-term describes the periodic influence of the underlying lattice; the quantity $d$ is thus the periodicity of the surface energy as a function of height and it is also the step height in the smooth facetted state. Note that, in the direction under consideration, $d$ is usually different from the lattice spacing $a$. This lattice potential is what anchors the surface to the lattice planes at low temperature. As for the quantity $\gamma$, it is the surface stiffness of the crystal and deserves a paragraph of comments.

As it is well known from the Laplace equation, the curvature of a free liquid surface is equal to the ratio of the pressure difference across the surface to the surface tension $\alpha$, which is the free energy per unit area. A crystal being anisotropic, there is not only a tension which tends to minimize the surface area, but also a torque which tends to rotate the surface towards a direction with minimum surface energy [see (Herring, 1953) or (Nozières, 1992)]. As a result, it is the surface stiffness tensor

$$\gamma_{ij} \; = \; \alpha + \frac{\partial^2 \alpha}{\partial \phi_i \partial \phi_j} \, , \qquad (5)$$

which governs the equilibrium curvatures of the crystal surface ($\phi_{i,j}$ are the reference angles). In the case of a liquid-solid interface, one can write a generalized Laplace equation as

$$\left( \frac{\rho_C}{\rho_L} \; - \; 1 \right) \delta P \; = \; \frac{\gamma_1}{R_1} \; + \; \frac{\gamma_2}{R_2} \, , \qquad (6)$$

where $\gamma_1$ and $\gamma_2$ are the two components of the surface stiffness tensor after diagonalization and $R_1$ and $R_2$ are the two radii of curvature in the corresponding directions. The pressure difference $\delta P = (P_L - P_{L0})$ is the departure from the liquid-solid equilibrium pressure $P_{L0}$ when the interface is flat[2]. Once multiplied by the density factor in Eq. (6), this pressure term is a generalization of the pressure difference across the interface (the problem here is that, except if the solid is under hydrostatic equilibrium, its stress tensor is not isotropic, so that the solid pressure is not a well defined quantity). In the case of the (0001) surfaces of the hcp $^4$He crystals, and in the absence of gravity, the surface has a cylindrical symmetry axis [0001] since $\gamma_1 = \gamma_2$, and the right-hand side of Eq. (6) simplifies to $2\gamma/R$ with $\gamma = \alpha \; + \; \partial^2\alpha/\partial\phi^2$.

The hamiltonian in Eq. (4) is often called the "continuous sine-Gordon" hamiltonian because it uses continuous variables and a sinusoidal potential. Its form calls for a few more remarks. The roughening transition is a macroscopic phenomenon and one is interested in the properties of the surface at a large scale. This is what justifies the use of continuous variables. At these large scales, the amplitude of fluctuations is always smaller than their wavelength, so that the local slopes are small ( $\nabla z \ll 1$). This is why only the leading term with $(\nabla z)^2$ is kept in the expansion for the surface shape. Furthermore, it is assumed that $V/\gamma < 1$: the crystal surface is weakly coupled to the lattice. This "weak-coupling approximation" is shown to be valid close to the roughening transition temperature, where critical behaviors are calculated. It also justifies the use of the first harmonic only, a cosine term, instead of a periodic function of arbitrary shape [see (Nozières, 1992)].

Although the algebra involved in the renormalization calculation of the roughening transition is tedious, its principle is simple. One calculates the free energy of the surface by averaging on fluctuations with larger and larger scale. At each scale $L$, the hamiltonian keeps the same form, Eq. (4), but its coefficients $\gamma(L)$ and $V(L)$ are now scale-dependent, i.e., "renormalized" because fluctuations with larger and larger wavelengths are progressively accounted for. By comparing coarse graining at scale $L$ and at scale $L + dL$, one obtains coupled differential equations for $\gamma(L)$ and $V(L)$; their integration gives the "renormalization trajectories", i.e., the scale-dependence of these two quantities. The important result of this theory is that there are two different behaviors.

If $T > T_R$, the potential energy $U = VL^2$ renormalizes to zero at large $L$. The interface becomes free from the

---

[2] $P_{L0}$ is also called the melting pressure $P_m$ of the solid; for a gas-solid interface, just replace liquid by gas in the above expressions.

influence of the crystal lattice, like a free liquid surface. Its fluctuations diverge at large distance, as described by the height-height correlation function

$$G(r) = < [z(r) - z(0)]^2 > = \frac{k_B T}{2\pi\gamma} \ln \frac{r}{L_0}, \qquad (7)$$

which is the same as for a free liquid surface ($L_0$ is the cutoff of fluctuations at a small scale). Physically, one understands that the fluctuations are so large that the crystal surface wanders over many periods $d$, so that the potential $V cos(2\pi z/d)$ is averaged to zero.

On the contrary, if $T < T_R$, the potential energy $U$ diverges at a large scale. Actually, as soon as $U$ becomes larger than $k_B T$ one understands that it should kill the fluctuations and the renormalization should stop. This renormalization is "truncated" at a maximum scale $L_{max}$ which appears in the problem. As a result, the height-height correlation function saturates:

$$\lim_{r\to\infty} G(r) = \frac{k_B T}{2\pi\gamma} \ln \frac{L_{max}}{L_0}. \qquad (8)$$

We thus understand that the crystal surface is "rough" like a free liquid surface at high temperature, and "smooth" at low temperature. The difference between these two states is *not* at the atomic scale. It is at the larger scale $L_{max}$ where fluctuations are either free or killed by the lattice. It is thus preferable to avoid expressions like "atomically smooth" or "atomically rough", which have been used by many authors in the past.

The quantity $L_{max}$ appears in Eq. (8) as a correlation length, but one usually defines the correlation length $\xi$ from the step profile which can be calculated within this sine-Gordon model. The step which we consider here is a *macroscopic* step. It is the surface defect whose existence is forced by pinning the crystal surface, say, at the height $z = 0$ on the left ($x = -\infty$) and at $z = +d$ on the right ($x = +\infty$). Its profile is given by

$$z(x) = \frac{2d}{\pi} \arctan \left[\exp \frac{x}{\xi}\right]. \qquad (9)$$

Close to $T_R$, the theory predicts that $\xi \approx L_{max}/2$, but the exact value depends on the way how the renormalization is truncated [see below and (Balibar *et al.*, 1993)]. $L_{max}$ is the minimum size for a smooth state to be defined, and it is not surprising to find that it is related to the step width, but, here again, there are numerical factors which need to be considered for a comparison with experiments. If one defines a step width $w$ as the horizontal distance necessary for the surface height to go from $0.1d$ to $0.9d$, then Eq. (9) implies that

$$w \approx 4\xi \approx 2L_{max}. \qquad (10)$$

At $T = T_R$, the renormalization goes to a "fixed point", where $U = 0$ and the surface stiffness has the universal value $\gamma(T_R)$ given by

$$k_B T_R = \frac{2}{\pi} \gamma(T_R)\, d^2. \qquad (11)$$

This is known as the "universal relation of roughening". It was first obtained by Fisher and Weeks (1983) and by Jayaprakash *et al.* (1983). It is universal in the sense that it does not depend on any microscopic detail such as the interatomic interactions and so on. Note that $\gamma(T_R)$ is the critical value of the surface stiffness in the right direction and exactly at the critical temperature $T_R$. Equation (11) refers to a surface with a cylindrical symmetry. For an arbitrary symmetry, when there are two different stiffness components, Fisher and Weeks (1983) showed that the universal relation writes as

$$k_B T_R = \frac{2}{\pi} (\gamma_1\gamma_2)^{1/2}\, d^2. \qquad (12)$$

There are two other predictions about critical behaviors near $T_R$. The first one concerns the step free energy $\beta$, which is predicted to vanish exponentially according to

$$\beta \propto \exp\left[-\frac{\pi}{2\sqrt{tt_c}}\right]. \qquad (13)$$

Here $t = 1 - T/T_R$ is the reduced temperature and the parameter $t_c$ is defined as

$$t_c = \frac{2\pi^2\sqrt{A(2)}U_0}{\gamma_0 d^2}, \qquad (14)$$

where $A(2) \simeq 0.4$ and the index "$_0$" as in $\gamma_0$ and in $U_0 = V_0 L_0^2$ means the unrenormalized value at the microscopic scale $L_0$. The parameter $t_c$ indicates the strength of the coupling of the crystal surface to the underlying lattice. It is weak if $t_c < 1$. Note that the critical domain in temperature is large if this coupling is weak and *vice versa*. It has been found that the correlation length $\xi$ diverges exponentially near $T_R$ since

$$\xi \approx \frac{k_B T_R}{\pi\beta}. \qquad (15)$$

The theory also predicts that the magnitude of $t_c$ controls the amplitude of the renormalization of the surface stiffness since

$$\gamma(T_R) = \gamma_0(1 + t_c/2). \qquad (16)$$

Another important prediction concerns the temperature dependence of $\gamma$. Below $T_R$ the stiffness is infinite, so that the crystal curvature is zero (the facet is flat). This is because, the step energy being non-zero, the angular variation of the surface energy $\alpha(\phi)$ has a linear cusp

$$\alpha(\phi) = \alpha_0 + \frac{\beta}{d}|\phi| \qquad (17)$$

around the smooth ($\phi = 0$) direction. As for above $T_R$, the surface stiffness reaches its universal value $\gamma(T_R)$ with a square root cusp:

$$\frac{\gamma(T)}{\gamma(T_R)} \approx 1 - \sqrt{|t|t_c}. \qquad (18)$$

Consequently, as temperature decreases, the crystal curvature shows a square root cusp till it reaches a universal value where it jumps to zero. Such square root cusps and universal jumps are found with all Kosterlitz-Thouless type of transitions. Depending on the system under consideration, the physical quantity showing this remarkable behavior is different. For example, it is the superfluid density for the superfluid transition of films, the shear modulus for the melting of 2D crystals, the magnetization in the "XY"-model of spins, the dielectric constant in the Coulomb gas, etc.

### 2. Vicinal surfaces and dynamic roughening

Several experiments also needed predictions for crystal surfaces whose orientations were tilted by a small angle $\phi$ with respect to the high-symmetry facetted ones (vicinal surfaces). Nozières calculated the properties of such surfaces within a slightly modified version of his first original theory. He replaced the potential term $V cos(2\pi z/d)$ in Eq. (4) by $V cos[2\pi(z-\phi x)/d]$. A new scale appeared in the problem, which was the average distance between steps, $l = d/\phi$. At a scale larger than $l$, the surface extends over more than one period $d$, so that the lattice potential is zero and the renormalization stops. In other words, the tilt angle introduces a "finite size effect" in the renormalization procedure. The exact scale at which it stops has been found numerically to be $L = l/6$ (Nozières and Gallet, 1987), and we will see below that this numerical factor "6" is important. The RG theory was thus able to predict also the angular variation of $\gamma(\phi)$ at small $\phi$ and near $T_R$.

Another kind of finite size effect appears when the crystal grows (or melts) with some finite velocity $v = \dot{z}$. Nozières' theory of this dynamic situation follows an approach first introduced by Chui and Weeks (1978). It uses the same renormalization group (RG) technique, but it is now applied to the Langevin equation of motion of the surface position $z(x,y)$:

$$\frac{\rho_C}{k}\dot{z} = \rho_C\delta\mu + \gamma\Delta z - \frac{2\pi}{d}V\sin\frac{2\pi z}{d} + R(z,t) \quad (19)$$

instead of the hamiltonian of Eq. (4). In this new equation, the important coefficient $k$ is the surface mobility, sometimes called the "growth coefficient" ($1/k$ is consequently the friction coefficient or the growth resistance); we will discuss it more extensively in Section IV; $R(z,t)$ is the random force at the origin of fluctuations and $\delta\mu = \mu_L - \mu_C$ is the difference in chemical potential between the liquid and crystal, which drives the net growth.

In the limit of $\delta\mu$ tending to zero (zero growth velocity), Nozières and Gallet (1987) have found a critical behavior for the mobility $k$ which has a square root cusp similar to the one found for the surface stiffness:

$$\frac{k(T)}{k(T_R)} \approx 1 - \sqrt{5.66\,|t|t_c}\ , \quad (20)$$

but this time, the mobility $k(T_R)$ is not universal. Now, as soon as a finite departure from equilibrium produces a net growth with some average velocity $v$, the roughening transition is blurred. Indeed, a time scale appears which is $\tau = d/v$, the time necessary for the crystal surface to move by one layer $d$. During $\tau$, the surface fluctuations diffuse by a distance $(k\gamma\tau/\rho_C)^{1/2}$ according to Eq. (19), which is a diffusion equation. As a result, the renormalization cannot proceed beyond this new scale. If it is larger than the correlation length $\xi$, there is no change. If it is smaller, then the renormalization stops before the lattice potential diverges, and the surface is dynamically rough. The criterion for the "dynamic roughening" is thus $\xi \approx (\rho_C\tau/k\gamma)^{1/2}$, which can be rewritten as

$$\frac{\beta^2}{d\rho_C\delta\mu k_B T} \approx 1\ . \quad (21)$$

There is a simple physical interpretation of this criterion. Indeed, on a smooth facet, and if the step free energy is small enough as happens close to $T_R$, the growth of a crystal proceeds by nucleation of terraces. In order to grow in size, these terraces need to have a radius larger than a critical value

$$r_c = \frac{\beta}{d\rho_C\delta\mu}\ . \quad (22)$$

Equation (21) means that this critical radius is comparable to the correlation length $\xi \approx k_B T_R/\beta$: dynamic roughening occurs if the critical radius for nucleation is smaller than the step width, which is also the minimum size for the definition of a smooth state. Let us finally remark that this dynamic roughening is different from another type of roughening (Kardar *et al.*, 1986), as explained by (Balibar and Bouchaud, 1992).

## C. $^4$He crystals

### 1. The (0001) surface

Balibar *et al.* (1993) summarized and discussed the way how the Paris group compared the RG theory of roughening with the surface properties of $^4$He crystals in the [0001] direction. Wolf *et al.* (1985) had measured the equilibrium shape of $^4$He crystals at a known overpressure $\delta P$. From this they obtained that the large scale angular variation of the surface stiffness of crystals was

$$\gamma_0(\phi) = 0.245\,(1 - 12\,\phi^2)\ \mathrm{erg/cm^2}\,. \quad (23)$$

They found that this angular variation was independent of temperature. They expected this result since they had to calculate the second derivative of the profile, and this could not be done in an angular domain smaller than about 10 degrees. This was not small enough to catch the critical behavior of $\gamma$. Indeed, as it appeared at the end of the analysis, the critical angular domain was only about 2 to 3 degrees. As a consequence, they considered 0.245

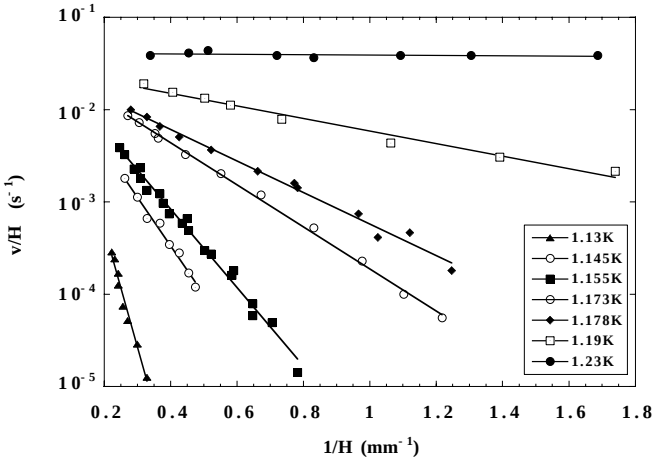


FIG. 22 . Experimental measurement by Wolf *et al.* (1985) of the growth characteristics of a c-facet on $^4$He crystals: semi-log plot of the growth velocity $V$ divided by a departure in height $H$ from the equilibrium position ($H = 0$), as a function of $1/H$. The difference in chemical potential across the interface is $\delta\mu = (\delta\rho/\rho_C)gH$. A good agreement was found with Eq. (24), from which values of the step free energy could be obtained.

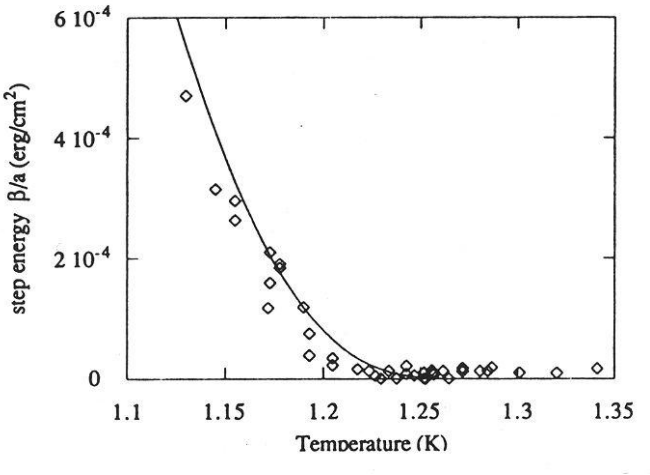


FIG. 23 . The temperature variation of the step free energy $\beta$ on the c-facets in $^4$He. The symbols correspond to the successive experiments by Wolf *et al.* (1985) and by Gallet *et al.* (1987). The solid line is the last fit of the RG theory by Nozières and Gallet (1987) which was done by Balibar *et al.* (1993) using the parameters of Eq. (25).

erg/cm$^2$ as the value of the non-renormalized quantity $\gamma_0$ in Eq. (16).

Wolf *et al.* (1985) and Gallet *et al.* (1987) measured also the step free energy of the (0001) or c-facets. This was done by studying the relaxation of a horizontal crystal surface towards its equilibrium height. In this case, in Eq. (19), the difference in chemical potential $\delta\mu$ is due to the hydrostatic equilibrium in the liquid; it is proportional to the departure $H$ from the equilibrium height. The visual observation technique of Wolf *et al.* was improved by Gallet *et al.* who used interferometry (see Section II.B.2). In the temperature range from 1.13 to 1.23 K, they found that the crystal growth apparently proceeded by 2D nucleation of terraces. If true, the growth velocity had to be given by

$$v = k\delta\mu \exp\left(-\frac{\pi\,\beta^2}{3\,d\,\rho_C\,\delta\mu\,k_B T}\right) . \qquad (24)$$

In this equation, the factor "3" indicates that terraces coalesce to form new atomic layers. As shown in Fig. 22, good agreement with this exponential behavior was found over several decades in the velocity values, and this allowed them to determine the step free energy $\beta$.

Figure 23 shows measurements of the step free energy close to $T_{R1}$ (Gallet *et al.*, 1987; Wolf *et al.*, 1985). In this figure, the solid line corresponds to a numerical integration of the Nozières' renormalization equations, which tend to the exponential form of Eq. (13) in the vicinity of the roughening transition. The best fit was obtained by Balibar *et al.* (1993) with the following set of parameter values:

$$T_{R1} = 1.30\,\mathrm{K}\ ;\ t_c = 0.58\ ;\ L_0 = 4d \approx 2\xi_0. \qquad (25)$$

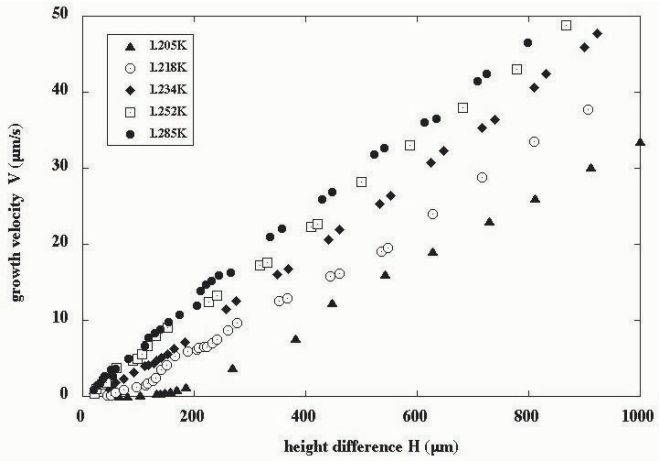


FIG. 24 . As the temperature approaches the roughening temperature $T_{R1} = 1.3$ K, the growth characteristics evolves smoothly from non-linear to linear behavior. These measurements were made by Gallet *et al.* (1987) and analyzed using the RG theory of dynamic roughening (see Fig. 25).

In reality, these three parameters were determined not only from the fit of the step free energy but also from the fit of the critical variation of the growth velocity of facets. The temperature 1.2 K appeared to be the threshold for dynamic roughening in these experiments, so that Eq. (24) could not be used above this temperature. Figure 24 shows that the growth characteristics $v(\delta\mu)$ is still slightly nonlinear at 1.2 K and evolves continuously into a linear regime near 1.3 K. This kind of evolution of growth is a central characteristics of the roughening transition and it is described by the dynamic part of the Nozières' theory, which could also be fitted with these

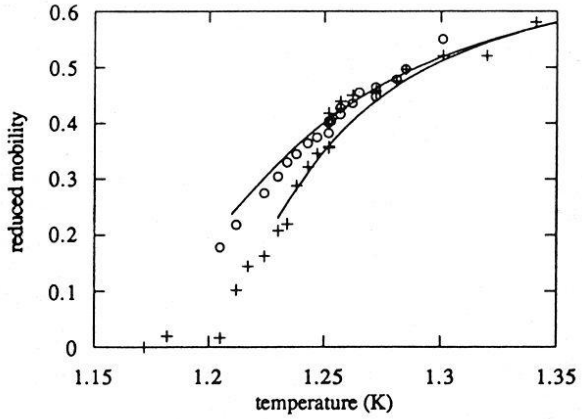


FIG. 25 . Measurements of the growth velocity of the c-facets by Gallet *et al.* (1987). Open circles correspond to a 0.7 mm height difference, and crosses to 0.07 mm. The "reduced velocity" is the ratio of the velocity $V$ of the (0001) surface to the velocity $V_r$ of a typical rough surface at the same temperature (taken in another crystalline direction). The two solid lines are theoretical fits by Balibar *et al.* (1993) using the theory of dynamic roughening by Nozières and Gallet (1987) and the parameters from Eq. (25).

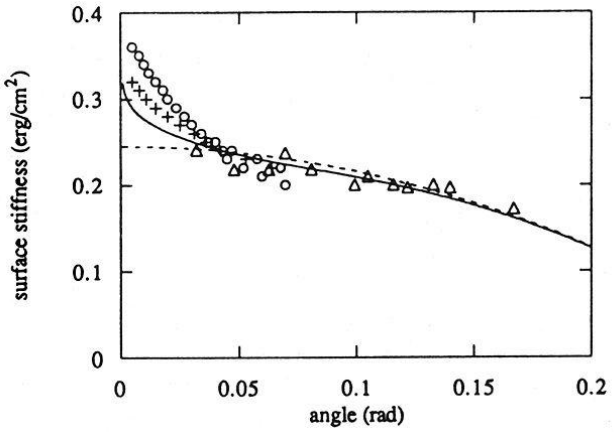


FIG. 26 . Angular variation of the surface stiffness close to the [0001] direction. The measurements are by Babkin *et al.* (1985) at 1.2 K (circles and crosses), by Andreeva *et al.* (triangles) at 0.4 K, and by Wolf *et al.* (1985) [dotted line, Eq. (23), in the interval from 1.18 to 1.41 K]. Given the scatter in the data, the agreement is good with the result from the RG theory at 1.2 K [solid line (Balibar *et al.*, 1993)]. It confirms that the critical angular domain is small, about 2 or 3 degrees, the only region where the surface feels the formation of the facet and where the stiffness has some temperature variation.

data as shown in Fig. 25. In this figure, three sets of experimental data points are shown which correspond to three different values of $\delta\mu$. The velocity of facets has been normalized by the velocity of rough surfaces in other crystalline directions. The parameters used for the theory are the same as above [Eq. (25)].

Figure 25 also illustrates the dynamic roughening. When submitted to a larger driving force $\delta\mu$, the transition from large growth velocity (in the rough state) to small growth velocity (in the smooth state) is broader than in the case when the driving force is small. At the intermediate temperature of 1.23 K, the applied force drives the surface into a faster growing, i.e., more rough state. In the limit of vanishingly small force, the velocity would jump sharply to zero at the roughening transition. Note also that the normalized velocity depends on $\delta\mu$ only below the roughening transition: this is where the growth is nonlinear.

Once this agreement was found and the parameters adjusted [Eq. (25)], Balibar *et al.* (1993) compared the RG theory with other measurements of the surface stiffness which had been done in Moscow (Andreeva *et al.*, 1989; Babkin *et al.*, 1985). The solid line in Fig. 26 is a numerical calculation of the angular variation of $\gamma$ at 1.2 K, the temperature of Babkin's measurements. The stiffness variation has an inflexion point in between 2 and 3 degrees, where it departs from Wolf's measurement of its noncritical behavior [Eq. (23)]. This angular range is directly connected to the value of $L_0$. Indeed, as explained above, the renormalization stops at the scale $L_{max} = l/6 = d/6\phi$. With $L_0 = 4d$, the Nozières' theory predicts no renormalization if $\phi$ is larger than $1/24$ rad = 2.4 degrees. This is remarkably consistent with Fig. 26. As we shall see in Section III.C.5, it has been further checked by the later studies of stepped surfaces (Rolley *et al.*, 1994b, 1995b), with an excellent agreement again.

Finally, the amplitude of the renormalization of $\gamma$ is also correct: Babkin's data tend to the universal value of

$$\gamma(T_{R1}) = 0.315 \text{ erg/cm}^2 = 0.245(1+\frac{0.58}{2})\text{erg/cm}^2 \quad (26)$$

at $\phi = 0$, more precisely to a slightly larger value because the measurements were unfortunately done at 1.2 K instead of 1.3 K (at that time, the exact value of $T_{R1}$ was not yet precisely known). This further confirms the values of $t_c$ and $T_{R1}$. Despite the scatter in the data, Babkin's measurements can be considered as the best available check of the universal relation of roughening [Eq. (11)].

A few additional comments are needed because, at the time of their publications, the Moscow group considered their results as contradictory to the RG theory [see, for example, Keshishev and Andreeva (1991)]. They first considered the value of $\gamma$ as too high by about 20%, but this was because they took $T_{R1}$ as 1.20 K. However, with $T_{R1} = 1.30$ K, good agreement is found with the Moscow measurements whose typical error bar is at least 10%, given the scatter in their experimental data. Furthermore, they objected that no temperature dependence of $\gamma$ was observed. This was because they did not look at a sufficiently small angle, nor at temperatures low enough to be in the critical domain. Later Rolley *et al.* (1994b, 1995b) performed experiments down to 40 mK and between 0.3 and 6 degrees. Their results showed a drastic

change as soon as the step width was small enough, once more in a very good agreement with the predictions from the RG theory (see Section III.C.5).

Although a rather good agreement was found between the RG theory and the properties of the c-facet in $^4$He, so that the validity of this theory looks well established now, there remains at least two problems which need to be clarified. The first one was pointed out by Balibar *et al.* (1993). As explained above, the renormalization stops at the maximum scale $L_{max}$ if $T < T_R$, a procedure which is often called a "truncated renormalization". In their analysis, the Paris group stopped the renormalization when the lattice potential $U$ equals $k_BT$. Gallet *et al.* (1987) found this physically correct because, beyond the corresponding length scale, the lattice potential is too large and kills the fluctuations. This implies the relation $\xi \approx L_{max}/2$. However, as explained by (Nozières, 1992), the weak coupling approximation needs in fact $4\pi U/k_BT \ll 1$ to be justified, so that the renormalization should perhaps be stopped when $U = k_BT/4\pi$ more than $U = k_BT$.

As explained by Balibar *et al.* (1993), a good fit of the experimental results was possible by changing the maximum scale slightly, but not if the renormalization was stopped when $U = k_BT/4\pi$. The exact maximum scale is in fact an additional adjustable parameter which is not explicit, but raises an interesting difficulty. In order to solve it, one would need independent measurements of both the correlation length $\xi$ and the step free energy $\beta$. The exact scale at which renormalization has to be stopped could then be more accurately determined and the other parameters slightly modified. The correlation length $\xi$ could perhaps be obtained from a measurement of the height-height correlation function in an X-ray scattering experiment. This looks difficult but an important challenge. Another experiment was suggested by (Giorgini and Bowley, 1995) to obtain more information on the best truncation scale, namely a measurement of the response of the interface, near the roughening transition temperature, to an external drive at a few kHz.

The second problem came very recently from critics by (Todoshchenko *et al.*, 2004) of the way how the experimental data were analyzed in the work of Wolf *et al.* (1985), Gallet *et al.* (1987), and Balibar *et al.* (1993). Todoshchenko's argument is that the assumption of a 2D nucleation mechanism is not well justified because the step mobility should be larger by a factor $\xi/d$ than the mobility $k$ of rough surfaces ([as Gallet *et al.* (1987) erroneously assumed]. If the facets have no dislocations at all, then, of course, Gallet's assumption holds; but if the mechanism is in fact the spiral growth due to the Frank-Read sources, then a fit with a quadratic law leads to new values for the step free energy $\beta$ which are larger than previously thought. From new fits with the RG theory, where the renormalization was stopped when $U = k_BT/4\pi$ this time, Todoshchenko *et al.* obtained values for the three parameters $T_{R1}, t_c$ and $L_0$ which are slightly smaller than those obtained by the Paris group [Eq. (25)]. That recent critics asks for further examination of the critical behavior near the roughening transition temperature, especially for new independent measurements of both $\beta$ and $\xi$.

### 2. Quantum roughening and mean field theories

A certain number of other theoretical ideas have been proposed. Andreev and Parshin (1978) (AP) first introduced the idea of quantum kinks. AP had noticed that, similarly to other point defects in quantum systems [see (Andreev and Lifshitz, 1969)], kinks on steps behave as delocalized quasiparticles. The energy of the ground state of such a quasiparticle is always lower than the energy of a localized state. According to AP, this effect is strong enough to make the net kink energy negative, i.e., "zero-point kinks" should exist. The step with such kinks, a "quantum rough step", should be very mobile at low temperatures, in contrast to classical steps. For a further discussion on the properties of quantum kinks and steps, see Sections IV.C.3 and V.A.2.

The presence of zero-point kinks decreases the step energy, therefore AP further proposed that this effect could be strong enough to make also the step energy negative, i.e., "zero-point steps" should exist. In such a case the smooth state of a given facet would be unstable against "quantum roughening", even at $T = 0$. However, Fisher and Weeks (1983) have shown that this is impossible: the step energy cannot be zero at $T = 0$. Here we meet with a fundamental difference in the role of quantum fluctuations in 1D and 2D cases, first suggested by Fisher and Weeks. As we have seen, the roughening transition is a problem of divergence of fluctuations at a large scale. In the 2D case the integral of quantum fluctuations leads to a finite contribution to the height-height correlation function which cannot diverge at $T = 0$, so that the thickness of the crystal surface is always finite. As a consequence, the crystal surface is always sensitive to the periodic potential of the lattice; the energy of the above defined *macroscopic* steps is always positive at $T = 0$, whatever happens to the steps at a microscopic scale. In contrast, in the 1D case the height-height correlation function of quantum fluctuations may diverge at a large scale, the pinning of a step to the lattice potential may be eliminated, and the step may be indeed quantum rough. The absence of quantum roughening in the 2D case was further demonstrated by solving various quantum models of crystal surfaces (Bol'shov *et al.*, 1984; Fradkin, 1983; Iordanskii and Korshunov, 1983, 1984).

We now understand that quantum effects enter in the determination of the surface thickness and the step width at $T = 0$, and *a priori* calculation of the parameters $t_c$ or $L_0$ would have to consider them: with more quantum fluctuations, the crystal surface and the steps at it are thicker at $T = 0$, the length $L_0$ is also larger, so that the surface should be more weakly coupled to the lattice (the coupling parameter $t_c$ should be smaller as well as the

step energy at $T = 0$). But the universal relation does not depend on this. Iordanskii and Korshunov (1984) mention a small dependence of the surface stiffness on quantum effects, but the quantity which they consider is $\gamma_0$, not $\gamma(T_R)$.

From the theoretical point of view, there is one more question of general interest: weather facets can appear as a result of a phase transition other than the Kosterlitz-Thouless one? Of course it could be the first order transition caused by some bulk transformation or even without it (Fisher and Weeks, 1983; Keshishev *et al.*, 1982; Nozières, 1992). To our knowledge, there is no manifestation of such transitions in helium crystals. Another possibility was studied by Andreev (1981), who proposed a mean field theory of faceting, similar to the Landau theory of the second order phase transitions. In the Andreev's approach, the rough surface plays the role of the symmetric phase and the step free energy the role of the order parameter. This theory predicts that the step free energy should vanish near $T_R$ according to the square root law $\beta \propto \sqrt{T_R - T}$ and that the surface stiffness should continuously diverge to infinity as a function of angle at $T_R$. Furthermore, Andreev predicted the existence of surfaces with one zero curvature only, i.e., with a cylindrical shape. None of these predictions were observed in experiments (Babkin *et al.*, 1984; Gallet *et al.*, 1987; Wolf *et al.*, 1985). In fact, as clearly stated by Iordanskii and Korshunov (1984), the mean field theory "has no range of applicability because of the governing role played by fluctuations".

### 3. Other facets in $^4$He

Let us now examine the other facets in $^4$He. Here again, there has been some controversy in the past. The analysis of the data on the (0001) facets showed that several measurements are needed for a precise comparison with the RG theory. In the case of the $(10\bar{1}0)$ and $(10\bar{1}1)$ facets, the comparison is more difficult due to the existence of two components of the surface stiffness tensor instead of one. Not only it is hard to obtain a crystal with vertical $[10\bar{1}0]$ or $[10\bar{1}1]$ axes, but this would not be even sufficient: one would need to rotate the crystal around this vertical axis and find the values of the two principal components of the stiffness tensor at the right temperature and in the precise directions where facets appear. This might be done hopefully in the future, but, for the moment, let us consider the available experimental data.

Supposing that the roughening temperature $T_{R2} = 1$ K for the $(10\bar{1}0)$ surfaces, it would be consistent with the RG theory if the geometric mean $(\gamma_1\gamma_2)^{1/2}$ of its two surface stiffness components is 0.21 erg/cm$^2$ at 1 K since the step height is 3.18 Å in this direction. Wolf *et al.* (1985) have measured the average value $\gamma = 0.19$ erg/cm$^2$ for this direction at 0.95 K and Andreeva *et al.* (1989) have measured 0.36 erg/cm$^2$ 1.5 degrees away from the $[10\bar{1}0]$ direction at 0.4 K. Andreeva and Keshishev (1990) have measured also 0.21 erg/cm$^2$ 13 degrees away from the $[10\bar{1}0]$ direction while Edwards *et al.* (1991) have estimated the two surface stiffness coefficients to be 0.2 erg/cm$^2$ and 0.16 erg/cm$^2$, correspondingly. Clearly, more precise measurements are needed in this direction, but there is no contradiction with the universal relation from the RG theory: the measured values of the surface stiffness components have the right order of magnitude.

As for the $[10\bar{1}1]$ direction, the lack of precise measurements is similar. If we assume that the roughening temperature $T_{R3}$ is as high as 0.43 K, as proposed by Keshishev and Andreeva (1991), then the mean surface stiffness $(\gamma_1\gamma_2)^{1/2}$ should be 0.11 erg/cm$^2$ for this third direction, where the step height is 2.80 Å. Only one component, $\gamma_1 = 0.22$ erg/cm$^2$, has been measured by Keshishev and Andreeva (1991). Agreement with the RG theory would need the other component $\gamma_2$ to be much smaller, but this is not unreasonable since a value as low as 0.08 erg/cm$^2$ has been measured in the $[11\bar{2}0]$ direction by Keshishev and Andreeva (1991). In fact, the study of the $[10\bar{1}1]$ direction would perhaps be easier to do than of the $[10\bar{1}0]$ direction because the stiffness could be measured from the dispersion of crystallization waves around 0.4 K (at 1 K and above, they are overdamped).

What about other directions then? How can it be that no more than three types of facets have yet been observed? In the $[11\bar{2}0]$ direction, the step height is 1.83 Å, thus if the average stiffness is about 0.2 erg/cm$^2$, the facets should appear below $T_{R4} = 0.3$ K [below 0.15 K if $(\gamma_1\gamma_2)^{1/2} = 0.1$ erg/cm$^2$]. Puech *et al.* (1983) have found an anomaly at 0.21 K which might be due to this fourth roughening transition, but no systematic search of higher order facets has yet been done in $^4$He. When crystal grows (slowly enough that no dynamic roughening occurs), the facet sizes are enhanced because they grow more slowly than the adjacent rough surfaces. Since the growth rate depends on the step energy, the facets with large Miller indices grow faster than those with small indices, and they are more difficult to see on the growth shapes. Furthermore, the hcp structure is highly anisotropic, so that the growth shapes of hcp $^4$He crystals are usually dominated by the [0001] and $[10\bar{1}0]$ facets. The $[10\bar{1}1]$ facets are very often absent on the growth shapes, and usually not as clearly visible as in Fig. 2. Is this a sufficient argument to explain that only three facets have been observed in $^4$He? May be, but a more systematic study would be useful.

If one looked at the equilibrium shapes, it would be also difficult because the equilibrium facet size is proportional to the step energy. For the (0001) facet in the low temperature limit, Rolley *et al.* (1995b) found that the step energy $\beta/d$ was equal to 0.014 erg/cm$^2$, less than one tenth of the surface tension value, so that the equilibrium facet radius should be less that one tenth of the typical crystal radius. The sizes of facets with higher Miller indices would be even smaller and thus these facets would be even more difficult to see on the equilibrium shapes of crystals. One possibility would be to enhance the facet

size with the help of gravity which assumes having a properly oriented crystal. This might produce a picture similar to the one shown in Fig. 18.

Note finally that, for the bcc $^4$He crystals which exist above 1.46 K and have a surface tension value less than 0.12 erg/cm$^2$ (Balibar *et al.*, 1979; Gallet *et al.*, 1984), the universal relation [Eq. (11)] predicts the first roughening transition for the (110) surfaces to take place below 0.45 K. This is, of course, consistent with the observations that the bcc $^4$He crystals are rough in their whole domain of existence. As for the bcc $^3$He crystals, their roughening transition temperatures are considered in Section III.D.

#### 4. Surface tension of $^4$He crystals

As we have seen above, the surface stiffness of $^4$He crystals is known in various directions and it has a substantial anisotropy. The Moscow group has investigated the general shape of $\gamma$ in all directions (Andreeva and Keshishev, 1991; Andreeva *et al.*, 1989; Keshishev and Andreeva, 1991). The surface stiffness could also be extracted from the equilibrium shape of free standing crystals and Wulff (1901) has introduced a geometric construction of the equilibrium crystal shape from the polar plot of $\gamma$. Even the values for the step energies could be extracted from the facet sizes on the equilibrium crystal shapes, but it has been observed that the facet sizes are hysteretic. The facet sizes depend on the history of a crystal because, when they grow from the motion of steps attached to the screw dislocations (see Section V), there is a threshold force below which the steps do not move [see (Nozières, 1992) again].

One should not forget also that only rough $^4$He crystal surfaces have a fast dynamics. Even for the extraction of the values of the surface stiffness of rough surfaces, the inverse Wulff's construction of $\gamma$ from an equilibrium shape would not be easy. One would need to know the exact pressure difference from the equilibrium pressure to obtain the absolute value of the surface stiffness. Furthermore, one would need a very good resolution on the measured shape to obtain its exact local curvature everywhere. Eventually, the crystal shape is sensitive to defects. All these difficulties probably explain why the surface stiffness of classical crystals is rarely accurately known, so that an accurate experimental check of Eq. (11) is usually impossible.

The method of Andreeva *et al.* (1989) and Keshishev and Andreeva (1991) was different: they used the dispersion relation of crystallization waves to determine $\gamma$. Some of their results are shown in Figs. 27 and 28. Further analysis of these data was performed in order to extract the surface tension $\alpha$ (Andreeva and Keshishev, 1991; Edwards *et al.*, 1991). It was found that $\alpha$ typically varies from 0.16 to 0.18 erg/cm$^2$. The anisotropy of $\alpha$ is much smaller than for $\gamma$. The value of $\alpha$ is important for the study of the nucleation of solid helium,

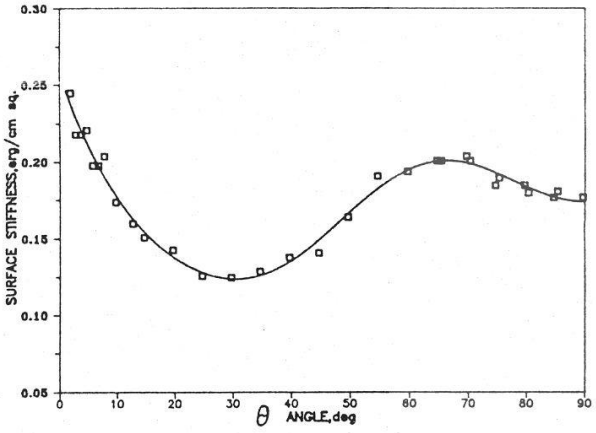


FIG. 27 . A set of measurements of the surface stiffness $\gamma$ of the hcp $^4$He crystals in the $(10\bar{1}0)$ plane. The angle $\phi = 0$ corresponds to the (0001) plane and $\phi = 90$ degrees to the $(11\bar{2}0)$ plane (Andreeva and Keshishev, 1991).

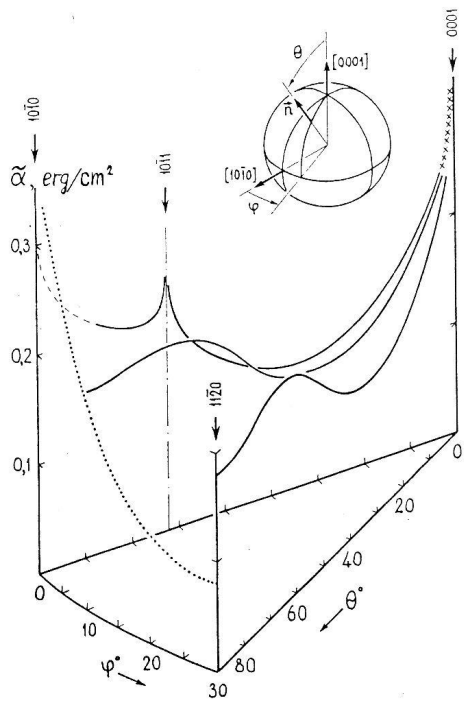


FIG. 28 . General variation of the surface stiffness $\gamma$ of $^4$He crystals as measured from the dispersion relation of crystallization waves by Andreeva *et al.* (1989) and Keshishev and Andreeva (1991).

where it is the free energy of the liquid-solid interface which matters, not the stiffness [see (Balibar, 2002) for a review].

The shape of the facet edges at a crystal surface has attracted a lot of attention. It is related to the interaction between steps. Consider a vicinal surface, i.e., a surface which is tilted by a small angle $\phi$ with respect to a certain facet (the temperature has to be lower than the roughening temperature of that facet). If $\phi$ is small enough, the steps are well separated and we call this vicinal surface a "stepped surface" because its properties are determined by the steps. The surface energy of the stepped surface does not depend on the sign of $\phi$ and it can be expanded as

$$\alpha(\phi) = [\alpha_0 + \frac{\beta}{d}\tan|\phi| + \frac{\delta}{d^3}\tan^3|\phi|]\cos\phi\,. \quad (27)$$

In this equation, we have assumed that the interaction energy between steps is a repulsion inversely proportional to the square of their mutual distance $l$, so that it writes as $(\delta/d^2)\tan^2\phi$. From Equation (27), one can derive the values of the two components of the surface stiffness tensor for such a vicinal surface:

$$\gamma_{//} = \frac{6\delta}{d^3}\phi\,, \quad (28)$$

and

$$\gamma_{\perp} = \frac{\beta}{d}\frac{1}{\phi}\,. \quad (29)$$

Just like a corrugated iron sheet, the stepped surface should be easy to bend in one direction and it should be very stiff in the direction perpendicular to the first one. The physics is simple: if one bends the surface in a plane perpendicular to the steps, one changes the distance between the steps, and the energy cost depends on the interaction between steps, which is small if the steps are far apart (small $\phi$). On the contrary, if one bends the surface along the steps, one forces the steps themselves to bend, that is to increase their length; the associated cost is now a step energy and the step bending is proportional to the inverse step density, i.e., to $1/\phi$ (see Fig. 29).

Several kinds of interactions have been predicted to exist between steps. The dominant ones are the elastic interaction $\delta_{el}$ and the entropic interaction $\delta_S$. Both of them vary as $1/l^2$ but with different coefficients. Let us start with the entropic interaction. It comes from a no-crossing condition. If two neighboring steps crossed, a local overhang would appear at the surface (see Fig. 30), and that is, of course, unlikely. Steps are thus confined by their neighbors, so that their long-wavelength fluctuations are cut and their entropy consequently reduced. This is a fundamental effect which has an equivalent in one more dimension: the entropic repulsion between fluctuating membranes known as the "Helfrich interaction" (Helfrich, 1978). Its exact magnitude was first calculated from an analogy with one-dimensional Fermi particles,

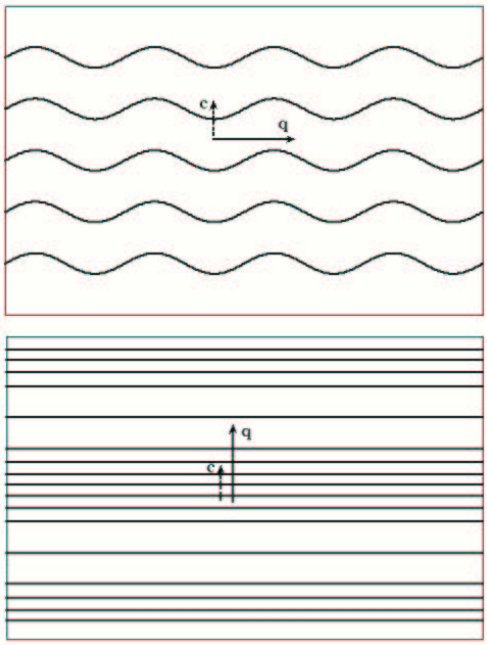


FIG. 29 . Bending of a vicinal surface is easy in a plane parallel to the $c$-axis, but difficult in the plane perpendicular to it. For waves propagating with $q//c$, the relevant surface stiffness component $\gamma_{//}$ is proportional to the interaction between steps and vanishes as the tilt angle $\phi$ tends to zero. On the contrary, the component $\gamma_{\perp}$ is proportional to the step energy $\beta$ and diverges as $1/\phi$.

whose trajectories in a space-time plane are lines which do not cross (Bartelt *et al.*, 1990; Jayaprakash and Saam, 1984; Williams and Bartelt, 1991). After correction of a numerical error [see note 34 in (Balibar and Nozières, 1994)], the result of this calculation agreed with the one obtained with a different method (Akutsu *et al.*, 1988):

$$\frac{\delta_S}{l^2} = \frac{\pi^2}{6}\frac{(k_B T)^2}{\beta\, l^2}. \quad (30)$$

This is another remarkable result which is universal in the same sense as Eq. (11).

The elastic interaction was first calculated by Marchenko and Parshin (1980a). Its physical origin is the overlap of the strain fields around each step. The atoms in the step have an environment which is different from the one of the bulk atoms. As a consequence, there is a force doublet on each step which induces a local strain field. Since the elastic energy is the integral of the square of the strain, the elastic energy of two steps is different from the sum of the elastic energies of two single steps: the cross term in the calculation gives the elastic interaction, which is repulsive for identical steps. Nozières (1992) wrote it as

$$\frac{\delta_{el}}{l^2} = \frac{2}{\pi}\frac{(1-\sigma_P^2)(\vec{f}_1\cdot\vec{f}_2)}{E\, l^2}\,, \quad (31)$$

where $\sigma_P \simeq 1/3$ is the Poisson ratio, $E$ is the Young modulus ($3.05 \times 10^8$ erg/cm$^3$ for the hcp $^4$He crystals)

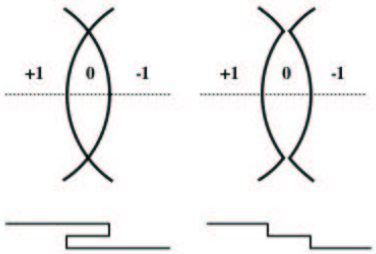


FIG. 30 . A crossing between steps (left) would induce a local overhang at the surface (cross-section below); this is rather unlikely, so that steps do not cross (right). The no-crossing condition for steps implies a reduction of the step entropy, hence a repulsive interaction.

and $\vec{f}_{1,2}$ are the force doublets on each step. Each of these doublets is made of the local stretch of the surface $f^x$ and of the local torque $f^z$ which tends to twist the crystal.

As explained by Marchenko and Parshin (1980a), $f^z = \sigma^s d$, where $\sigma^s$ is a surface stress (Andreev and Kosevich, 1981; Marchenko and Parshin, 1980a; Suttleworth, 1950). In the case of $^4$He crystals, Edwards *et al.* (1991) estimated this surface stress to be 0.6 erg/cm$^2$ from the pressure variation of the surface tension, and suggested to measure it from the transmission of phonons through the liquid-solid interface as a function of the direction of incidence. This does not seem to be an easy experiment to do, but $\sigma^s$ has to be comparable to the surface tension or surface stiffness. If one estimates also $f^x$ as $\gamma$, one finds the elastic interaction to be of the order of $\gamma^2/E\,l^2$.

Since they had not observed the anisotropy predicted by Eqs. (28) and (29), Andreeva *et al.* (1989) questioned the validity of the whole above reasoning. In fact, Rolley *et al.* (1994b, 1995b) found this anisotropy when studying vicinal surfaces at lower temperature and with a smaller tilt angle. Both groups measured the surface stiffness from the dispersion of crystallization waves at surfaces with variable orientation. They changed this orientation by rotating the cell containing a crystal with horizontal surface (see Fig. 14). Figure 40 presents all their experimental results. Only the low temperature and low tilt angle measurements by Rolley *et al.* could show the expected anisotropy of the surface stiffness tensor close to the c-facet. This experiment is described in more details in Section IV.B; Rolley's main results are that

(1) at low temperature, the step energy is $\beta/d = 14 \pm 0.5$ erg/cm$^2$ for ultrapure $^4$He crystals. In the presence of $^3$He impurities, Rolley *et al.* found the lower value $\beta/d = 11 \pm 1 \times 10^{-3}$ erg/cm$^2$, and they attributed the difference to adsorption, as explained in Section IV.C.8.

(2) the step-step interactions are consistent with the $1/l^2$ interactions predicted by Eqs. (30) and (31).

Eventually, hydrodynamic interactions were also calculated by (Uwaha, 1989, 1990). The fluctuations of steps induce some flow field around them, and if steps are close to each other, these fields overlap. Since the kinetic energy is quadratic, this phenomenon leads to a hydrodynamic repulsion between steps. Uwaha first calculated the interaction at $T = 0$ and found a $1/l^2$ repulsion. At high enough temperature, Uwaha predicted a crossover to $1/l$ interactions. Rolley *et al.* (1995b) could not verify Uwaha's predictions because these hydrodynamic interaction were too small in their experimental conditions.

### 6. Facet edges and related shape problems

The nature of step-step interactions has a direct consequence on the equilibrium shape of crystals. As calculated by Jayaprakash *et al.* (1983) and Jayaprakash and Saam (1984), the shape of the crystal profile near the facet edge has to obey a power law equation with a "3/2" exponent if the interaction energy is proportional to $1/l^2$. Suppose that the facet is some portion at $x < 0$ of the horizontal plane $z = 0$, then the shape of the crystal edge should be described by $z \propto x^{3/2}$. Jayaprakash *et al.* obtained this result by using Andreev's analysis of the Wulff construction (Andreev, 1981; Wulff, 1901). The "3/2" exponent is different from the mean field exponent "2"; it relates the problem of crystal shapes to the Pokrovsky-Talapov transition of crystalline layers on incommensurate substrates (Gruber and Mullins, 1967; Jayaprakash and Saam, 1984; Jayaprakash *et al.*, 1983; Rottman *et al.*, 1984).

Several experimental attempts were made to check this new universal property. For $^4$He crystals, (Carmi *et al.*, 1987) found an exponent 1.55 ± 0.06 between 0.9 and 1.1 K; (Gallet, 1986) found 1.55 ± 0.3 from fits in a small angular domain (from 0.14 to 0.18 rad), and a higher value at larger tilt angle. He also noticed that the fit of the exponent is so sensitive to the choice of the edge position $x = 0$ that its error bar cannot be small. Furthermore, it was noticed that, for large crystals and horizontal facets, gravity might change the exponent from "3/2" to "3" (Avron and Zia, 1988). Finally, (Jayaprakash *et al.*, 1984; Rottman *et al.*, 1984) discussed the finite-size effects which could be responsible for some rounding of the crystal profile very close to the facet edge; however, (Parshin *et al.*, 1988) showed with direct calculations of the shape that the exponent "3/2" holds down to an atomic scale.

The most accurate experimental attempt was done by the Helsinki group. Babkin *et al.* (1985) measured the equilibrium profile of $^4$He crystals near the edge of the c-facets, using their high-resolution interferometric techniques in the temperature interval from 0.05 to 0.7 K (Babkin *et al.*, 1995). They studied very high quality crystals, whose growth threshold was about 1 $\mu$bar, meaning an average density of screw dislocations or pinning centers of about 10 cm$^{-2}$ only. They confirmed the "3/2" exponent but also obtained unexpected results.

Figure 31(a) shows their measured surface profile at

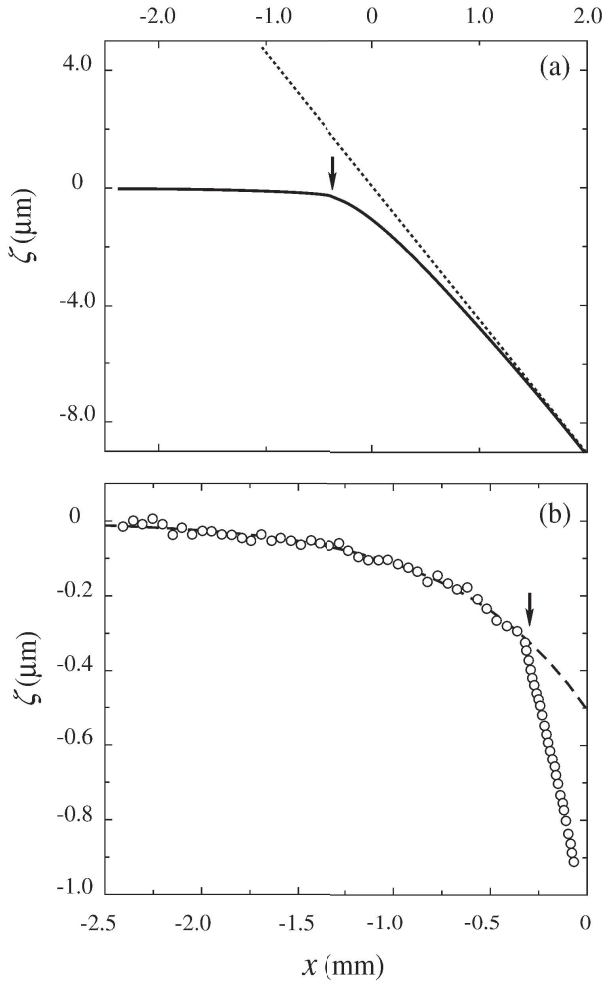


FIG. 31 . Surface profile of a $^4$He crystal at 0.05 K (a) in a wide angular region $0 \leq \Theta \leq 4.5$ mrad; the dashed line corresponds to the gravitational horizon and the arrow indicates the slope discontinuity, and (b) at small $\Theta$ (magnified view); the line is an exponential fit as explained in text (Babkin *et al.*, 1995).

0.05 K. The facet is shown on the left side at $\zeta = 0$. Far away from the edge the horizontal crystal profile follows the dashed line, the gravitational horizon. Figure 31(b) shows a magnified view of the same profile near the facet edge. There are two remarkable features. First, there is a discontinuity (marked by the arrow): the slope jumps from $\phi_{c1} = 0.43$ mrad to $\phi_{c2} = 2.3$ mrad, indicating a separation between two regions with distinct properties. In the right side region the profile could be fitted with the form $\zeta \sim x^\theta$, with $\theta$ between 1.3 and 1.8, in agreement with the "3/2" prediction. As in the Gallet's analysis, the large error bar in the determination of the exponent comes from the uncertainty in the determination of the facet edge position. As for the left side region, which should be a flat facet, it appeared curved at that scale. The deviation from a flat plane was well represented by an exponential law $\zeta \propto \exp(-x/x_0)$, where $x$ was calculated from the facet edge and $x_0$ was a temperature dependent constant.

Several possible ideas were proposed to explain this surprising curvature of facets. Since there are dislocations emerging on the facet, there is a finite density of steps on this facet and these steps could be polarized by the growth (Uwaha and Nozières, 1987); they could also be pinned by defects (Thuneberg, 1997), and the flatness of the facet can be affected by these phenomena. However, the density of dislocations and other pinning defects in these crystals looked to be too small for these explanations to be accepted. Another possibility was that the six-fold symmetry of the facet was broken, so that two different surface states could exist, with the same surface energy but with different orientations of the surface stress tensor; this would lead to a logarithmic interaction between steps (Alerhand *et al.*, 1998; Marchenko, 1981a), with an exponential bending of facets and a slope discontinuity as observed in the experiment. However, the origin of the symmetry breaking, if real, is unknown, so that this explanation looks rather speculative. Before accepting this explanation, one would like some independent observations to be done, and some physical arguments to be found, in support of the idea that a reconstruction of the c-facet takes place, leading to a new surface state.

Eventually, another explanation was proposed, which involved the existence of thermally excited dislocation loops at the interface (Andreev, 1990). This idea arose a lively discussion on the effect of dislocations, dislocation loops, point defects of different nature on the long-range order in 3D and 2D systems, and on the surface roughening in particular (Andreev, 1995; Andreev and Melnikovsky, 2001; Armour *et al.*, 1998; Bowley and Armour, 1997; Thuneberg, 1997). Andreev introduced the idea of thermodynamical equilibrium plasticity and argued that even point defects might destroy faceting. On the contrary, Armour *et al.* came to the conclusion that closely spaced pairs of dislocations with opposite signs can only slightly reduce the temperature of the roughening transition. They also predicted that, if the dislocations are randomly distributed, the interface seems to have a glassy, non-faceted low temperature state, and it undergoes a super-roughening transition, which is not a "true" phase transition (i.e., not infinitely sharp in the thermodynamical limit); its rounding would be detectable only on huge length scales (Toner and DiVincenzo, 1990).

To our knowledge, the whole issue is still an open problem. Turning back to Babkin's experiments, the activation energy of Andreev's loops was later estimated by the Helsinki group (Saramäki *et al.*, 1998), who found it larger than 18 K, and this looks too high to produce any observable effect at temperatures as low as 0.05 K. Thus, no satisfactory explanation exists for the observed curvature of the c-facets in Babkin's experiments, nor for the slope discontinuity at the edge of the facets.

Additional support to the existence of $1/l^2$ interactions were obtained in $^3$He from the growth of stepped crystal surfaces (see Section V.A.3)(Tsepelin *et al.*, 2002a).

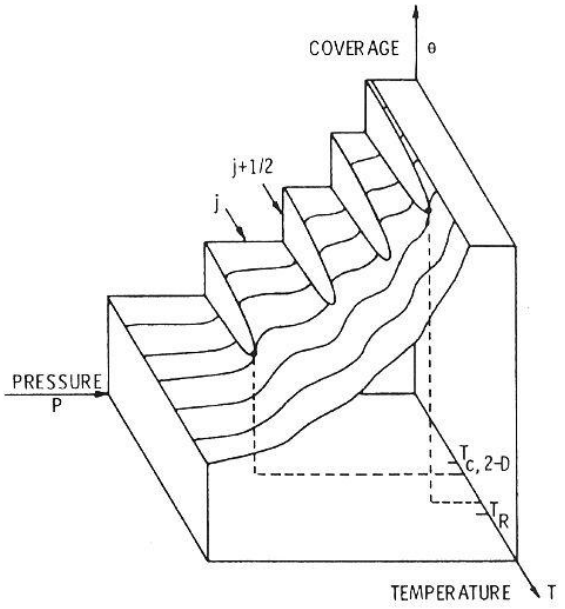


FIG. 32 . Adsorption isotherms of solid $^4$He on graphite. At low temperature, the coverage shows jumps, i.e., first order transitions, between layers with integer numbers of layers [noted $j$ by Ramesh *et al.* (1984)]. The first order transitions have critical end points at successive temperatures $T_c$ which depend on the number of atomic layers.

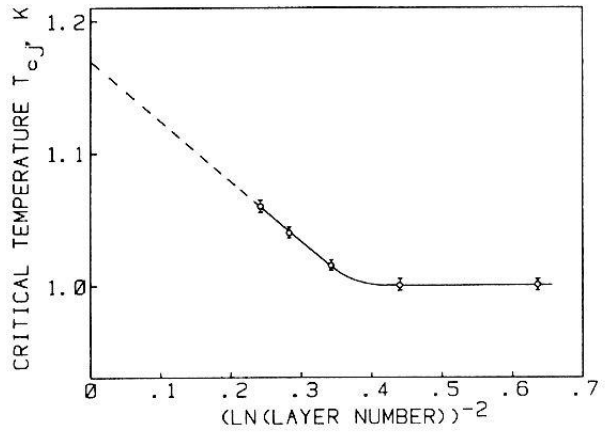


FIG. 33 . Extrapolation of the critical layering transition temperatures $T_c(n)$ as a function of the number $n$ of layers, more precisely $(\ln n)^{-2}$. According to Huse (1984) and Nightingale *et al.* (1984), $T_c$ tends to the roughening temperature $T_R$ at infinite thickness (Ramesh *et al.*, 1984).

### 7. Roughening and layering transitions

As already mentioned in Section II.C, $^4$He crystals grow by epitaxy on clean graphite substrates. Maynard and his group carefully studied the variation of the thickness of the adsorbed film of solid $^4$He as a function of pressure and temperature (Ramesh and Maynard, 1982; Ramesh *et al.*, 1984). As shown in Fig. 32, the shape of the adsorption isotherms evolves with temperature. At high enough temperature the coverage is a continuous function of pressure $P$. As $P$ approaches the equilibrium pressure $P_{eq}$, the coverage increases; it shows structures but it evolves continuously. At low temperatures, the isotherms show jumps in thickness, i.e., first order transitions between films with integer numbers of atomic layers. Each of these "layering transitions" has a critical temperature $T_{cn}$, which depends on the number $n$ of layers.

This phenomenon was related to roughening by (Huse, 1984) and by (Nightingale *et al.*, 1984). This is because the physics is similar: the liquid-solid interface can either be anchored by the lattice potential, in which case it occupies positions corresponding to an integer number of layers adsorbed on the graphite substrate, or it is free to occupy any position. However, the critical layering transitions are different from the roughening transition because of the van der Waals attraction which confines the interface fluctuations. For the first layer, for example, the attraction is so strong that atoms can be in the first or in the second layer only. In this case, the system is strictly equivalent to the 2D Ising model, with a second order phase transition, not with a Kosterlitz-Thouless one. As the film thickness increases, fluctuations feel a weaker and weaker van der Waals attraction and the critical layering transition was predicted to evolve into the roughening transition. More precisely, Huse and Nightingale *et al.* predicted that $T_{cn}$ tends linearly to $T_R$ as a function of $[\ln(n)]^{-2}$. This prediction was qualitatively verified by Ramesh *et al.*, as shown in Fig. 33 at a time when $T_{R1}$ of $^4$He crystals was not yet accurately known. It would be very interesting to extend Ramesh's measurements beyond 8 layers, the maximum thickness in Ramesh's experiment, in order to obtain a better check of this prediction.

Later on the same group, (McKenna *et al.*, 1992) discovered a surprising phenomenon. As temperature was lowered below about 0.5 K, their fourth sound measurement technique showed the existence of a feature at a half filling of layers. It seems that layers are being completed in two stages, not in a single one as was expected before. They first proposed to relate this observation to the existence of quantum kinks whose mobility drastically changes when thermal rotons disappear or when $^3$He impurities adsorb on the steps. They proposed another possible interpretation, namely that some reconstruction of the (0001) surface could occur if one forces a half filling of layers. Such ideas were also proposed by (Gridin *et al.*, 1984) who observed similar features in their adsorption isotherms. The whole issue looks interesting and undecided yet.

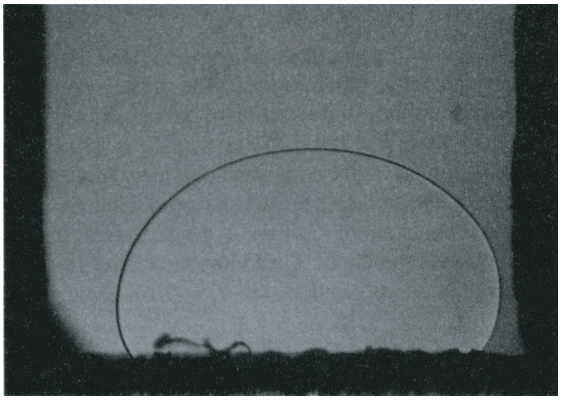

FIG. 34 . $^3$He crystal in equilibrium at 320 mK (Rolley *et al.*, 1989). Their analysis of such equilibrium shapes allowed to measure the surface stiffness of $^3$He crystals (see Fig. 35).

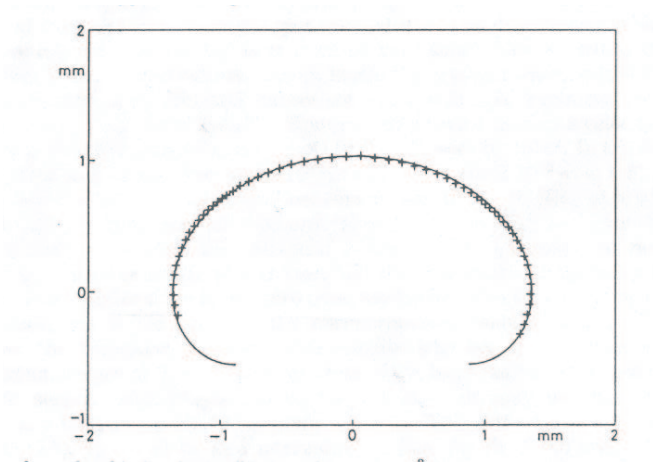


FIG. 35 . When the size of a crystal is larger than the capillary length, its equilibrium shape depends on both the gravity $g$ and the surface stiffness $\gamma$. From a fit with Laplace equation, Rolley *et al.* (1989) obtained $\gamma = 0.06$ erg/cm$^2$.

### D. $^3$He crystals

#### 1. Surface tension of $^3$He crystals

In $^3$He, crystallization waves could propagate only at sub-millikelvin temperatures. At higher temperatures the surface stiffness of $^3$He crystals can be measured from the equilibrium crystal shape, but it is difficult because the crystal shape can be easily distorted by defects, impurities or temperature gradients. The crystal size should be larger than the capillary length, which is about 1 mm. Owing to the large latent heat of crystallization, the relaxation time of the crystal shape is very long (many hours or even days), except in the vicinity of the melting curve minimum ($T_{min} = 320$ mK), where the latent heat vanishes.

Rolley *et al.* (1989) have made such measurements between 150 and 330 mK. Figure 34 shows the equilibrium shape of one of their crystals at 320 mK. As shown in Fig. 35, the measured profile fits very well with a single value of the surface stiffness $\gamma$; this proves that the stiffness is close to isotropic, consequently equal to the the surface tension $\alpha$, as usually found for the bcc structures. Moreover, the measured value of $\alpha = 0.060 \pm 0.011$ erg/cm$^2$ (see Fig. 35) does not depend on temperature within the experimental accuracy. (Rolley *et al.*, 1994a) later estimated the anisotropy of $\gamma$ from the shape of quasi-spherical liquid inclusions inside crystals. Good fits were obtained with $\gamma(\phi) = \gamma_0[1 + \epsilon\cos(4\phi)]$, and $\epsilon = 0.02 \pm 0.01$, as found for other bcc structures.

An important observation is the absence of visible facets above 150 mK on these $^3$He crystal shapes. More recently, the surface stiffness of $^3$He crystals has been measured down to 80 mK by the Helsinki group (Todoshchenko *et al.*, 2004). They used a Fabry-Pérot multiple-beam interferometer (see Section II.B.2) and observed the whole crystal shape, not only the profile. The results of Todoshchenko *et al.* confirm those by Rolley *et al.* (1989).

FIG. 36 . $^3$He crystals growing at 80 mK (Rolley *et al.*, 1986). The facets are the (110) surfaces.

#### 2. Roughening transitions in $^3$He

In $^3$He, Rolley *et al.* first observed (110) facets below 80 mK (Rolley *et al.*, 1986), later up to 100 mK (Rolley *et al.*, 1989) (see Fig. 36). Two other types of facets [(100) and (211)] were seen by Wagner *et al.* (1996) in the millikelvin range, during growth of the crystals from the A-phase of superfluid $^3$He (see Fig. 37). More recently, the Helsinki group observed up to eleven different types of facets at 0.55 mK (Alles *et al.*, 2001; Tsepelin *et al.*, 2001) (see Fig. 38). Thanks to their interferometer, facets could be observed even when they occupied a small fraction of an otherwise rounded surface. With the same setup it was observed that at least three types of facets exist up to 55 mK (Todoshchenko *et al.*, 2003).

From all these publications, it appears that the max-

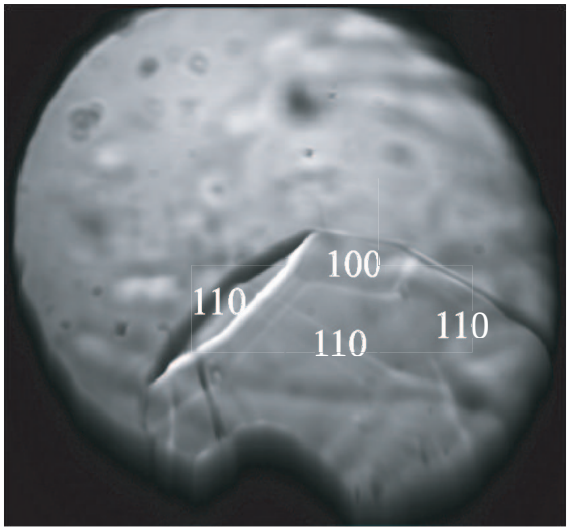


FIG. 37 . Growing $^3$He crystal at 2.2 mK (Wagner *et al.*, 1996). Three types of facets [(110), (100) and (211)] were identified from a comparison of this image with computer simulations. The (211) facets are barely visible in between some of the two neighboring (110) facets.

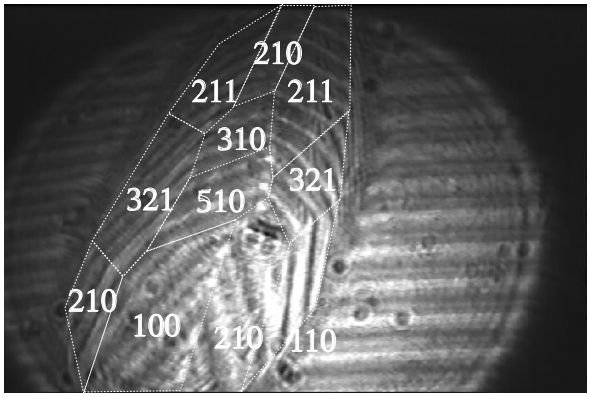


FIG. 38 . The interferogram of a growing $^3$He crystal at 0.55 mK revealing seven different types of facets which are labelled with Miller indices (Alles *et al.*, 2001).

imum temperatures at which facets can be seen in $^3$He are definitely lower that expected from the universal relation [Eq. (11)]. This was already noticed by Rolley *et al.* (1989) who deduced from their measured value of $\gamma$ that the roughening temperature of the (110) facets should be about 260 mK. Table I shows the maximum temperatures at which facets have been observed by the Helsinki group and a simple estimate of the corresponding roughening temperatures. For this estimation, the critical variation of $\gamma$ was neglected: Eq. (11) was used with $\gamma = 0.06$ erg/cm$^2$ and the respective values of step heights for each orientation.

In order to explain this discrepancy, Rolley *et al.* (1989) invoked dynamic roughening. Since a $^3$He atom is lighter than a $^4$He one, they noticed that the zero-point motion of atoms in the lattice was even larger in $^3$He than in $^4$He: $0.37a$ in $^3$He compared to $0.24a$ in $^4$He, according to (Pierre *et al.*, 1985). From this they concluded that the coupling of the liquid-solid interface to the crystal lattice should be even weaker in $^3$He than in $^4$He. This is because the lattice potential is expected to decrease exponentially with the interface width (Nozières, 1992). As a consequence, the step energies of facets should be very small. This means that it would be nearly impossible to see the facets on the equilibrium shapes of crystals, as noticed in all experiments; as for the growth shapes, they would reveal the existence of facets only if the growth speed was slow enough to avoid dynamic roughening. Within this model, they used Eq. (21) to estimate the step free energy for the (110) facets at 100 mK, and found $\beta_{110} \approx 1.2 \times 10^{-11}$ erg/cm. Under these conditions, the correlation length had to be $\xi_{110} \approx 3 \times 10^{-6}$ cm, i.e., by two orders of magnitude larger than the lattice constant of $^3$He crystals. Such an extremely weak coupling leads to very wide steps and it is possible. Its verification is in progress in the Helsinki group.

There appeared a serious difficulty when Tsepelin *et al.* (2002a) measured the step free energy at 0.55 mK, where the solid is ordered in its antiferromagnetic state and is in contact with the B-phase of superfluid $^3$He. They found $\beta_{110} = 6.6 \times 10^{-10}$ erg/cm, about fifty times more than the Rolley's estimate at 100 mK. If the coupling is really weak, it seems impossible to imagine that the step free energy increases that much from 100 to 0.55 mK. Moreover, Tsepelin's value is about one third of the product $\gamma d$ $= 1.8 \times 10^{-9}$ erg/cm$^2$, indicating strong coupling at low temperature. They also noticed that facets could be observed even during slow melting, not only during growth, and this confirms that the step energy is comparable to

TABLE I . For bcc $^3$He crystals, the calculated roughening transition temperatures ($T_{calc}$) are systematically larger than the maximum temperatures at which facets have been observed ($T_{obs}^{max}$); the different facets are represented by their respective Miller indices.

| Miller index | $T_{calc}$ (mK) | $T_{obs}^{max}$ (mK) |
|---|---|---|
| 110 | 260 | 100 |
| 100 | 130 | 55 |
| 211 | 86.6 | 55 |
| 310 | 52 | 0.55 |
| 111 | 43.3 | 0.55 |
| 321 | 37.1 | 0.55 |
| 411 | 28.8 | 0.55 |
| 210 | 26 | 0.55 |
| 510 | 20 | 0.55 |
| 431 | 20 | 0.55 |
| 311 | 11.8 | 0.55 |

the surface energy $\gamma d$. Another indication of strong coupling at low temperature comes from the comparison of the step energy values on successive facets: Tsepelin *et al.* (2002a) showed that the $1/l^2$ law seems to hold down to interstep distances $l$ of order $d$, and this is contradictory with a large step width (see Section V.A.3).

Altogether, these measurements lead to a series of unanswered questions in $^3$He: is the liquid-solid interface strongly or weakly coupled to the crystal lattice; is it possible that the strength of this coupling changes with temperature; what could be the effect of the superfluid transitions on the surface properties of a crystal; what about the magnetic ordering transition in the solid; could it be that the RG theory of roughening does not apply to $^3$He for some unknown reason? The whole issue is under investigation by the Helsinki group who has undertaken systematic measurements in the whole temperature range from 0.5 to 120 mK along the melting curve of $^3$He.

## IV. DYNAMICS OF ROUGH SURFACES

### A. Crystallization waves and the unusual growth dynamics of rough $^4$He surfaces

In 1978, Andreev and Parshin realized that at low temperatures, when all individual degrees of freedom are frozen, the melting and crystallization of helium from the superfluid are quantum collective processes, which can proceed without energy dissipation. Therefore the liquid-solid interface could oscillate as freely as the surface of a non-viscous classical liquid (Andreev and Parshin, 1978). As we shall see, the dispersion relation of crystallization waves is similar to that of ordinary surface waves because the potential energy is due to the same gravity and surface tension terms. One difference is that the mass flow, hence the kinetic energy, comes from the difference between the crystal density $\rho_C$ and the liquid density $\rho_L$: any growth or melting leading to a displacement of the interface requires a mass flow in the liquid which is proportional to the difference $\delta\rho = \rho_C - \rho_L$. Another difference is that a crystal being anisotropic, the crystallization waves are not isotropic either. Eventually, the attenuation of ordinary surface waves originates in the viscous dissipation in the bulk of the liquid while for crystallization waves it is mainly a surface mechanism.

In order to derive the dispersion relation, one proceeds as follows. Let us call $\zeta(x)$ the displacement of the crystal surface from its average horizontal position. Mass conservation implies a velocity $v_L$ in the liquid, which is related to the velocity $\dot{\zeta}$ of the surface by

$$v_L = \frac{\rho_L - \rho_C}{\rho_L}\dot{\zeta} \,. \tag{32}$$

If there is no dissipation, the difference in chemical potential $\delta\mu = \mu_L - \mu_C$ is zero at the interface. Since the chemical potentials $\mu_{C,L}$ are taken per unit mass, they obey

$$\frac{\partial\mu}{\partial P} = \frac{1}{\rho} \,. \tag{33}$$

Furthermore, the mechanical equilibrium of the interface implies that

$$P_C - P_L = (\alpha + \frac{\partial^2\alpha}{\partial x^2})\frac{\partial^2\zeta}{\partial x^2} = \gamma_x \frac{\partial^2\zeta}{\partial x^2} \,, \tag{34}$$

where $\alpha$ is the surface tension and $\gamma_x$ the surface stiffness in the $x$-direction. The two above equations can be combined as

$$\left(\frac{1}{\rho_L} - \frac{1}{\rho_C}\right)(\delta P_L - \rho_L g\zeta) + \frac{1}{\rho_C}\gamma_x \frac{\partial^2\zeta}{\partial x^2} = 0 \,. \tag{35}$$

Finally, at low enough frequency, these waves propagate with velocities which are small compared with the sound velocity, so that the fluid can be considered as incompressible, and the equations for a potential flow are

$$v_L = \nabla\psi \,, \tag{36}$$

$$\delta P_L = -\rho_L \dot{\psi} \,. \tag{37}$$

For a sinusoidal wave $\zeta(x,t) = \zeta_0 \exp(ikx - i\omega t)$, one finds a potential $\psi = \psi_0 \exp(ikx - i\omega t - kz)$, where $z$ is the vertical coordinate, and one obtains the dispersion relation

$$\omega^2 = \frac{\rho_L}{\delta\rho^2}\gamma_x q^3 + g\frac{\rho_L}{\delta\rho}q \,. \tag{38}$$

The first term describes the capillary waves which are anisotropic because $\gamma_x$ depends on orientation; it dominates at high frequencies (short wavelengths); the second term involves $g$, the acceleration of gravity. As usual, the crossover from the capillary to gravitational waves occurs for wavelengths larger than the capillary length

$$l_c = \sqrt{\frac{\gamma}{\delta\rho g}} \,. \tag{39}$$

Equation 38 was first verified by Keshishev *et al.* (1979) between 70 Hz and 5 kHz (see Fig. 39), later by Rolley *et al.* (1994b). From such graphs, very accurate measurements of the surface stiffness could be made in different crystalline directions (see, for example, Figs. 27 and 28).

Supposing now that growth and melting dissipate a small amount of energy, a finite velocity $v$ of the liquid-solid interface produces a small difference in chemical potential $\delta\mu$ between the solid and liquid; the dissipation can be described by the growth coefficient $k$ in the equation

$$v = k\delta\mu \,. \tag{40}$$

As a consequence, Eq. (35) has to be replaced by the more general form

$$\left(\frac{1}{\rho_L} - \frac{1}{\rho_C}\right)(\delta P_L - \rho_L g\zeta) + \frac{1}{\rho_C}\gamma_x \frac{\partial^2\zeta}{\partial x^2} = \frac{1}{k}\dot{\zeta} \,, \tag{41}$$

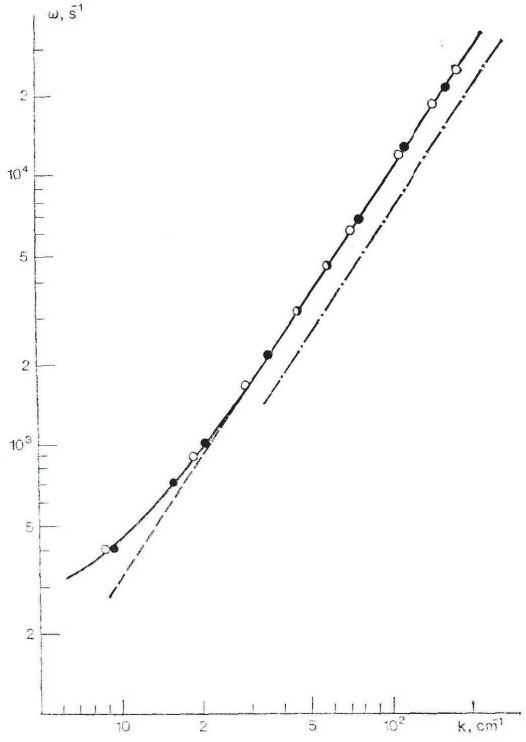


FIG. 39 . The measurements by Keshishev *et al.* (1979) of the dispersion of crystallization waves. At high enough frequencies, a "3/2" power law was found, in a very good agreement with Eq. (38). Below about 20 $cm^{-1}$, the slight deviation from the "3/2" power law indicates the crossover to the gravitational waves.

and the dispersion relation acquires an imaginary term:

$$\omega^2 = \frac{\rho_L}{\delta\rho^2}q^3 + g\frac{\rho_L}{\delta\rho}q - \frac{\rho_C\rho_L}{\delta\rho^2}\frac{i\omega q}{k} . \qquad (42)$$

Keshishev *et al.* (1979) obtained the first measurements of the dissipative coefficient $k$ from the damping of the waves (see, for example, Fig. 15). A more elaborate theoretical description of the dissipative coefficients is presented in Section IV.C.1, together with a comparison with several experiments. Corrections to the above equations have been calculated by (Uwaha and Baym, 1982) who considered the effect of compressibility at high frequency (see Section IV.C.9). Other corrections have to be introduced if the crystal is under stress (see Section VI.A).

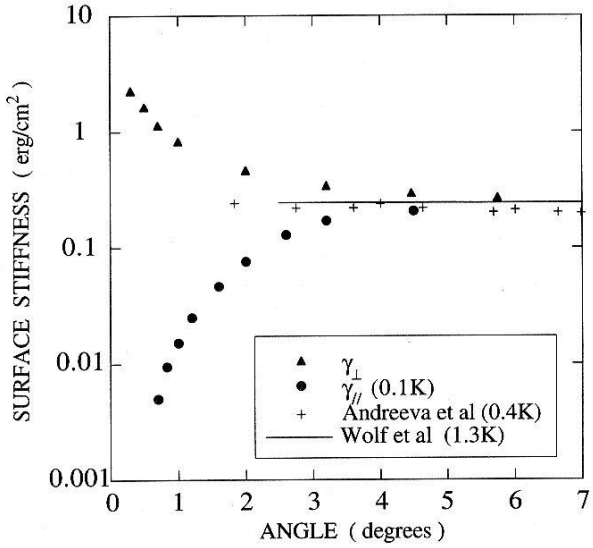


FIG. 40 . As measured by Rolley *et al.* (1994b,1995b), the stepped surfaces show a large anisotropy as their tilt angle $\phi$ with respect to a high symmetry plane tends to zero. One component of the surface stiffness sensor tends to zero while the other one diverges, as predicted by Eqs. (28) and (29).

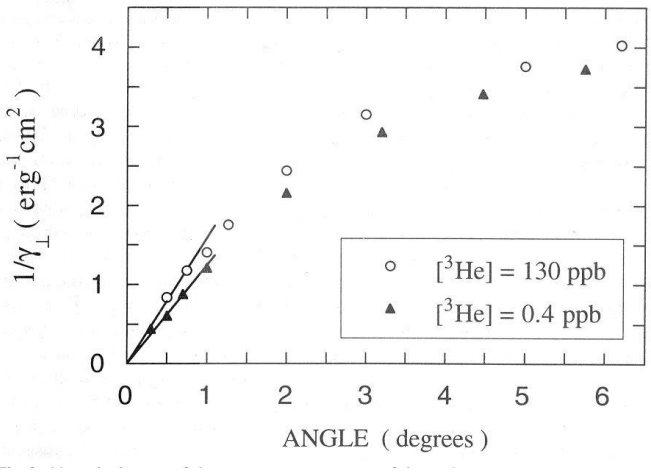


FIG. 41 . With this measurement, Rolley *et al.* (1995a) verified that the surface stiffness coefficient $\gamma_\perp$ is inversely proportional to the tilt angle $\phi$, as predicted by Eq. (29); from the initial slope, they measured the step free energy $\beta/d$ = 0.014 erg/$cm^2$ for ultrapure $^4$He (0.011 erg/$cm^2$ with 130 ppb of $^3$He impurities).

### B. Crystallization waves on $^4$He vicinal surfaces

Rolley *et al.* (1994b,1995a,b) studied crystallization waves on the vicinal surfaces, i.e., on surfaces with an orientation close to that of facetted ones. They were interested in investigating the properties of stepped surfaces, which are particular vicinal surfaces where steps are well separated and control the surface properties of crystals. They measured the energy of steps on the (0001) surfaces as well as their mutual interactions.

As described in Section II.C, they were able to rotate their crystals in two perpendicular directions and study

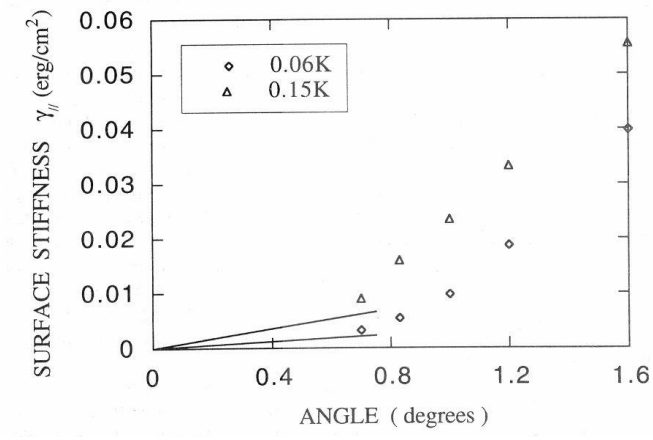


FIG. 42 . Rolley *et al.* (1994b,1995b) verified that the stiffness coefficient $\gamma_{//}$ vanishes as the tilt angle $\phi$ tends to zero. They could not measure it down to small enough angle to verify the linear asymptotic behavior predicted by Eq. (28), but their measurements are consistent with Eqs. (30) and (31) (solid lines).

the case were the wavevector $k$ was parallel to the projection of the c-axis on the surface, or the case where $k$ was perpendicular to it. They obtained the angular variation of the two corresponding components $\gamma_{//}$ and $\gamma_{\perp}$ of the surface stiffness tensor. Figure 40 shows that $\gamma_{//}$ decreases while $\gamma_{\perp}$ increases as the surface approaches the (0001) basal planes, i.e., as its tilt angle $\phi$ tends to zero.

Rolley *et al.* (1995b) compared this behavior with the predictions of Eqs. (28) and (29). As shown in Fig. 41, the component $\gamma_{\perp}$ was found to be inversely proportional to the tilt angle $\phi$ and the low temperature value

$$\beta_0/d = 14 \pm 0.5 \times 10^{-3}\ \mathrm{erg/cm^2} \qquad (43)$$

of the step energy was inferred from this measurement. This value was found close to the value ($17 \times 10^{-3}$ erg/cm$^2$) which had been predicted with the parameters of the RG theory. Although these parameters had been adjusted by comparing with measurements close to the roughening transition temperature, the extrapolation of the theory far from the roughening transition was considered as a good approximation because the value of the parameter $t_c$ indicated weak coupling even at low temperature. For a more accurate calculation of $\beta_0$, one would need to go beyond the first approximations of the Nozières' theory. One attempt has been made by (Hazareesing and Bouchaud, 2000) who used a more elaborate renormalization method ("functional renormalization").

Rolley *et al.* (1994b,1995b) also showed that the $\phi$-dependence of the component $\gamma_{//}$ approached the prediction of Eq. (29). They could make measurements down to $\phi = 0.7$ degree (see Fig. 42), but they found that this was not small enough to reach the linear behavior, characteristic to well separated steps. This is because the steps were confirmed to be very wide. As can be seen from Fig. 40, it is only below the crossover angle $\theta_c \approx 2.5$ degrees where the surface stiffness components depart from the roughly isotropic value of 0.245 erg/cm$^2$, which had been previously measured by Andreeva *et al.* (1987-92) and by Wolf, Gallet *et al.* (1985-87). This finding agreed with the RG theory, which predicted a crossover angle $\theta_c \approx d/6L_0 \approx 1/24$ rad [see Eq. (25)]. Andreeva *et al.* (1989) had questioned the existence of the stepped behavior but, after the work of Rolley *et al.* , it was shown to exist only at rather small $\phi$ and at low enough temperature for the wide steps to be well separated [remember that an estimate of the step width was given as $w \approx 4\xi \approx 2L_{max}$ in Eq. (10)].

Although the steps were not fully separated at $\phi = 0.7$ degree, Rolley *et al.* compared their measurements with the predictions for the interaction between two steps with a distance $l = d/\phi$ apart. In his mean field theory, Andreev had assumed a $\phi$-independent value of $\gamma_{//}$, implying a $1/l$ interaction between steps (Andreev, 1981; Andreev and Knizhnik, 1982); this was clearly ruled out. Rolley *et al.* compared their results with the prediction of entropic and elastic interactions which varied as $1/l^2$ (see Section III.C.5). From the temperature variation and the known value of $\beta_0$, they found good agreement with the entropic interaction, in particular with Akutsu's universal coefficient $(\pi^2/6)$ in Eq. (30) which had been a matter of debate for some time (Akutsu *et al.*, 1988). From an estimate of the temperature independent term in the interaction, they found agreement with the prediction of Marchenko and Parshin (1980a) for the elastic interaction, if the surface stress was roughly equal to the surface stiffness $\gamma_0 = 0.245$ erg/cm$^2$. It would be useful to measure this interaction at a smaller tilt angle for the steps to be better separated, and to extend the theory of the step-step interactions to the case where, steps being close to each other, their interaction depends on their structure, primarily on their width.

## C. Surface dissipation in $^4$He

### 1. Heat and mass flow: the Onsager matrix

When Keshishev *et al.* (1981) had measured the damping of crystallization waves, several authors started to calculate the dissipation at the liquid-solid interface (Andreev and Knizhnik, 1982; Bowley and Edwards, 1983; Castaing and Nozières, 1980; Huber and Maris, 1981). Keshishev *et al.* found that the inverse attenuation length of the waves varied as $\omega^{1/3}$, in agreement with Eq. (42). It corresponds to a damping rate proportional to the wavevector $q$, and confirms that the dissipation takes place at the crystal surface; a viscous dissipation in the bulk would lead to a damping proportional to $q^2$. Furthermore, they found that the growth resistance $k^{-1}$

could be decomposed as a sum of three terms:

$$k^{-1} = A_0 + B_0 T^4 + C_0 \exp - \left(\frac{\Delta}{T}\right) . \qquad (44)$$

The constant term $A_0$ was not reproducible from one crystal to another and was therefore attributed to defects or impurities; the two other terms were respectively attributed to the scattering of phonons and rotons by the moving liquid-solid interface.

Andreev and Parshin (1978) assumed that the dissipation was due to the total reflection of phonons and rotons and they first predicted that the growth resistance should be proportional to $T^4$ in the low temperature limit. Andreev and Knizhnik (1982) later distinguished "ballistic" and "hydrodynamic" regimes. The ballistic regime corresponds to a situation where the size of the system is smaller than the mean free path $l_{mf}$ of excitations. In this case the interface moves with respect to an excitation gas which is at rest in the frame of the experimental cell. For crystallization waves, this means $ql_{mf} > 1$, or $\omega\tau > 1$ if $\tau$ is the collision time of the excitations. In the opposite limit, the excitations move with the interface and the dissipation is due to the viscosity of the excitation system in the adjacent bulk phases; it does not take place at the interface. This is a remarkable situation: the transformation of the condensate into a crystalline phase is accompanied by no dissipation at all at the interface. In a classical system, the sticking atoms have to release their momentum, consequently some kinetic energy, so that the dissipation has to take place at the interface.

Castaing and Nozières (1980) formulated the whole problem in the frame of an Onsager matrix relating currents to the differences in chemical potential ($\delta\mu = \mu_L - \mu_C$) and in temperature ($\delta T = T_L - T_C$) between the two phases; more precisely, they linearized the relation between the two forces $\delta\mu/T$ and $\delta T/T^2$, and the mass current $J$ and heat current $J_E$ flowing through the interface. They were followed by numerous authors who used different notations. In order to avoid confusion with the lattice spacing $a$ and the sound velocity $c$, we here define the Onsager matrix coefficients $A$, $B$ and $C$ by the following relations:

$$\frac{\delta\mu}{T} = AJ + BJ_E , \qquad (45)$$

$$\frac{\delta T}{T^2} = BJ + CJ_E . \qquad (46)$$

The Onsager matrix being symmetric, its cross coefficient $B$ is the same in the two equations. Furthermore, the condition that the dissipation, i.e., the entropy production

$$\dot{S} = J\left(\frac{\delta\mu}{T}\right) + J_E\left(\frac{\delta T}{T^2}\right) \qquad (47)$$

is positive, requires $B^2 < AC$. In the absence of mass current ($J = 0$), one sees that the coefficient $C$ describes the thermal resistance of the interface, known as the "Kapitza resistance" $R_K = (\delta T/J_E)$. The two quantities are related by

$$R_K = CT^2 . \qquad (48)$$

As for the growth coefficient $k$ which was introduced above, this general formulation shows that two different cases have to be distinguished. The growth is called "adiabatic" if there is no heat current ($J_E = 0$). In this case, the "adiabatic growth coefficient" (also called "adiabatic interface mobility") is

$$k_E = \frac{1}{\rho_C AT} . \qquad (49)$$

If the growth is "isothermal" in the sense that $\delta T = 0$, then the "isothermal growth coefficient" is different and given by

$$k_T = \frac{k_E}{1 - B^2/AC} . \qquad (50)$$

The cross coefficient $B$ describes the way how the two entropies are shared between the two sides of the interface during growth. Its physical meaning was clarified by (Balibar *et al.*, 1991a), using the previous work of (Nozières and Uwaha, 1987). They represented the flow of heat and entropy at the interface as shown in Fig. 43. In this figure, $Q_C$ is the heat flow from the walls into the crystal and $Q_L$ is the heat flow from the liquid into the walls. One has:

$$Q_C = JTS_C - J_E , \qquad (51)$$

$$Q_L = JTS_L - J_E . \qquad (52)$$

$$(53)$$

Furthermore, the heat current $J_E$ which flows through the interface can be expressed as

$$J_E = \frac{\delta T}{R_K} - J\frac{B}{C} , \qquad (54)$$

so that

$$Q_C = J(TS_C - B/C) - \delta T/R_K , \qquad (55)$$

$$Q_L = J(TS_L + B/C) - \delta T/R_K . \qquad (56)$$

One now understands that $\delta T/R_K$ is the heat which is *conducted* through the interface, and that $(-B/CT)$ is the entropy per unit mass which is *carried* through the interface by the mass current $J$.

### 2. The growth resistance: phonon contribution

Bowley and Edwards (1983) first calculated the growth resistance $k_T^{-1}$ in the low temperature limit where they assumed phonons to dominate and to be ballistic. The dissipation is the work of the phonon radiation pressure on the moving interface: as it moves, the interface perturbs the distribution of phonons, and it is the relaxation

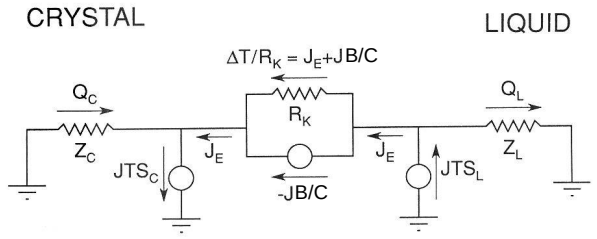


FIG. 43 . Diagram of entropy conservation at the liquid-solid interface during growth, as represented by Balibar *et al.* (1991a) following Nozières and Uwaha (1987).

of the perturbed distribution towards equlibrium, which produces entropy. In a first step, and following Castaing and Nozières (1980), they assumed that, due to the high mobility of the interface at low temperature, all phonons were totally reflected at the interface (see the next subsection). They also neglected mode conversion and found that

$$k^{-1} = \frac{\hbar\pi^2}{30\rho_C}\left(\frac{k_B T}{\hbar}\right)^4 \left[\frac{1}{c_L^4} + \frac{2}{c_t^4} + \frac{1}{c_l^4}\right] , \qquad (57)$$

where $c_L$ is the sound velocity in the liquid, $c_t$ and $c_l$ are the respective velocities of the transverse and longitudinal sounds in the crystal. At low temperature, the above equation predicts that the growth resistance is dominated by the phonons with the smallest velocity, i.e., by the transverse phonons in the crystal. The result by Bowley and Edwards is more general than the one obtained by Andreev and Knizhnik (1982) who only calculated the contribution from phonons in the liquid.

Equation 57 also explains the anisotropy of the growth resistance: it depends on the sound velocities in the crystal. Finally, Bowley and Edwards showed that the effect of phonon transmission was small, a reduction of the growth resistance by about 3% only; they also showed that the effect of mode conversion is even smaller.

How does the above theory compares with experiments? Equation (57) predicts that the growth resistance is proportional to $T^4$ with a coefficient between 3.06 and 3.32 cm·s$^{-1}$·K$^{-4}$. Keshishev *et al.* (1981) had found $2.6T^4$ for one crystal and $3.4T^4$ for another crystal. The agreement is obviously good, but a precise comparison would need to know the exact orientation of these crystals. Furthermore, Keshishev's data were taken in the temperature range from 0.36 to 0.59 K, where the phonons in the crystal are not expected to be ballistic (Golub and Svatko, 1980). This was later confirmed by Wang and Agnolet (1992a). Below 0.25 K, Wang and Agnolet observed the coefficients varying from crystal to crystal in the range from 2.7 to 3.5. They also found a systematic drop of this coefficient above 0.25 K, when the crystal phonons entered a hydrodynamic regime, so

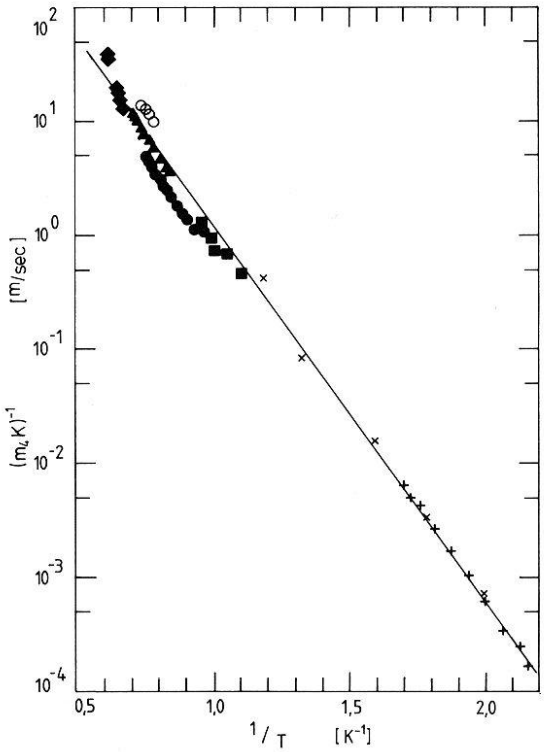


FIG. 44 . The roton contribution to the growth resistance $k^{-1}$ of solid $^4$He [noted $(m_4K)^{-1}$ by Bodensohn *et al.* (1986)]. The different symbols respectively correspond to the experiments by Keshishev *et al.* (1981) (+), Castaing *et al.* (1980) (x) and Bodensohn *et al.* (1986) (circles, squares and diamonds). The solid line is a best fit with a simple exponential function [Eq. (60)]. The phonon contribution has been subtracted in the case of Keshishev's measurements.

that, progressively, only the contribution from the liquid phonons was left. The crossover from a ballistic to a hydrodynamic regime of crystal phonons was also the explanation for the frequency dependence of the damping of crystallization waves, which was measured by Rolley *et al.* (1995b).

### 3. Rotons and kinks

At even higher temperature, none of the phonons are ballistic and their contribution to the growth resistance is negligible; the thermodynamics of liquid helium is dominated by rotons. Rotons are totally reflected at the interface because their velocities are very different from that of phonons in the crystal. There are two different types of reflections because there are two sorts of rotons, which were named $R^+$ and $R^-$ by (Wyborn and Wyatt, 1990). $R^+$ rotons have their momentum parallel to their group velocity while $R^-$ rotons have it antiparallel. A normal reflection corresponds to rotons staying in the same category and an "Andreev reflection" corresponds to the op-

posite case, when there is conversion from one type into another. Assuming ballistic rotons and a fraction $\xi_A$ of Andreev reflections, Bowley and Edwards (1983) found a roton contribution to the growth resistance:

$$k_{rot}^{-1} = (1-\xi_A)\frac{\hbar(q_0/\hbar)^4}{4\pi^2\rho_C}\exp(-\Delta/k_BT) \qquad (58)$$

$$\simeq 2.36\times10^5(1-\xi_A)\exp(-7.21/T)\ \text{cm/s}\,, \qquad (59)$$

where $q_0$ is the roton minimum wavevector; this result agreed with Keshishev's experimental results if $\xi_A \simeq 0.3$ to 0.4. However, they also pointed out an important difficulty which remained as a puzzle for several years (Castaing, 1984; Edwards *et al.*, 1990). As shown in Fig. 44, all experiments (Bodensohn *et al.*, 1986; Castaing *et al.*, 1980; Keshishev *et al.*, 1981) agreed with each other and showed a unique exponential increase of the growth resistance in the whole temperature range from 0.45 K to 1.7 K.

Bodensohn *et al.* (1986) gave a simple law for the growth resistance:

$$k^{-1} = 2.4\times10^5\exp{-(7.8/T)}\ \text{cm/s}\,, \qquad (60)$$

which was close to Eq. (59). But the roton-roton mean free path was certainly smaller than the wavelength of Keshishev's waves; it was also smaller than the size of the experimental cell used by Castaing *et al.* (1980), who measured the temperature dependence of the sound transmission (see below). As for Bodensohn *et al.* (1986), they measured the relaxation of a surface deformation by charging the liquid-solid interface and applying a variable electric field to it; once more, the size of their experimental cell was much larger than the roton mean free path. If rotons were in a hydrodynamic regime, i.e., moving with the interface, the growth resistance should have been much smaller.

Castaing (1984) first proposed that rotons were moving with the interface, but were scattered by the lattice potential which was immobile with respect to the cell walls. He also questioned the validity of the assumption by Andreev and Knizhnik (1982) of a fraction $\xi_A = 1$ of Andreev reflections of rotons. Later, Edwards *et al.* (1990) proposed that, at the scale of rotons, i.e., at an atomic scale, rough helium surfaces have a large density of microscopic steps with moving kinks (note that these microscopic steps should not be confused with the macroscopic steps which are considered in Section III). Even if the roton distribution moved with the interface, the kinks moved with respect to it. Edwards *et al.* developed a theory for the roton-kink collisions, in which the kink mass $m_k$ was an important parameter. This mass has been introduced by Kosevich and Kosevich (1981) as a consequence of the flow of superfluid towards the kink which acts as a moving sink. The existence of a kink mass implies the existence of a surface inertia $m_I$, which is proportional to $m_k$.

Furthermore, as explained by (Puech and Castaing, 1982), the surface inertia has a direct consequence on the transmission coefficient $\tau$ of phonons through the liquid-solid interface, consequently on its Kapitza resistance (see below). From a fit of both $\tau$ and the roton contribution to the growth resistance $k_{rot}^{-1}$, Edwards *et al.* (1990) obtained a kink mass

$$m_k^0 = 0.002 m_4 \qquad (61)$$

at $T = 0$, in agreement with the prediction $m_k \simeq m_4(v_L/v_C - 1)^2/2\pi$ by Kosevich and Kosevich (1981). They also found that this mass increased with temperature (see Fig. 45). This time, they found good agreement with the measurements of $k_{rot}^{-1}$ if the fraction $\xi_A$ was nearly zero. Their latest theoretical result was

$$k_{rot}^{-1} = (0.25+0.3T)(2.36\times10^5)\exp(-7.21/T) \qquad (62)$$

in cm/s again and in good agreement with all available experimental results (see Fig. 44). As explained in the next section, the value of the surface inertia was confirmed by the series of experiments done by Poitrenaud and her group.

Andreev and Knizhnik (1982) had assumed a fraction ( $\xi_A = 1$) by considering that rotons were reflected by a plane rigid boundary. In their model, Edwards *et al.* (1990) considered a rough surface with a large density of moving kinks, a rather different picture which implied $\xi_A \simeq 0$. Note finally that all these comparisons use the theoretical value of the isothermal growth coefficient $k_T$, but experiments only measure some approximation of $k_T$. For example, Balibar *et al.* (1991a) explained that, in the experiment by Bodensohn *et al.* (1986), there should be a small temperature difference across the interface, so that, in fact, an effective growth resistance

$$k_{eff}^{-1} = k_T^{-1} + \frac{\rho_C R_K}{T}(TS_C)^2 \qquad (63)$$

was measured, where $S_C$ is the crystal entropy per unit mass. Consequently, a small negative correction should be applied to their measurements of $k_T^{-1}$, from - 20% at 0.9 K to - 2% at 1.4 K.

### 4. Sound transmission and surface inertia

As we now understand, one cannot calculate the growth coefficient nor the Kapitza resistance without calculating the sound or phonon transmission. Castaing and Nozières (1980) had first noticed that the high mobility of the liquid-solid interface of $^4$He strongly affects the transmission of sound through it. They showed that the transmission probability $\tau$ from the liquid to solid is related to the interface mobility $k$ by

$$\tau^{-1} = \frac{Z_C+Z_L}{2Z_C} + \frac{kZ_L\rho_C}{2}\left(\frac{\rho_C-\rho_L}{\rho_C\rho_L}\right)^2\,, \qquad (64)$$

where the quantities $Z_C$ and $Z_L$ are the respective acoustic impedances in the crystal and in the liquid. The

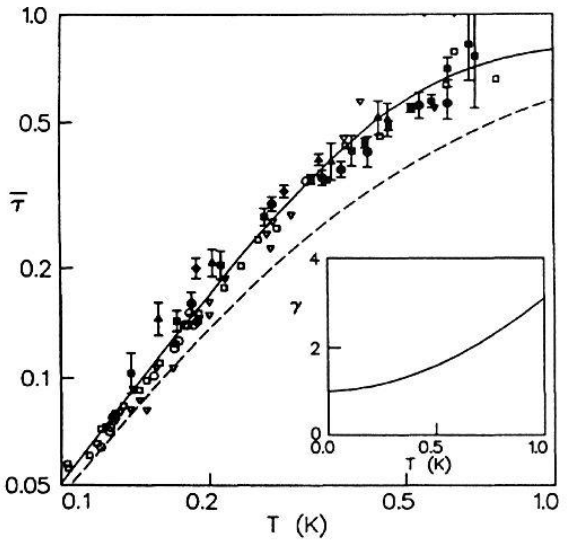


FIG. 45 . The transmission coefficient of thermal phonons through the liquid-solid interface of $^4$He. Various symbols refer to the measurements by (Wolf *et al.*, 1983b) (filled symbols) and (Puech and Castaing, 1982) (open symbols). The dashed curve was calculated by Edwards *et al.* (1990) using a temperature independent surface inertia $m_I^0 = 2.1\times\ 10^{-10}$ g/cm$^3$. A better fit was obtained with a temperature dependent inertia $m_I = \gamma m_I^0$, where $\gamma = m_k(T)/m_k^0$ is a kink mass ratio shown in the insert.

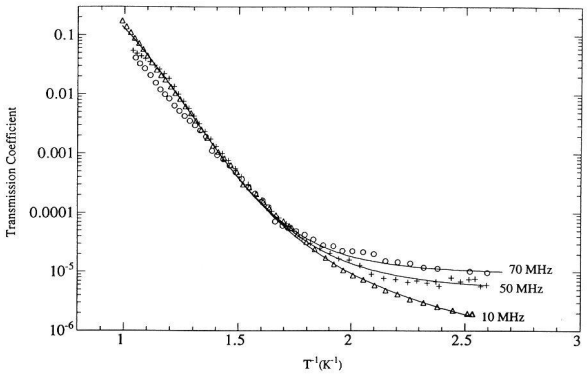


FIG. 46 . The transmission coefficient of acoustic waves in $^4$He as a function of the inverse temperature $1/T$ and at three different frequencies. These measurements by Amrit *et al.* (1995b) show that at low enough temperature, the mobility of rough crystal surfaces is limited by the surface inertia, so that the transmission is larger at higher frequency.

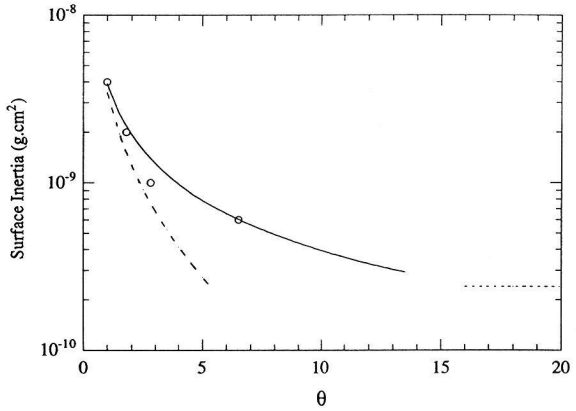


FIG. 47 . The surface inertia was deduced in $^4$He by Amrit *et al.* (1995b) from their sound transmission measurements. This graphs shows its angular dependence, which was found to be in a good agreement with the theory of Edwards *et al.* (1990) (solid line). The broken line represents the theory of Kosevich and Kosevich (1981) in the limit of well separated steps, i.e., with a small tilt angle. The horizontal dotted line indicates the surface inertia of rough surface at a large tilt angle.

physical interpretation of this effect is as follows. If the liquid-solid interface was immobile, the transmission probability would be equal to the usual impedance ratio $2Z_C/(Z_C + Z_L)$. On the contrary, if the interface was infinitely mobile, it would move in phase with any acoustic wave or incident phonon, so that there would be no difference in chemical potential across it, the pressure in the solid would always be equal to the equilibrium melting pressure, and no sound would be transmitted. In reality, we have seen above that the growth coefficient $k$ is limited by interactions with the thermal density of excitations (phonons and rotons), so that $\tau$ depends on temperature.

Furthermore, Marchenko and Parshin (1980b) showed that, if the incidence angle of the incoming phonon is non-zero, a capillary wave is produced at the interface, which couples to phonons in the solid. As a result, they found a probability $\tau$ to be proportional to the square of the phonon frequency, and consequently a Kapitza resistance proportional to $T^{-5}$ instead of $T^{-3}$, the usual behavior. Eventually, as we saw above, the interface has a non-zero inertia so that it cannot respond immediately to any perturbation. This was first predicted by Kosevich and Kosevich (1981), who proposed a hydrodynamic origin for this inertia. They found that the dispersion relation of crystallization waves departs from Eq. (38) when their wavelength is comparable to the average distance between steps. Puech and Castaing (1982) later explained that the local rearrangement of atoms passing from the liquid to the solid phase would induce the existence of a surface inertia even if $\rho_C$ was equal to $\rho_L$.

The surface inertia was measured by Poitrenaud and her group (Amrit *et al.*, 1995a,b; Poitrenaud *et al.*, 1989; Poitrenaud and Legros, 1989). They measured the transmission of sound as a function of frequency (in the range from 10 to 70 MHz), crystal orientation and temperature. Figure 46 shows that at low enough temperature the surface inertia limits the mobility of rough surfaces so that

the transmission of sound is larger at higher frequency. They wrote an acoustic impedance $\zeta_I$ for the interface as

$$\zeta_I = \left(\frac{\rho_C \rho_L}{\rho_C - \rho_L}\right)^2 \left[\frac{1}{\rho_C k} + i\frac{\omega m_I}{\rho_L \rho_C}\right] , \qquad (65)$$

where $m_I$ is the surface inertia, or dynamic mass per unit area. The real part of the impedance is due to the finite value of $k$, while the imaginary term originates in the inertia $m_I$. This inertia was related to the kink mass $m_k(T)$ by Edwards *et al.* (1990):

$$m_I = \frac{m_k n_k}{\sigma_C n_s \zeta} . \qquad (66)$$

In the above equation, the cross section $\sigma_C$ is related to the surface of a kink $\sigma$ by $\sigma_C = \sigma\rho_L/\rho_C$, $n_s$ is the density of steps on the crystal surface and $n_k$ is the density of kinks on the steps; as for $\zeta$, it is a dimensionless roughness factor which depends on the density difference between the plus and minus kinks on steps ($\zeta = \sigma_C < (n_+ - n_-)^2 >$). Amrit *et al.* (1995b) found a good agreement between their measurements and the theory of Edwards *et al.* (1990) as shown in Fig. 47. According to their latest estimates, the inertia of rough surfaces is

$$m_I = (2.4 \pm 0.5) \times 10^{-10}\ \mathrm{g/cm^2} , \qquad (67)$$

increasing by more than a factor of ten as the surface orientation tends to the facetted one.

### 5. Heat flow: the Kapitza resistance

The Kapitza resistance $R_K$ can be expressed as

$$R_K = \frac{3}{4}\rho_L S_{\phi L} c_L \bar{\tau} , \qquad (68)$$

where $\bar{\tau}$ is the average transmission probability for the phonons from the liquid into the crystal, and $S_{\phi L}$ is the phonon part of the liquid entropy (Maris and Huber, 1982). There have been three series of measurements on the Kapitza resistance. The first one was done by (Huber and Maris, 1981, 1982). They used a heat pulse technique at temperatures between 0.1 and 0.4 K. They found significant variations from crystal to crystal, which they attributed to unknown changes in crystal orientation. Their results could be represented as $5 \times 10^8\, T^5 < R_K^{-1} < 10^9\, T^5$ erg·s$^{-1}$K$^{-1}$cm$^{-2}$. This indicated a transmission probability for thermal phonons which was about $7T^2$, larger than predicted by the capillary theory of Marchenko and Parshin (1980b) (about $3T^2$).

Similarly, (Puech and Castaing, 1982; Puech *et al.*, 1982) found that Marchenko's capillary effect was not sufficient to explain their experimental measurements on the Kapitza resistance, so that the consideration of a surface inertia was necessary. For their final fit shown in Fig. 45, Edwards *et al.* (1990) considered both the results by Puech *et al.* (1982) and the later results by Wolf *et al.* (1983b). The experiment by Wolf *et al.* was primarily designed to measure the Onsager cross coefficient (see below). Its results for the transmission probability were summarized as $\tau = 5.4T^2$ for the rough surfaces. They found a somewhat larger value for a crystal surface close to the [0001] direction. As shown in Fig. 45, they were well interpreted in terms of the calculated surface inertia (Edwards *et al.*, 1990). In summary, the Kapitza resistance of the liquid-solid interface in $^4$He is anomalous in the sense that its limiting behavior at low temperature is proportional to $T^5$ instead of $T^3$ for immobile surfaces. The coefficient of the $T^5$ law is well understood as mainly due to the limitation of the mobility by the surface inertia.

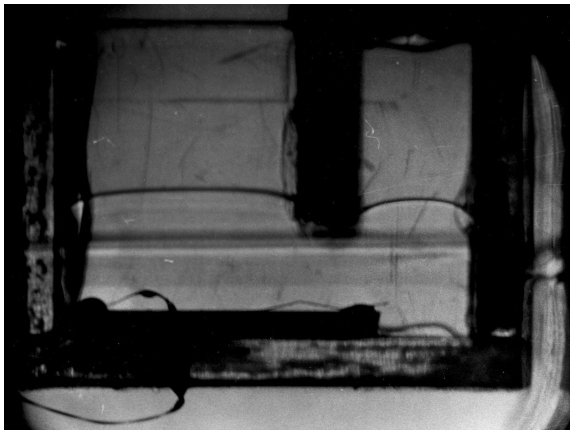

FIG. 48 . The setup used by Wolf *et al.* (1983b) to measure the Onsager cross coefficient $B$ and the Kapitza resistance $R_K$ at the surface of $^4$He crystals. A heat current is applied at the bottom of a transparent box. It flows through the left side which is open; on the contrary, the right side is closed by a superleak which ensures thermodynamic equilibrium but does not allow any heat flow. The double horizontal line across the whole box is the liquid-solid interface outside the box; in this case ($J_E = 0.503$ mW/cm$^2$ and $T = 0.27$ K) it was about 2 mm below the levels inside the box. From the level changes at the two sides of the box, both the pressure and the temperature of the crystal were measured, and $R_K$ and $B$ deduced.

### 6. The Onsager cross coefficient

Wolf *et al.* (1983b) designed an experiment to measure the Onsager cross coefficient $B$ by measuring the difference in chemical potential $\delta\mu$ which was induced across the liquid-solid interface of $^4$He by a heat current flowing through it. For this, they had to know the changes in pressure and temperature on both sides of the interface. This was obtained by looking at level changes of the interfaces in a transparent box with two sides (see Fig. 48). The heat current was generated at the bottom

of the solid. It flowed up through the left side into the liquid. The right side was closed by a porous plug which allowed a superfluid current to flow, consequently thermodynamic equilibrium to be reached, but no heat. The height changes were related to the changes in pressure from the hydrostatic equilibrium in the liquid. The level on the right was different from the left because of a heat current flowing only through the left side. Various corrections were considered such as a fountain pressure, and a limited thermal conductivity of the bulk phases.

From the difference in temperature, the Kapitza resistance $R_K$ was measured, as discussed above. From dimensional considerations, Bowley and Edwards (1983) expected the quantity $B\rho_C c_L T$ to be of the order of one. They predicted a slight dependence on the mobility of the interface, and it was important to know if phonons were ballistic in both the liquid and the solid, or only in the liquid. For ballistic phonons on both sides, they predicted $B\rho_C c_L T$ = -1.6 if the surface was immobile and -1.5 if it was infinitely mobile; if phonons were ballistic in the liquid only, they predicted a smaller coefficient, respectively equal to -0.7 and -0.6 in the two above situations.

Wolf's experimental result was -1.1 $\pm$ 0.4 in the temperature interval from 0.2 to 0.6 K, where the crystal phonons should have been in a hydrodynamic regime. This was considered as a qualitative agreement with the predictions. A more precise analysis would be useful but no other experimental measurement has been attempted.

### 7. Mobility of vicinal surfaces

When studying crystallization waves in $^4$He at vicinal surfaces, Rolley *et al.* (1995b) measured their damping and obtained the mobility of vicinal surfaces as a function of temperature and the tilt angle. Their results are shown in Fig. 49. This figure shows that the proximity of the c-facet has a strong influence on the growth rate. Furthermore, this influence extends on a much larger angular domain than for the surface stiffness, 15 degrees at least compared to about 2.5 degrees. For the intermediate orientations ($2 < \phi < 8$ degrees), the temperature dependence was also found to be closer to $T^6$ than $T^4$. Andreeva *et al.* had found qualitatively similar results in 1987-92. This was surprising because Nozières and Uwaha (1987) had predicted a $T^3$ variation for the stepped surfaces.

In their analysis, Rolley *et al.* (1995b) explained all these results by considering the crossover from the coherent to incoherent scattering of phonons by steps. This depends on a comparison between the step density $n_s$ and the phonon wavevector $q_{ph}$. Phonons are scattered incoherently, that is independently by the individual steps if their wavelength is smaller than the typical spacing between steps, equivalently if the ratio $n_s/q_{ph}$ is less than 1. A typical phonon wavevector is $q_{ph} = 2.7 k_B T/\hbar c$ with $c \simeq$ 400m/s, a typical sound velocity. Rolley *et al.* normalized the mobility $k$ of the vicinal surface by the typical mobility of a rough surface $k_{rough}$ and plotted this normalized mobility as a function of the quantity $n_s/q_{ph}$. Figure 50 shows that all their results collapsed on a universal curve, in strong support of their starting idea.

Nozières and Uwaha (1987) had calculated $k$ in the incoherent regime, and found a $T^3$ law. In this incoherent regime the growth resistance is larger than in the coherent regime, because there is an additional channel for a momentum exchange: in addition to the perpendicular momentum, the parallel component is not conserved dur-

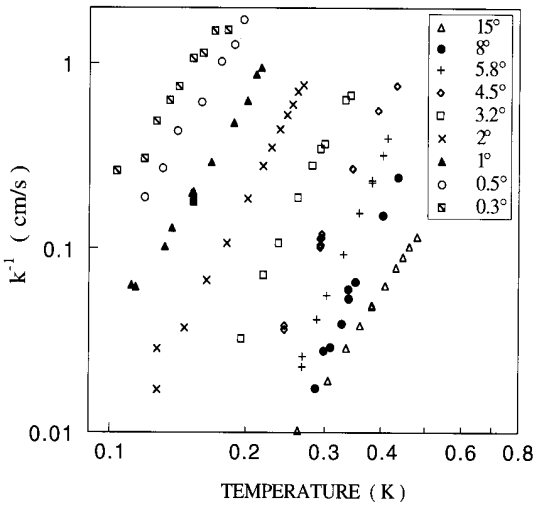


FIG. 49 . The growth resistance of vicinal surfaces of $^4$He crystals as a function of temperature and orientation, as measured by Rolley *et al.* (1995b); the angles measure a tilt with respect to the c-facet.

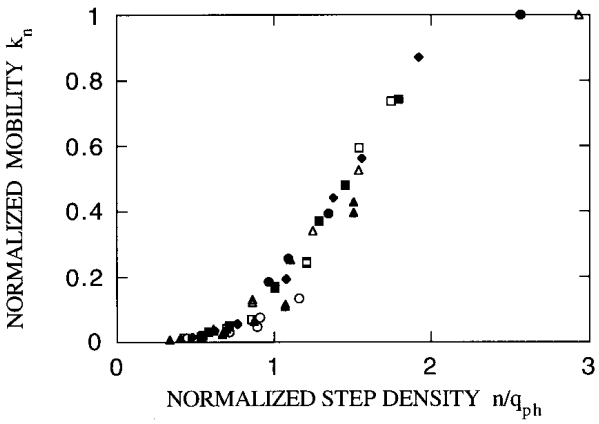


FIG. 50 . Once the growth resistance of vicinal surfaces of $^4$He crystals is normalized by the one of rough surfaces, and plotted against the product $n_s/q_{ph}$ of the step density by the phonon wavevector, all measurements collapse on a single curve (Rolley *et al.*, 1995b).

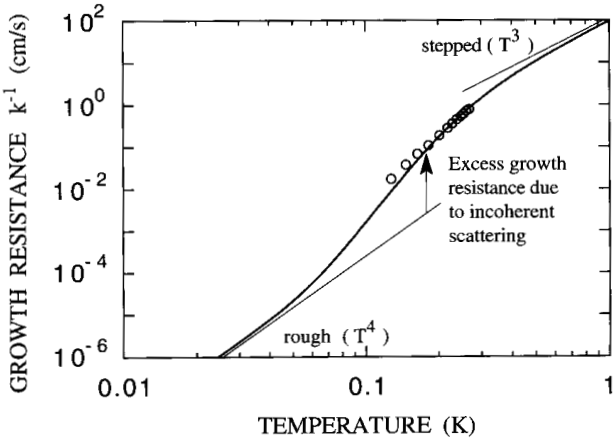


FIG. 51 . A sketch by Rolley *et al.* (1995b) of the temperature dependence of the growth resistance of $^4$He crystals, for a vicinal surface tilted by 2 degrees with respect to the c-facet. In the crossover, which corresponds to the phonon wavelength being comparable to the interstep distance, the growth resistance increases faster than $T^4$ (coherent scattering for rough surfaces or stepped surfaces at low temperature) and $T^3$ (incoherent scattering for stepped surfaces at higher temperature)

ing the collision. Nozières and Uwaha also calculated an expression for the crossover to the coherent regime which is $T^4$ as for rough surfaces, where the average distance between steps is always smaller than the typical phonon wavelength. Rolley *et al.* (1995b) simplified Nozieres' expression and found very good agreement with all their experimental results. At low temperature, the phonon wavelength is larger than the interstep distance, so that the scattering is coherent as for rough surfaces ($T^4$). As $T$ increases, incoherent scattering starts and the growth resistance increases even faster before reaching a $T^3$ behavior (see Fig. 51). The crossover angle depends on temperature of course, and it is larger than the crossover angle for the stiffness component $\gamma_{//}$ because it is related to a different criterion, namely $n_s/q_{ph} \approx 1$ instead of $l/3w \approx 1$.

### 8. Effect of $^3$He impurities

Despite several attempts to understand the effect of $^3$He impurities on the surface properties of $^4$He crystals, this subject looks far from being completely understood. This is probably because $^3$He impurities can affect both the static and dynamic properties, and in many different ways which depend on both the temperature and the concentration of impurities.

Early visual observations by Landau *et al.* (1980) showed that $^3$He impurities changed crystal shapes. The same Haifa group later claimed that the roughening temperature was lowered by 20% when about 1 ppm of $^3$He was added (Carmi *et al.*, 1985, 1989). They attributed this effect to a decrease of the surface tension value by 15% (at 1 K), which was caused by $^3$He adsorption but which was independent of the $^3$He concentration in the range from 0.8 to 150 ppm. They estimated the binding energy of $^3$He atoms to be about 10 K, but this looks rather large compared to 2.9 K, the theoretical estimate by (Treiner, 1993) of the binding energy on a solid substrate.

A more direct estimate of the binding energy was found by (Wang and Agnolet, 1992b), who measured the surface stiffness of $^4$He crystals around 1 K for $^3$He concentrations ranging from 4.5 to 50 ppb. They estimated the binding energy to be 3.4 K. Further evidence of the existence of bound states for $^3$He atoms at the liquid-solid interface of $^4$He was obtained by (Rolley *et al.*, 1995a), who compared the normal purity $^4$He containing 130 ppb of $^3$He with ultrapure $^4$He containing only 0.4 ppb. They found a change in the surface energy $\delta\alpha \approx -15 \times 10^{-3}$ erg/cm$^2$ at 0.2 K, and nearly no change above 0.4 K. They also found that the step energy was lowered from $\beta/d = 14 \pm 0.5$ erg/cm$^2$ in an ultrapure $^4$He to $11 \pm 1$ erg/cm$^2$ in a normal purity $^4$He. In this experiment, most $^3$He impurities were probably bound to vortices in the heat exchangers and the exact concentration in the bulk liquid was not precisely known. Despite these difficulties, they estimated the binding energy to be 4.3 K and the presence of a step to increase locally the binding energy by about 10 mK. They also estimated the maximum density of adsorbed impurities as 0.4 atomic layer. Clearly, a more systematic study of these adsorption phenomena is needed.

As for the influence of $^3$He impurities on the growth resistance of $^4$He crystals, the situation is not completely clear either. After the early estimate by (Castaing *et al.*, 1982), (Bowley and Edwards, 1983) calculated the contribution to $k^{-1}$ of the scattering of $^3$He atoms by the moving interface. This was done in the case where $^3$He atoms are ballistic, either forming a degenerate or a non-degenerate Fermi gas. The crystallization wave experiments by (Wang and Agnolet, 1992b, 1994) showed a large increase in the growth resistance, increasing exponentially in the region $0.2 < T < 0.3$ K for rather small concentrations (12 to 158 ppb). These results seemed much larger than the effect calculated by Bowley and Edwards. It was rather attributed to the diffusion of $^3$He in a $^4$He crystal. For this mechanism, (Kagan, 1986) had calculated a growth resistance

$$k_{diff}^{-1} = \frac{k_B T X_C}{m_4 \sqrt{\omega D_C}}\,, \tag{69}$$

where $X_C$ is the concentration of $^3$He impurities in a crystal and $D_C$ their diffusion coefficient, $\omega$ the frequency of the waves and $m_4$ the mass of a $^4$He atom. From the phase diagram of helium mixtures [see (Edwards and Balibar, 1989)], $X_C$ was known to be related to the con-

centration $X_L$ in the liquid by

$$\frac{X_C}{X_L} = 2\left(\frac{1.696}{T}\right)^{3/2} \exp\left(-1.36/T\right), \qquad (70)$$

and good agreement was found with the data.

Another series of measurements was performed by (Susuki *et al.*, 1997) at higher temperature (around 0.8 K) and with higher concentrations (5 and 10 ppm). Susuki *et al.* found that the growth resistance was larger by a factor of about 2 or 3 than in pure $^4$He, with no strong dependence on the concentration and the temperature variation, similarly to the resistance due to the roton scattering. Their results contradicted predictions by (Burmistrov and Dubovskii, 1993) who claimed that the additional dissipation was due to the flow of $^3$He in the liquid, in front of the moving interface, so that the growth velocity should strongly depend on $^3$He concentration and should be a non-linear function of $\delta\mu$. Instead, Susuki *et al.* proposed that the additional resistance was due to the flow of heat in the solid, so that an effective growth resistance was measured to be equal to

$$k_{eff}^{-1} = k_T^{-1} + \frac{\rho_C R_K}{T}(TS_L)^2 . \qquad (71)$$

This equation is similar to Eq. (63) but it contains the liquid entropy instead of the crystal entropy. Susuki *et al.* justified this by claiming that, in the presence of 10 ppm $^3$He impurities, the thermal conductivity of the superfluid $^4$He was so much reduced that the heat could flow more easily in the crystal. This is another interesting effect which would probably deserve some more systematic study.

Eventually, the effect of $^3$He impurities on the Kapitza resistance was also investigated. (Graf *et al.*, 1984, 1985) studied mixtures with concentrations $X_3 = 1.1 \times 10^{-4}, 1.9 \times 10^{-4}, 4.7 \times 10^{-4}$, and $15 \times 10^{-4}$. By carefully fitting the time evolution of the temperature of the crystal and of the liquid, after a heat pulse was applied in the crystal, they could measure three different quantities, namely the heat conduction $\sigma_{CL}$ from the crystal to the phonons in the liquid $^4$He, the conduction $\sigma_{C3}$ to the $^3$He impurities, and the coupling $\Gamma_{L3}$ between the $^3$He and the phonons in the liquid $^4$He. Their results confirmed their prediction of a direct coupling of crystal phonons with $^3$He impurities. They explained that, if the surface is rough, and consequently mobile, a phonon incident from the crystal side produces a large motion of the interface which acts a piston on the $^3$He atoms and directly transfers energy to them. Within this model, they estimated the additional thermal conductivity as

$$\sigma_{C3} = 9.4 \times 10^9 T^{7/2} X_3 \cdot \mathrm{erg} \cdot \mathrm{s}^{-1}\mathrm{cm}^{-2}\mathrm{K}^{-1} . \qquad (72)$$

With no adjustable parameter, this agreed with their experimental results. If, due to impurities, the liquid-solid interface had been smooth instead of rough, their theory predicted that $\sigma_{C3}$ had the same temperature variation but with a magnitude of 100 times smaller. They also verified that $\sigma_{CL}$ varied proportionally to $T^5$, as expected for rough surfaces.

The few examples above demonstrate the rich variety of phenomena which appear in the presence of impurities, and also the lack of a complete understanding of the whole field.

## 9. High frequency and high speed limitations

In deriving the crystallization waves spectrum (see Section IV.A), the compressibility of the liquid was neglected, as well as the elastic properties of the crystal. However, a second type of wave can propagate at the liquid-solid interface; this is an elastic Rayleigh wave with no mass transfer between the liquid and solid and in which the restoring force is provided by the elasticity of the solid. In the long-wave limit, when one can neglect the capillary effects, the spectrum of these waves is exactly as if the solid was in contact with vacuum (Marchenko and Parshin, 1980b). Indeed, as it was mentioned above, due to the very high mobility of the interface, the crystal oscillates at a constant chemical potential at the interface, hence at a constant pressure, exactly as if it was a crystal-vacuum interface. Capillary effects lead to a velocity dispersion but not to damping, since the sound velocity in liquid helium is larger than the velocity of transverse waves in solid helium. In contrast, the velocity of surface acoustic waves on the helium facets (without melting) essentially depends on the properties of the liquid even in the long-wave limit.

Uwaha and Baym (1982) calculated the spectrum and damping of surface waves at higher frequencies, when the two types of waves become coupled since their velocities are comparable. This happens when the wavevector $q$ exceeds $10^6$ cm$^{-1}$ (still much less than the atomic wave vectors). For even shorter wavelengths the spectrum of these mixed waves tends to the linear one with the velocity slightly below the velocity of Rayleigh waves without melting. The damping due to the growth resistance decreases with increasing $q$. An interesting feature of these oscillations is that in the limit of large $q$ the surface tension term dominates in the boundary conditions. As a result, the elastic displacement of the surface and the displacement due to crystallization almost compensate each other, and the total displacement of the surface becomes small compared to those in the liquid and solid.

In these calculations, as well as in calculations of the anomalous Kapitza resistance (Marchenko and Parshin, 1980b; Maris and Huber, 1982; Puech and Castaing, 1982) it was assumed that the processes of crystallization and melting remain practically dissipationless even at very high frequencies, up to $\omega \sim 10^{10}...10^{11}$rad/s. This arises an important question on possible high speed and frequency limitations of the very concept of nondissipative crystallization. According to Andreev and Parshin

(1978), such a limit is due to the finite probability of quantum tunnelling of an individual helium atom across the liquid-solid interface, $\Omega \sim 10^{11}...10^{12}$rad/s. As we have seen, experimental data on the Kapitza resistance in $^4$He agree well with the theory at temperatures up to 1 K at least and thus confirm that $\Omega$ is high compared to the characteristic frequency of thermal phonons at 1 K. Moreover, the analysis made by Edwards *et al.* (1990) showed that the best fit is obtained on the basis of the concept of very light quantum kinks: the width of their energy band is estimated to be 30 K! This value exceeds even the Debye temperature, which means that the concept of nondissipative crystallization has no specific frequency limitations in application to real helium.

As for the high growth speed limitations, the situation is different. Graf and Maris (1987) measured the transmission of high-amplitude sound waves across the rough superfluid-solid interface of $^4$He at temperatures from 0.1 to 1 K. They used these results to determine the growth coefficient $k$ as a function of the growth velocity $v$. They found that $k$ decreases rapidly as $v$ approaches the characteristic ("critical") velocity $v_c$, which was found varying from 1600 to 5100 cm/s for different samples. This value is surprisingly low, by about one order of magnitude lower than the sound velocity. In terms of the above discussed $\Omega$, this result would mean that $\Omega \approx v_c/a \approx 10^{11}$rad/s; the width of the kink's energy band would be much smaller than 60 K.

Edwards *et al.* (1990) suggested the following mechanism for the decrease of the growth coefficient at high growth velocities: the kinks are accelerated by the driving force, so that their energy and density at the crystal surface deviate from the equilibrium values. This tendency is counteracted by thermal fluctuations and heat exchange with the surroundings, which results in additional dissipation, hence in a decrease of the growth coefficient. The following simple argument shows that this mechanism may be really important in the experiments by Graf and Maris, who used 2.15 MHz acoustic waves with pressure amplitudes up to 0.4 bar. Let us estimate the change in the momentum of an individual kink $\delta q$ as a subject to a driving force $f = a^2(\rho_C - \rho_L)/\rho_L \delta P$: $\delta q \sim f/\omega = 3 \times 10^{-18}$g·cm/s. This is much higher than the atomic momentum $q \approx \pi\hbar/a = 10^{-19}$g·cm/s, which demonstrates that the crystal surface should be very far from equilibrium unless an effective relaxation mechanism intervenes.

Of course, for a complete understanding of all processes involved in the very fast growth of helium crystals, more experiments are needed, in particular a systematic studies at different surface orientations, including vicinal surfaces. Note also that the maximum growth velocity reached by Graf and Maris (1987), about 10 m/s, was exceeded in the experiments by (Balibar *et al.*, 2003): using high intensity ultrasound waves with a pressure amplitude up to 20 bar, they observed small crystals growing with 100 m/s, at a significant fraction of the sound velocity.

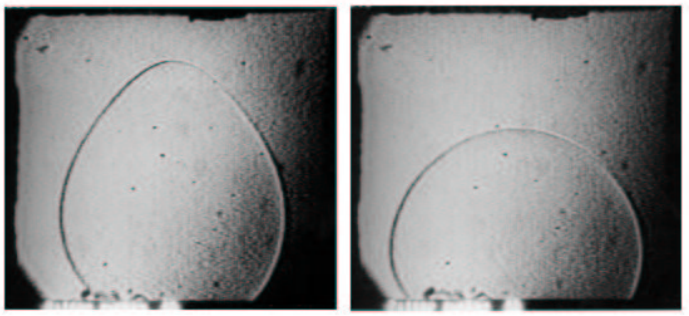

FIG. 52 . A $^3$He crystal relaxing towards its equilibrium shape (Graner *et al.*, 1989). The time delay between the two photographs is 10 s. The temperature is close to $T_{min} = 320$ mK.

### D. The case of $^3$He

#### 1. High temperatures

The growth dynamics of $^3$He crystals is very different from that of $^4$He. At high temperature, i.e., above the superfluid transition temperature $T_c = 2.5$ mK, liquid $^3$He is a viscous Fermi liquid with a low thermal conductivity. Furthermore, the latent heat of crystallization is large, so that the growth dynamics is limited by a large bulk resistance, as in classical systems. The surface resistance could only be measured near $T_{min} = 320$ mK, the minimum of the melting curve, where the latent heat vanishes. As we shall see, this surface resistance is much larger in $^3$He than in $^4$He, because the excitations in the liquid are Fermi quasiparticles with a large momentum instead of phonons or rotons.

A rough theoretical estimate of the intrinsic growth coefficient $k$ was first given by Andreev and Parshin (1978). Assuming that the dissipation comes from the collisions of Fermi quasiparticles in the liquid with the moving interface, they obtained $k \sim m_3/p_F$, the mass of a $^3$He atom divided by the Fermi momentum. They had assumed that the correlation time of the surface fluctuations is short compared to the average duration of an individual collision. However, both times should be comparable to the inverse exchange frequency in the liquid and this assumption is not well justified. In the opposite situation, the quasiparticles should interact with the crystal lattice rather than with the moving interface; with this assumption, Puech *et al.* (1986a) obtained

$$k = (3\tau_s/4)(m_3/p_F)[\rho_C \rho_L/(\rho_C - \rho_L)^2] , \qquad (73)$$

where $\tau_s$ is the sticking probability of quasiparticles on the crystal surface. Due to its large density factor, this equation predicts that the mobility is larger by about two orders of magnitude than first predicted by Andreev and Parshin (1978).

Accurate measurements were performed by Graner *et*

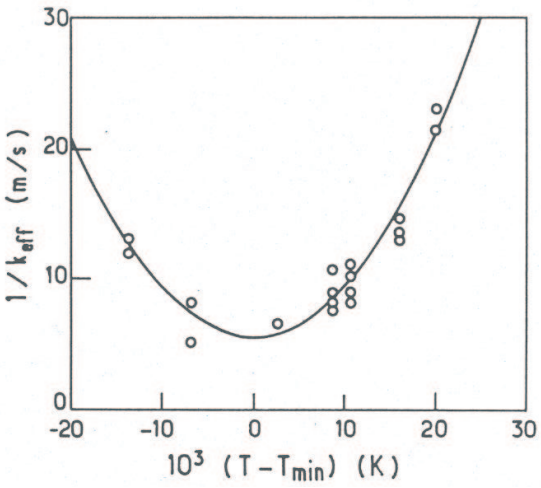


FIG. 53 . Inverse mobility of the liquid-solid interface of $^3$He near the melting curve minimum at 320 mK (Graner *et al.*, 1989). The solid line is a fit with Eq. (74).

*al.* (1989); they confirmed Puech's model and gave some information on the other kinetic coefficients. Graner *et al.* recorded the shape relaxation of crystals near $T_{min}$. The crystals evolved at a constant volume so that no heat had to flow in or out of the cell, even at temperatures slightly away from $T_{min}$, where the latent heat was not strictly zero. Heat had to be transferred from the melting top of the crystal to its growing sides (see Fig. 52). In their analysis, they followed Puech *et al.* (1986a) and assumed that most of this latent heat was liberated on the liquid side, which meant $-B/C \approx TS_C$. This was justified by Puech *et al.* (1986a) and Graner *et al.* (1990) by explaining that quasiparticles sticking to the solid exchange energy more easily with other quasiparticles in the liquid than with phonons in the solid which have rather long wavelengths. Furthermore, since $Z_C \ll R_K \ll Z_L$, they assumed that the latent heat $L = T(S_L - S_C)$ mainly flowed through the interface and through the crystal, so that the effective growth resistance was

$$k_{eff}^{-1} = k_T^{-1} + \frac{R_K \rho_C}{T} L^2 \,. \tag{74}$$

A fit with their experimental measurements (see Fig. 53) lead (Balibar *et al.*, 1991b; Graner *et al.*, 1989, 1990) to the values

$$k_T = 0.18 \pm 0.04 \,\mathrm{s/m} \,, \tag{75}$$

which agreed with Eq. (73) if the sticking coefficient $\tau_s$ was about 0.1 at 320 mK, and

$$R_K(T = 320 \,\mathrm{mK}) = 1.3 \pm 0.3 \,\mathrm{cm}^2 \cdot \mathrm{K/W} \,. \tag{76}$$

Puech *et al.* (1986a) presented qualitative arguments to predict that the sticking probability $\tau_s$ should be proportional to $T$ in the low temperature limit. This would be interesting to study. As for $R_K$, Graner *et al.* (1990) proposed that its relatively small value arises from the coupling between transverse phonons in the crystal and transverse zero sound in the Fermi liquid. Using a more direct method, (Amrit and Bossy, 1990) measured the Kapitza resistance in a much wider temperature domain ($50 < T < 200$ mK); they found that

$$R_K T^3 = 0.03 \,\mathrm{cm}^2 \cdot \mathrm{K}^4/\mathrm{W} \,, \tag{77}$$

in a good agreement with both the measurements (Graner *et al.*, 1989) and the theoretical estimate (Graner *et al.*, 1990). They also performed careful pressure measurements during melting of a crystal in a tube and obtained $k = 0.18 \pm 0.02$ s/cm, confirming Graner's results (Amrit and Bossy, 1993).

In their discussion of the whole picture, (Balibar *et al.*, 1991b) insisted on the difference between $^3$He and $^4$He. In $^3$He, because of the low thermal conductivity of the liquid, an isothermal experiment is very hard to achieve, except when the latent heat is zero or at millikelvin temperatures where liquid $^3$He is superfluid. Furthermore, the adiabatic coefficient $k_E$ is very different from $k_T$, from the isothermal one, because the quantity $(1 - B^2/AC)$ is very small ($\approx 3 \times 10^{-4}$ at 320 mK). On the contrary, in $^4$He, $B^2/AC \ll 1$ so that $k_T \approx k_E$. In practice, the typical relaxation time of $^3$He crystals near 320 mK is comparable to that of $^4$He crystals at 1.2 K, but at 0.1 K, it is about three days in $^3$He and 3 $\mu$s for rough surfaces in $^4$He. This difference is only due to thermal effects. One can estimate the effect of viscosity in liquid $^3$He as

$$1/k \sim \frac{\nu}{R} \left(\frac{\rho_C - \rho_L}{\rho_L}\right)^2 \,, \tag{78}$$

where $R$ is the crystal size and $\nu$ the kinematic viscosity of the liquid. It is small in the hydrodynamic regime, where the mean free path of the Fermi quasiparticles is small compared with the crystal size.

### 2. Low temperatures

Below $T_c$, liquid $^3$He becomes superfluid, but this transition does not result in an immediate change of the growth kinetics: due to the extremely high viscosity of the normal component, the superfluid convection does not help in the heat transfer, the heat conductivity of the solid is very low, but the latent heat is still very large until the temperature is less than the magnetic ordering temperature $T_N$. As shown in Fig. 54 the mobility of rough surfaces increases very fast below $T_N$. This figure shows data obtained by different authors at temperatures down to 0.55 mK (Akimoto *et al.*, 1998; Kawaguchi *et al.*, 2002; Nomura *et al.*, 1994; Tsepelin *et al.*, 2002b). It is likely that, even at the lowest temperature, the bulk dissipation still dominates the growth resistance (Jochemsen, 2002).

In all these experiments there is a net crystal growth so that some latent heat has to be evacuated through

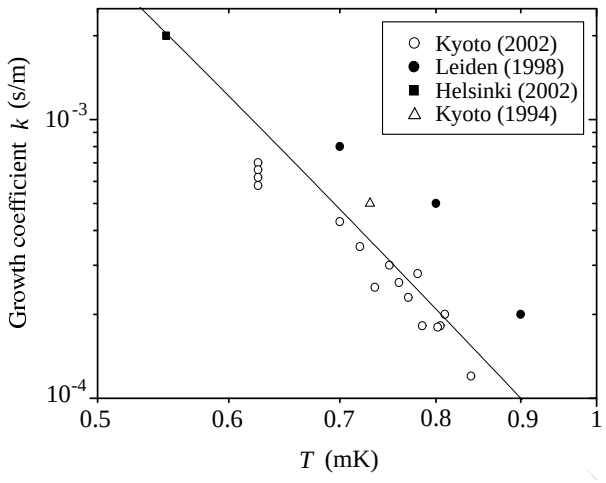


FIG. 54 . The measurements on the growth rates of $^3$He crystals below $T_N$, the antiferromagnetic transition temperature of bulk solid $^3$He. The solid line shows the $T^7$ dependence.

sintered silver heat exchangers ("sinter") to the thermal bath. Furthermore, the Kapitza resistance $R_K$ is small compared to the liquid thermal impedance (Feng *et al.*, 1993), and it can be neglected even if all the latent heat is liberated in the solid, as is expected from the arguments similar to the ones used above (in the very low temperature limit, one can neglect quasiparticles and magnons in the liquid, and the only remaining degrees of freedom are those of magnons in the solid). One can thus write

$$k_{eff}^{-1} = k^{-1} + \frac{\rho_C}{T} Z_L L^2 \,, \tag{79}$$

where $Z_L$ is the total impedance of the liquid including the impedance of the sinter. In the temperature range of Fig. 54, $Z_L$ is roughly temperature-independent (Osheroff and Richardson, 1985; Vollhardt and Wölfle, 1990; Wellard *et al.*, 1982). Taking into account that $L \sim T^4$, we obtain a temperature dependence for the second term in Eq. (79) which is close to $T^7$ (solid line in Fig. 54). Note that rather large scatter of the data obtained by different authors may be due to different magnitudes of $Z_L$ in their experimental cells. As for the first term in this equation, the intrinsic growth resistance, it is expected to behave as $T^4$ and to be by about thousand times smaller (see below).

As temperature is lowered below 0.4 mK, the mean free path of Fermi quasiparticles in the liquid becomes much larger than 1 cm, and the heat conductivity of the liquid starts to decrease exponentially, in proportion to the heat capacity of the liquid (Feng *et al.*, 1993; Vollhardt and Wölfle, 1990). The heat conduction across the liquid-solid boundary decreases also exponentially; in contrast, the (magnon) heat conductivity of the solid remains almost constant (Feng *et al.*, 1993; Osheroff *et al.*, 1991). As a result, the crystal becomes thermally isolated from the liquid during growth, its temperature is practically uniform and depends mainly on its thermal contact to the walls. Accordingly, the growth rate of such a crystal depends essentially on this thermal contact.

A different behavior is expected when the crystal changes shape at a constant volume. In this case the total enthalpy of the crystal remains constant, hence there is no need to evacuate any heat through the liquid or the sinter. The growth dynamics is now controlled by the thermal magnons in the crystal, and the situation looks very similar to the case of $^4$He in the phonon region; one only has to replace phonons by magnons [see (Andreev, 1982; Bowley and Edwards, 1983) for such a comparison]. Here too, one should distinguish the hydrodynamic regime from the ballistic one. In the hydrodynamic regime, when the magnon mean free path $l_m$ is much smaller than the characteristic size $R$ of the region, where growth or melting takes place, one can write

$$\frac{1}{k} = \rho_C T S_C^2 Z_C \tag{80}$$

with $Z_C \sim R/\kappa_C$ is the thermal impedance of the crystal. It has been found that $l_m \sim 1\ \mu$m at 0.4 mK and at lower temperatures $l_m$ increases as $T^{-2.5}$ or even faster (Osheroff *et al.*, 1991). It means that at sufficiently low temperatures one should expect thermal magnons to be ballistic and their interaction with the moving interface to be responsible for the growth resistance. In this case the resistance can be estimated [(Korshunov and Smirnov, 1982), see also (Andreev, 1996)] as

$$\frac{1}{k} \approx \frac{1}{\rho_C \hbar^3} \left(\frac{k_B T}{c_m}\right)^4 \,, \tag{81}$$

where the magnon velocity $c_m \approx 8$ cm/s (Osheroff *et al.*, 1991; Osheroff and Yu, 1980).

### 3. Crystallization waves in $^3$He

The possible observation of crystallization waves in $^3$He is a very interesting challenge. At temperatures low enough below $T_N$ thermal excitations disappear and one expects crystallization waves to propagate with a small damping, as in $^4$He. It is interesting to estimate the temperature range where it could happen. As for $^4$He, the quality factor of the waves is

$$Q = 2k \frac{\omega}{q} \frac{(\rho_C - \rho_L)^2}{\rho_C \rho_L} \,, \tag{82}$$

where $q$ is the wavevector. Taking $k$ from Eq. (81), and $\gamma = 0.06$ erg/cm$^2$ from Rolley *et al.* (1989), one sees that for wavelengths of the order of 1 mm or shorter, $q > 10^2$ cm$^{-1}$, $Q \gg 1$ at $T < 0.2$ mK.

As in the case of $^4$He, there is a very weak, temperature independent damping of crystallization waves in

$^3$He caused by their instability to the decay of one quantum into two quanta with lower energies (Andreev and Parshin, 1978; Saam, 1973). Another damping mechanism is specific for $^3$He, namely the Cerenkov radiation of magnons, whose velocity $c_m \approx 8$ cm/s is always smaller than the minimum phase velocity of crystallization waves (60 cm/s). This damping is much smaller than the one coming from the scattering of thermal magnons [(Eq. (81)], except if the temperature is lower than 10 $\mu$K (Korshunov and Smirnov, 1982).

In zero external magnetic field, the spin supercurrents which accompany the propagating crystallization wave (Korshunov and Smirnov, 1982; Marchenko, 1981b) are too small to produce any measurable effect on the dispersion relation. However, as has been shown by (Andreev, 1993), the situation changes in a non-zero field. In $^4$He, the kinetic energy of the wave is due to the mass flow, which is by itself a consequence of mass conservation. Here, the spin conservation during phase transformation and the large difference in the magnetic susceptibilities $\chi_C$ and $\chi_l$ imply that spin currents are generated by growth or melting. Thus, a magnetic contribution has to be added to the usual kinetic energy. The new magnetic terms being proportional to the square of the velocity of the interface, they constitute a magnetic kinetic energy. The dispersion relation can be written in the usual form

$$\omega^2 = \frac{\gamma q^2}{M(q)} \tag{83}$$

with the effective mass

$$M(q) = \rho_L d_m \left(\frac{H}{H_0}\right)^2 + \frac{(\rho_C - \rho_L)^2}{\rho_L q}\,, \tag{84}$$

where

$$d_m = \frac{\chi_L {c_{mL}}^2}{\chi_C c_{mC} \Omega_c + \chi_l c_{mL} \Omega_L} \tag{85}$$

and

$$H_0 = \frac{c_{mL}}{\chi_C}\sqrt{\rho_L \chi_L}\,. \tag{86}$$

In Equation (85) $\Omega_C$ is the antiferromagnetic resonance frequency in the solid and $\Omega_L$ is the frequency of the longitudinal NMR in $^3$He-B; both frequencies are of the order of $10^5$Hz; $H_0$ is of the order of the exchange field in the solid ($\sim$ 1 Tesla). The length $d_m$ is a few times smaller than the dipole length in the liquid, $l_D \sim 10^{-5}$ cm.

This result was obtained for magnetic fields less than 0.4 T, i.e., for a u2d2 phase of the crystal (and with superfluid $^3$He-B). Numerically, the magnetic contribution dominates the effective mass $M$ when $H \gg H_0(\rho_C - \rho_L)/\rho_L$. In this case the crystallization waves have a linear dispersion relation with a velocity

$$s = \frac{H_0}{H}\sqrt{\frac{\gamma}{\rho_L d_m}}\,. \tag{87}$$

It is important to note that the spin supercurrents do not contribute to the energy dissipation, nor do the mass currents. Therefore the damping should depend on the growth coefficient given by Eq. (81). Since the Q-factor increases proportionally to $\sqrt{M}$, working with non-zero field should allow to observe crystallization waves in $^3$He at temperatures slightly higher than in zero field. The whole issue is a quite remarkable and exciting challenge.

## V. DYNAMICS OF SMOOTH SURFACES

### A. Basic growth mechanisms

Contrary to rough surfaces, smooth surfaces grow layer by layer; it means that the growth is due to the transverse displacement of steps and it usually implies that the velocity $v$ is a non-linear function of the driving force $\delta\mu$. Either these steps are nucleated, or screw dislocations emerge on the facet so that steps are already present. These two different growth mechanisms are well known in the physics of classical crystals, and both have been observed in helium. As we shall see, a few other growth modes have been observed in helium, whose physical origins are not yet clear.

#### 1. 2D nucleation

In order to nucleate a new terrace on a dislocation-free facet, a step needs to be created. The free energy of a terrace with a radius $R$ is

$$F(R) = 2\pi R\beta - \pi R^2 d\rho_C \delta\mu\,. \tag{88}$$

The maximum free energy is reached for the critical radius

$$R_c = \frac{\beta}{d\rho_C \delta\mu}\,. \tag{89}$$

It is the nucleation barrier

$$E = \frac{\pi\beta^2}{d\rho_C \delta\mu} \tag{90}$$

for the nucleation of terraces. In their experimental study, Wolf *et al.* (1985) distinguished three different regimes. At high temperature and with a large driving force, terraces should nucleate everywhere at a high rate so that the surface is covered by terraces, this is the "dynamic roughening". At very low temperature, and with a moderate driving force, the nucleation probability should be small and the completion of each layer results from the growth of terraces nucleated one by one. In this case, the growth rate should be simply proportional to $\exp -(E/T)$ with $E$ given by the above equation. In practice, this mechanism is difficult to observe because, at low temperature, it is dominated by spiral growth from

Frank-Read pairs of dislocations. There is a small temperature domain in the vicinity of $T_R$, where terraces nucleate simultaneously at different places and have time to grow on the surface.

One thus has to consider the coalescence of terraces. There is a characteristic time in this process, which is $a/v$, the time for the completion of one layer if the growth velocity is $v$. The density of terraces is the product of this time $\tau$ by the nucleation rate $\Gamma$, so that the average distance between terraces is $1/(\Gamma\tau)^{1/2}$. Furthermore, within a time $\tau$ the terraces grow by an amount $v_{\rm step}\tau$. Coalescence occurs for

$$v_{\rm step}\tau = 1/(\Gamma\tau)^{1/2} \ , \tag{91}$$

and we find $\tau$ to be proportional to the cubic root of $\Gamma$. As a consequence, the Arrhenius factor in the growth velocity has to contain $\exp(-E/3T)$ instead of $\exp(-E/T)$. This explains the factor "3" in Eq. (24). This growth mode was apparently observed by Wolf *et al.* (1985) and Gallet *et al.* (1987) who used this model to extract the step free energy of the c-facets in $^4$He between 1.1 and 1.2 K.

In the limit of zero temperature, Eq. (24) predicts that the growth rate vanishes exponentially, but there is a non-zero probability of nucleation by quantum tunnelling in a system like $^4$He where dissipation can be neglected. The probability of quantum nucleation under the barrier $E(\delta\mu)$ has been calculated by (Andreev, 1982; Uwaha, 1983). In the quasi-classical approximation the tunnelling exponent depends on both the potential barrier and the kinetic energy of the system. The latter is due to the motion of the liquid which accompanies the formation of the nucleus. One finds

$$\Gamma_Q \sim \exp\left[-B\frac{\beta^{5/2}}{\hbar d{\rho_C}^{3/2}(\delta\mu)^2}\right] \ , \tag{92}$$

where $B$ is a number of the order of unity. In principle, this process could be observed at an overpressure $\delta p \sim 1$ bar in the case of the (0001) facets in $^4$He. Note that the quantum growth rate depends on $\delta\mu$ even more strongly than in the case of classical one.

### 2. Spiral growth

The spiral growth from Frank-Read sources was introduced by Burton *et al.* (1951) and has been reviewed by (Chernov, 1984). Figure 55 shows the main features of this phenomenon. It is important to realize that the growth rate of crystals does not depend on the number of sources; it is typically determined by the activity of a single source. As explained by Burton *et al.* (1951), this is a consequence of the no-crossing condition for steps (see Fig. 30). Furthermore, the average distance between moving steps is usually very large compared to their height; thus, the step velocity is much larger than the growth velocity of the facet itself. Since the step

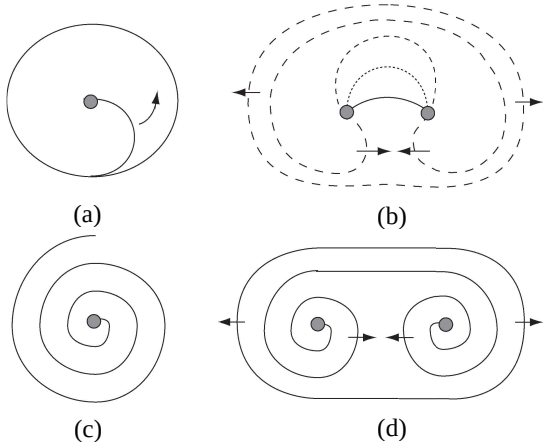


FIG. 55 . Spiral growth of a crystal induced by screw dislocations. Growth of a single dislocation under a small excess pressure (a) and of a Frank-Read source (b). At higher growth rates the dislocation winds around itself to produce a spiral as shown for a screw dislocation (c) and for a Frank-Read source (d). From Ruutu *et al.* (1998).

mobility is comparable to the mobility of rough surfaces, a facet grows much slowlier than a rough surface (under the same conditions). This in turn explains why the existence of facets is revealed by a slow growth (see Fig. 20). As a result, in the spiral growth regime, bulk dissipation is usually negligible and the growth is governed by the step dynamics only.

If one relates the step mobility $k_s$ to the step velocity $v_s$ by $v_s = k_s\delta\mu$, and if one assumes that $k_s$ is isotropic, then the asymptotic spacing between spiralling arms is

$$L \approx \frac{19}{K}\frac{\rho_L}{\rho_C - \rho_L}\frac{\beta}{d\delta p} \ , \tag{93}$$

where $K$ is the number of elementary steps produced by one dislocation [for the (0001) facet in $^4$He, $K = 2$](Burton *et al.*, 1951). The facet velocity $v$ is $v = v_s d/L$, or

$$v \approx \frac{K}{19}\frac{(\rho_C - \rho_L)^2 d^2}{\rho_L^2 \rho_C \beta}k_s(\delta p)^2 \ . \tag{94}$$

In helium, the step mobility has been the subject of a number of theoretical (Andreev and Parshin, 1978; Nozières and Gallet, 1987; Parshin, 1998; Ruutu *et al.*, 1998) and experimental studies (Rolley *et al.*, 1995b; Ruutu *et al.*, 1996, 1998; Tsepelin *et al.*, 1999).

When discussing the step motion in $^4$He, Andreev and Parshin (1978) first considered a $T = 0$ situation where all thermal processes are frozen out. They suggested that steps are rough, even in this limit, due to the existence of zero-point quantum kinks. A classical step should be smooth at $T = 0$ because the creation of kinks or pairs of kinks requires overcoming a finite energy barrier [see (Nozières, 1992)]. However, in $^4$He, kinks can easily tunnel from site to site and consequently form quasiparticles

which are delocalized and have a finite bandwidth $\Delta_k$. Andreev and Parshin (1978) estimated that $\Delta_k \approx \hbar\Omega \approx$ 1 to 10 K ($\Omega$ is the tunnelling frequency in the interface). They concluded that the bandwidth could be larger than the energy $\epsilon_{k0}$ of a localized kink, so that a finite density of quantum kinks could exist at $T = 0$. As explained in Section IV.C.3, this model was also used by (Edwards *et al.*, 1990, 1991) who found an even larger bandwidth, about 30 K. It is generally accepted now that quantum kinks can induce a quantum roughness of steps at $T = 0$. In their article, Andreev and Parshin further proposed that, similarly, there should be a finite density of zero point steps leading to quantum roughening of the surface at $T = 0$. However, we have seen in Section III.C.2 that this could not be true: at $T = 0$, the step energy is always positive, whatever its quantum fluctuations. Within their quantum solid-on-solid model, Iordanskii and Korshunov (1984) found that the step energy $\beta$ decays as $\exp(-c\sqrt{\Delta_k/\epsilon_{k0}})$ and is always positive; $c$ is a number of the order of unity.

If quantum roughening of steps occurs in all directions, then their mobility should be roughly isotropic. If the steps are smooth in some high symmetry directions, then a large anisotropy of the step mobility could be observed. No experiment has been attempted yet to verify such ideas. At $T \neq 0$, the step mobility has to be limited by the interactions with thermal excitations, as seen for rough surfaces. This was calculated by Nozières and Uwaha (1987) in the case of well separated steps. They considered the dissipation from the scattering of phonons. As already mentioned in Section IV.C.7, Nozières and Uwaha predicted a crossover from a $T^3$ behavior for incoherent scattering to a $T^4$ behavior for coherent scattering, i.e., in the case where the separation between steps is less than the phonon wavelength. This crossover was observed by Rolley *et al.* (1995b).

In the derivation of Eq. (91) all internal degrees of freedom of the step were ignored - the step was assumed to be "cold". At very low temperatures, it could be true only in the limit of a small driving force $\delta\mu$. At large $\delta\mu$ kinks on the step get accelerated and can reach the maximum possible velocity in the middle of the energy band before they release the excess kinetic energy. This is nothing but quantum localization by an external field, a phenomenon which manifests itself in the quantum diffusion of vacancies and impurities in solid helium (Andreev, 1982), in the electrical conductivity of superlattices (Esaki, 1992), and in other systems with narrow-band quasiparticles. In the regime of localization, the rate of energy dissipation $W_l = \rho_C d v_s \delta\mu$ does not depend on the driving force; it is determined by the emission of phonons at collisions of "hot" kinks with each other (Ruutu *et al.*, 1998). Thus $v_s \sim 1/\delta\mu$, and

$$k_s = \frac{W_l}{\rho_C d (\delta\mu)^2} \,. \qquad (95)$$

Ruutu *et al.* (1998) give the following rough estimate for $W_l$:

$$W_l \sim 10^{-3} \left(\frac{\rho_C - \rho_L}{\rho_L}\right)^4 \frac{\rho_L n_k^2 a^6 \Delta_k^8}{\hbar^3 (k_B \theta_D)^5} \,. \qquad (96)$$

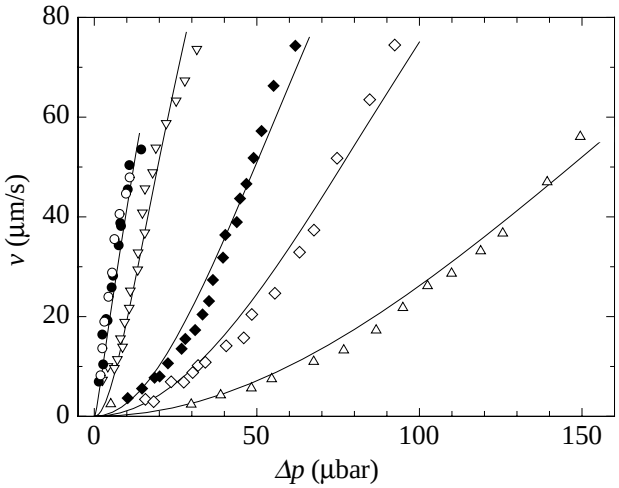


FIG. 56 . Velocity of the c-facet as a function of the driving pressure $\Delta p$: $T = 2$ mK (empty circles), 20 mK (filled circles), 50 mK (empty triangles, downwards), 100 mK (filled rotated squares), 150 mK (empty rotated squares), and 200 mK (empty triangles, upwards). Solid lines are just to guide the eyes. From Ruutu *et al.* (1998).

The spiral growth of $^4$He crystals has been studied by Ruutu *et al.* (1996, 1998). Figure 56 shows the results of Ruutu *et al.* (1998) for the c-facet between 2 and 200 mK. The velocity of the c-facets increases very fast when the temperature decreases. The quadratic dependence on the pressure difference $\delta p$ is expected in the regime of constant mobility [Eq. (94)]; however, it is observed only at high temperatures and low velocities. At low temperatures the dependence is almost linear and becomes even weaker at higher velocities. These results show that the classical picture of the step motion fails under these conditions where one should take into account non-linear effects in the step dynamics.

First of all, the experiments by Ruutu *et al.* have shown that, at low temperatures, the step velocities may be very high: for instance, using $v = 20$ $\mu$m/s, $\delta p = 4$ $\mu$bar, and Eq. (93), one obtains a step velocity $v_s \approx 200$ m/s, which is close to the sound velocity in helium. It means that at all temperatures, at least down to 2 mK, the density of kinks on the step is very high, of the order of the atomic density; otherwise the kink velocity would exceed the sound velocity, which is impossible. Moreover, one can estimate the lower limit for $\Delta_k$ by assuming, as usual, that $\epsilon_k = -\Delta_k \cos(pa/\hbar) + const.$ Then $v_k = \Delta_k a/2\hbar \sin(pa/\hbar)$, and $\Delta \geq 2\hbar v_k/a \approx 10$ K (with $v_k = 200$ m/s). With such a large value of $\Delta_k$, and considering that the density of kinks shows no tendency to decrease down to 2 mK, it seems that for all step orientations there is a high density of very mobile quantum kinks.

Furthermore, at such high velocities, the step inertia should be taken into account. As seen in Section IV.C.3, the step inertia originates from the hydrodynamic flow around it; the hydrodynamic mass of a step per unit length can be written as (Kosevich and Kosevich, 1981)

$$m_s = \frac{(\rho_C - \rho_L)^2 d^2}{\pi \rho_L} \log \frac{R}{\xi} , \qquad (97)$$

where $R$ is the characteristic large scale of the system; for the spiral growth $R \sim L$. The kinetic energy may exceed the step energy at rest $\beta$: for example, at $v_s = 200$ m/s, it should be five times larger. When accounting for the step inertia, the general form of the step motion equation writes in the Euler variables as

$$m_s \left( \frac{\partial v_s}{\partial t} + v_s \frac{\partial v_s}{\partial n} \right) = \rho_C d \left( \delta\mu - \frac{v_s}{k_s} \right) - \frac{\beta^*}{r_c(\vec{r})} , \qquad (98)$$

where $n$ is the normal of the step, $r_c(\vec{r})$ is the local radius of curvature, and $\beta^* = \beta + m_s v_s^2/2$ (Ruutu *et al.*, 1998).

In addition to the usual quadratic growth, Eq. (98) provides two new growth regimes: the "inertial" regime at very low temperatures with a linear dependence

$$v = K \frac{\rho_C d^2 \delta\mu}{2\pi\sqrt{2 m_s \beta}} , \qquad (99)$$

and the regime of localization at high driving forces, where the growth rate saturates:

$$v \approx K \frac{W_l d}{19\beta} . \qquad (100)$$

In Figure 56 the low temperature inertial regime is clearly seen. The step mass obtained from these data $m_s = (4 \ldots 5) \times 10^{-18}$ g/cm agrees quite well with the hydrodynamic mass given by Eq. (97). As for the regime of localization, there is a tendency to saturation only at the highest growth velocities, which allows to estimate $W_l$ roughly as $(1 \ldots 3) \times 10^{-3}$. With this value of $W_l$, one obtains from Eq. (96) that $\Delta_k \approx 10$ K (at $n_k a = 1$), in agreement with previous estimates.

The quadratic regime with constant mobility can also be seen in Fig. 56 at low velocities and higher temperatures. The corresponding step mobility was obtained by using Eq. (94); it is shown in Fig. 57 as a function of temperature (circles). As one can see, the temperature dependence of the measured mobility is very close to $T^{-3}$ between 20 and 200 mK, as predicted by Eq. (91). The absolute values of $k_s$ also agree well with this estimate. At lower temperatures, down to 2 mK, the mobility was too high to be measured. Note that in these experiments the spacing of the spiral arms was much larger than the wavelength of thermal phonons, and therefore the phonons were scattered incoherently from the steps. Figure 57 shows a comparison with the effective mobility obtained by Rolley *et al.* (1995b) for a vicinal surface tilted by 0.3 degrees (squares). The difference is probably due to the fact that, in Rolley's situation, the phonon scattering was intermediate between coherent and incoherent.

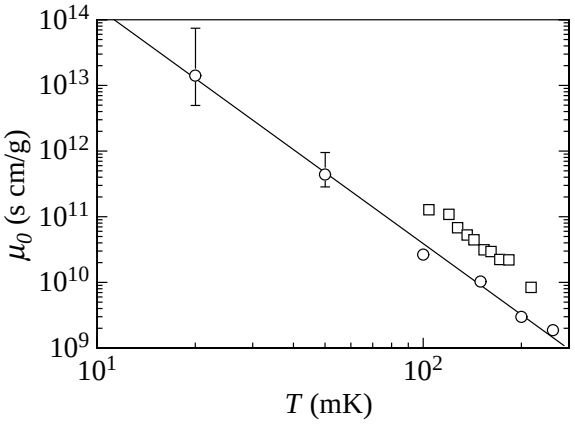


FIG. 57 . The step mobility as a function of temperature. The results by Ruutu *et al.* (1998) (circles) follow the $T^{-3}$ law predicted by Eq. (91). Rolley *et al.* (1995b) measured a slightly larger mobility (squares) probably because the phonon scattering was intermediate between coherent and incoherent in their experiment.

At low temperatures, where the effect of phonon scattering is weak, the step mobility becomes very sensitive to the presence of $^3$He impurities. There should be two contributions to the dissipation: one from impurities dissolved in the bulk liquid and another one from impurities absorbed on the interface (Parshin, 1998). Both contributions depend on the way how the step is "seen" by the $^3$He atoms, i.e., on the relation between the characteristic wavelength of impurities and the effective width of the step. In the interesting case of relatively short wavelengths, the impurities can be considered as probe particles for the step profile studies. The non-degenerate 3D gas gives a contribution

$$\frac{1}{k_s} = \frac{d\sqrt{2 m_3 T}}{\pi \xi_i} n_3 , \qquad (101)$$

where $m_3$ and $n_3$ are the effective mass and the concentration of $^3$He atoms in the liquid, respectively, and $\xi_i$ plays a role of some kind of correlation length for the step profile as seen by the impurity. This formula has been checked by Tsepelin *et al.* (1999). The results of Tsepelin *et al.* are shown in Fig. 58; they seem to agree reasonably well with the above prediction, but the value of $\xi_i = 8$ nm looks unexpectedly high.

One more non-linear effect in the step dynamics may originate in the Cerenkov emission of various excitations by a moving step (phonons and rotons in $^4$He, Fermi quasiparticles and magnons in $^3$He, etc.). This happens when the step velocity exceeds the phase velocity of excitations. If the intensity of this emission is sufficiently strong, the step mobility drops down to a very low value above some critical velocity $v_c$. This may limit the growth velocity more than the inertia if $v_c$ is relatively low (if $m_s v_c^2/2\beta < 1$) (Ruutu *et al.*, 1998). In this

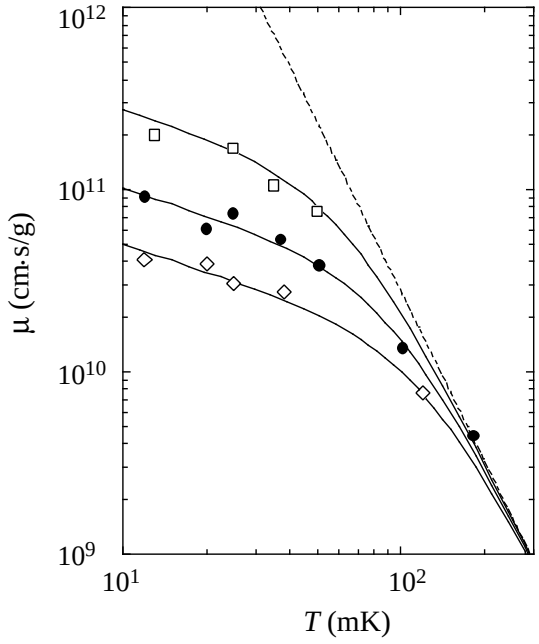


FIG. 58 . Step mobilities $\mu$ on the c-facets of $^4$He crystals calculated from the measurements with different $^3$He concentrations of 40 ppm (empty squares), 110 ppm (filled circles), and 220 ppm (empty rotated squares). The dashed line represents the data taken with regular $^4$He (0.1 ppm). The solid lines denote theoretical curves. From Tsepelin *et al.* (1999).

case, the solution of Eq. (98) yields

$$v = \frac{\rho_C v_c d^2}{2\pi(\beta + m_s v_c^2/2)}\delta\mu\,. \qquad (102)$$

As well as the radiation in the regime of localization, the Cerenkov radiation is due to the coupling of the step motion with other degrees of freedom in the bulk liquid or solid, or in the interface itself. According to Ruutu *et al.* (1998), this coupling is rather weak in the case of $^4$He rotons because the roton momentum is large. In contrast, the radiation of phonons is expected to be strong, but the corresponding critical velocity is too high, $m_s v_c^2/2\beta \approx 5$. Thus the observed linear dependence of the growth velocity is most probably due to the inertia.

In order to avoid misunderstanding, we note here that the Cerenkov emission is due to coherent motion of a continuous step with respect to the liquid or solid. This process is quite different from the emission of phonons (and other quasiparticles) in the regime of localization, when the step could be even at rest as a whole, but is very hot with respect to its internal degrees of freedom.

### 3. Facet growth in $^3$He

In $^3$He the critical velocities should be much lower than in $^4$He. This is first because the magnon velocity $v_m$ in the solid is low, and secondly because the pair-breaking velocity $v_{pb}$ is also low, approximately 7 cm/s (Feng *et al.*, 1993; Osheroff and Yu, 1980). The step-magnon coupling is expected to be rather strong because the moving step directly disturbs spins in the solid next to the interface. Therefore at $v_s > v_m$ the step mobility should be significantly lowered by the emission of magnons. As for the emission of quasiparticles in the liquid, this contribution is expected to be relatively weak due to the large value of the Fermi momentum, as in the case of rotons in $^4$He (Tsepelin *et al.*, 2002a).

The facet growth in $^3$He has been studied by several experimental groups (Akimoto *et al.*, 1998; Feng, 1991; Kawaguchi *et al.*, 2002; Nomura *et al.*, 1994; Tsepelin *et al.*, 2002a). In all measurements an almost linear dependence of $v(\delta\mu)$ was observed for overpressures of the order of a few mbar. This was interpreted as a spiral growth with a step velocity limited by the magnon velocity. In all but one case (Tsepelin *et al.*, 2002a) the crystal orientation was unknown; thus there is some uncertainty in the experimental data. Despite this uncertainty all data agree quite well with each other. Using Eq. (102), and neglecting the kinetic energy of steps, one can estimate the value of $\beta$ for facets growing in this regime. One finds a few times of $10^{-10}$ erg/cm.

The most complete data have been obtained by Tsepelin *et al.* (2002a). They were able to measure the growth velocities of ten different types of facets and to calculate the corresponding values of $\beta$ (see Fig. 59). Figure 59 shows that the dependence of $\beta$ on the step height $d$ is approximately $\beta \propto d^4$. This was expected for vicinal facets with an elastic interaction between steps. The somewhat surprising result is that the $d^4$ law extends down to a very small interstep distance. This indicates that the steps are narrow at low temperature in $^3$He, i.e., that the coupling to the crystal lattice is strong. Strong coupling is also indicated by the magnitude of the step energy which is comparable to the surface energy $\gamma d$, as already discussed in Section III.D.2. There is no clear interpretation to this surprising finding yet.

## B. Unusual growth modes of $^4$He facets

As explained above, a facet can grow only by 2D nucleation in the absence of screw dislocations, and this requires a typical overpressure of 1 bar. However, the Helsinki group has found a burst-like growth mode occurring on the c-facets of dislocation-free $^4$He crystals, when the overpressure was slowly increased up to some fraction of a mbar. Each fast growth event was signalled by about a 0.1 mbar drop of the overpressure (see Figure 60).

The nature of this burst-like growth mode is not clear yet. One possibility is that, while the overpressure increases, the facet touches the side wall (which is somewhat rough) at randomly distributed points. This could happen at $\delta p \sim \rho\gamma/l_r\delta\rho$, where $l_r$ is the scale of the

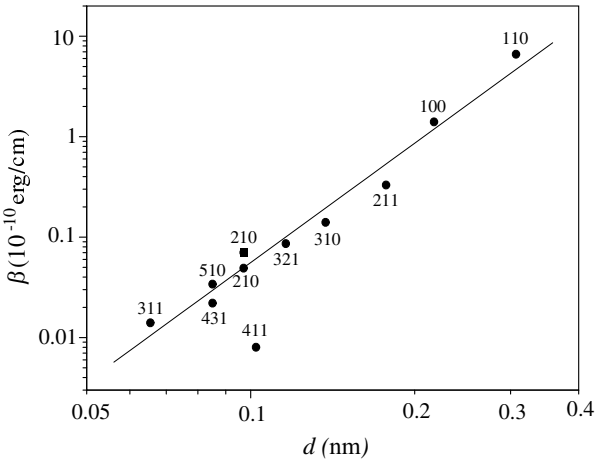


FIG. 59 . Step free energies of different facets at 0.55 mK, plotted versus corresponding step heights (Tsepelin *et al.*, 2002a).

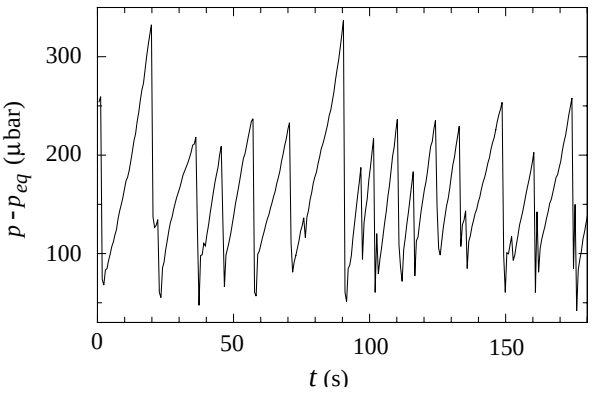


FIG. 60 . Burst-like growth of $^4$He crystals (Ruutu *et al.*, 1996).

wall roughness. Then new terraces can be spontaneously emitted from the contact region, where the threshold for such emission is estimated to be $\rho\beta/l_r\delta\rho$, a quantity much smaller than $\delta p$. The main problem is to explain why the observed values of $\delta p$ significantly increase with temperature or in the presence of $^3$He impurities. Both observations indicate that some dynamic process is involved, where the energy dissipation is important. Here, accounting for the surface oscillations caused by mechanical vibrations of the cryostat could help. On the other hand, this growth mode could be a manifestation of some intrinsic property of the facet, not directly related to the cell walls. Anyway, further experiments are needed to clarify this issue, perhaps with a cell with very smooth glass walls.

In the same series of experiments, a slow continuous movement of the c-facet was found in between the fast events. The facets grew with velocities of typically 0.5 nm/s, changing approximately linearly with the overpressure. Increasing the temperature or adding $^3$He impurities slowed down the growth velocity. An interesting explanation of this growth mode was proposed by Andreev and Melnikovsky (Andreev and Melnikovsky, 2001). They argued that the crystal could grow "from the bottom", due to a flux of vacancies. If so, the growth velocity of a facet should depend on the crystal height. They also predicted the existence of a maximum in the temperature dependence of the growth velocity if these vacancies are thermally activated, not if they are zero point vacancies. It would be interesting to test these predictions experimentally.

An anomalously fast growth mode was found for the facets of $^4$He crystals at high overpressures by (Tsymbalenko, 2000, 2003). The $^4$He crystals were nucleated on a needle by applying an electrical pulse, without direct contact to the cell wall. At low overpressures, the crystals grew relatively slowly, apparently by the usual spiral mechanism. Above some threshold pressure value which increased from about 1 mbar at 0.2 K to 14 mbar at 0.78 K, the crystals grew much faster, with velocities up to 3.5 m/s; this value is comparable to the maximum growth velocity found for rough surfaces by (Graf and Maris, 1987). The value of this pressure threshold, its dependence on temperature and the concentration of impurities are close to those observed in Helsinki for the burst-like growth. It means that these two observations might have the same physical explanation (Tsymbalenko, 2003). Note, however, that in Tsymbalenko's experiments the crystal is touching only the needle, so that only one facet touches the wall, in contrast with the experiments by Ruutu *et al.*

The two above examples show that the growth dynamics of helium crystals is not fully understood far from equilibrium, and some important growth mechanisms may be still missing from the theory. One possibility was suggested by Parshin and Tsymbalenko (Parshin and Tsymbalenko, 2003). Using the weak coupling approximation, they considered the non-linear dynamics of steps on a smooth superfluid-solid boundary, particularly the collisions of steps with opposite signs. In addition to the conventional annihilation of steps in such collisions, they found that under certain conditions transmission and reflection of steps could occur. The transmission of steps is similar to the transmission of sine-Gordon kinks and anti-kinks through each other; it becomes possible if the step velocities exceed some threshold value, which is estimated in the case of $^4$He to be about 100 m/s. This process results in a multiplication of preexisting steps and gives thus a qualitatively new mechanism for the facet growth in the absence of renewable sources such as screw dislocations.

## VI. INSTABILITIES AND OTHER PROPERTIES

### A. A mechanical instability

If a non-hydrostatic stress is applied to a crystal, the planar shape of its surface becomes unstable and peri-

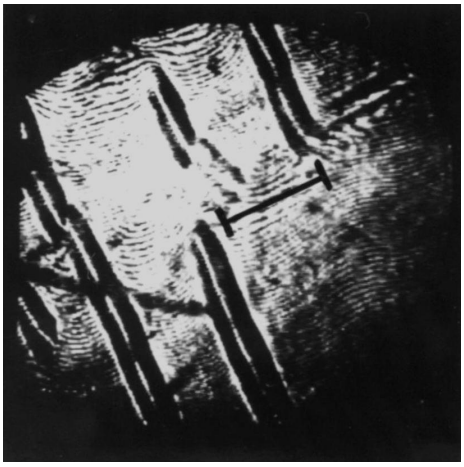

FIG. 61 . Bodensohn *et al.* (1986) observed a formation of parallel grooves at the surface of $^4$He crystals after a rapid quench in temperature at around 1 K. The distance between grooves was approximately $2\pi l_c \approx 6.3$ mm, the length of the scale bar on the image ($l_c$ is the capillary length). This was soon understood as a mechanical instability of the crystal surface, due to the appearance of stresses after the rapid quench in temperature (see text).

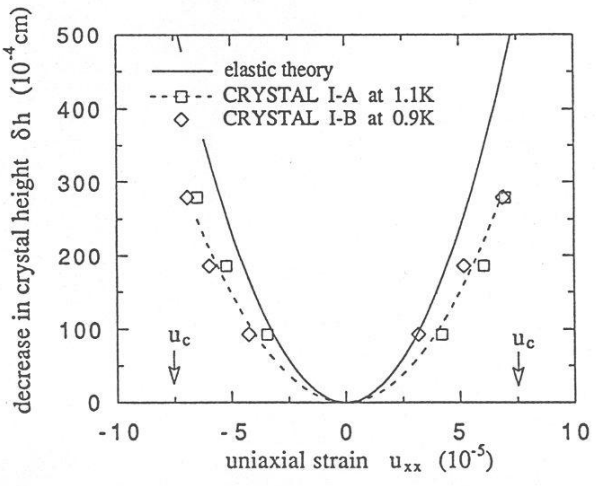


FIG. 62 . Torii and Balibar (1992) have measured the amount of melting which is produced when a uniaxial stress is applied to a $^4$He crystal in equilibrium with its superfluid phase; the experimental results (various symbols) are close to the prediction of Eq. (108) (solid line). An instability occurs at the threshold strain $u_c$ indicated by arrows.

odic grooves appear on the surface. This instability was first proposed by (Asaro and Tiller, 1972) as a possible precursor of fracture and corrosion, and later independently by (Grinfeld, 1986, 1993) who connected it to the spontaneous formation of quantum dots during the heteroepitaxy of semiconducting materials. Its mechanism was further investigated by (Nozières, 1992) and by (Balibar *et al.*, 1991b), who explained that the deformation of the crystal surface allows some release of the elastic energy at an expense of the surface energy which is favorable if the applied stress exceeds a certain threshold.

Consider a liquid-solid interface at $z = 0$ and suppose that a stress tensor $\sigma_{ij}$ is applied, which induces a deformation $u_{ij}$. The stress would be called hydrostatic if its tensor was diagonal, with $\sigma_{xx} = \sigma_{yy} = \sigma_{zz} = -P(z)$. Suppose that an extra stress $\sigma_0$ is applied in the $x$-direction and that the crystal has fixed boundaries in the $y$-direction; then the equilibrium conditions at the interface are:

$$\sigma_{zz} = -P_L \ , \ \sigma_{xy} = \sigma_{yx} = 0 \, , \tag{103}$$

$$\sigma_{xx} = \sigma_{zz} + \sigma_0 \ , \ u_{yy} = 0 \, , \tag{104}$$

$$\sigma_{xz} = \sigma_{yz} = 0 \, , \tag{105}$$

$$\frac{f_C - \sigma_{zz}}{\rho_C} = \mu_C^{eff} = \mu_L \, , \tag{106}$$

where the chemical potential of the crystal had to be generalized as $\mu_C^{eff}$ since the pressure in the crystal is not defined.

The extra uniaxial stress $\sigma_0$ shifts the equilibrium pressure in the liquid by an amount $\delta P_L$, which obeys

$$\delta\mu_C^{eff} = \frac{(1-\sigma_P^2)\sigma_0^2}{2\rho_C E} + \frac{\delta P_L}{\rho_C} = \delta\mu_L = \frac{\delta P_L}{\rho_L} \, , \tag{107}$$

and where $\sigma_P$ is the Poisson coefficient and $E$ the Young modulus of the crystal. Due to the gravity acceleration $g$, the crystal melts down by an amount

$$\delta h = \frac{(1-\sigma_P^2)\sigma_0^2}{2Eg(\rho_C - \rho_L)} \, . \tag{108}$$

A corrugation of the surface appears with a wavevector

$$q^* = \sqrt{\frac{(\rho_C - \rho_L)g}{\gamma}} \tag{109}$$

if the uniaxial stress $\sigma_0$ exceeds the threshold

$$\sigma^* = \sqrt{\frac{\gamma E q^*}{1-\sigma_P^2}} \, . \tag{110}$$

Well beyond this threshold, gravity becomes negligible and all Fourier components of the surface deformation are unstable up to a maximum wavevector

$$q_m = \frac{2\sigma_0^2}{E\gamma} \, . \tag{111}$$

In an early experiment, Bodensohn *et al.* (1986) noticed the formation of grooves at the surface of a crystal after rapid cooling above 1 K (see Fig. 61). Balibar *et al.* (1991a) proposed that the origin of the instability was the non-hydrostatic stress produced by cooling: above 1 K,

the melting pressure varies significantly with temperature so that cooling down a crystal in a box with fixed boundaries should produce horizontal stresses. This hypothesis was proved to be correct, and the mechanical origin of the instability clearly was evidenced by (Thiel *et al.*, 1992) who showed that grooves appeared either during cooling or warming, or after applying a horizontal stress with a piezoelectric bimorph. At nearly the same time, (Torii and Balibar, 1992) used piezoelectric cylinders to apply calibrated strains to $^4$He crystals. They first verified Eq. (108) (see Fig. 62). They also verified that an increasing number of grooves appears beyond the threshold $\sigma^*$ predicted by Eq. (109). However, no experiment has accurately tested yet Eq. (111), which predicts a wavelength $2\pi/q_m$ in the nanometer range for strains of a few percent (as found in semiconductor epitaxy).

Balibar *et al.* (1991a) also proposed that the crystallization waves are modified in the vicinity of this instability but this has not yet been checked either. Torii and Balibar (1992) and Thiel *et al.* (1992) observed that the groove direction depends on both the crystal orientation [the wavevector tends to be aligned perpendicular to the (0001) planes and perpendicular to the uniaxial stress]. These tendencies could be in conflict with some interesting experimental situations but this has not been investigated further.

### B. Hydrodynamic instabilities

Several interface instabilities have been considered, which originate from hydrodynamic phenomena. A first one is the Kelvin-Helmholtz instability, which is related to the generation of sea waves by wind: in the presence of a tangential flow in the superfluid above a crystal surface, crystallization waves are generated. Assuming that the interface is horizontal, the critical velocity for this instability is (Kagan, 1986; Parshin, 1985; Uwaha and Nozières, 1986):

$$v_c = \left( \frac{4\gamma(\rho_C - \rho_L)g}{\rho_L^2} \right)^{1/4} . \qquad (112)$$

Numerically, one finds $v_c = 4...5$ cm/s, depending on the surface orientation. Uwaha and Nozières (1986) considered the combined effect of a flow and electric charges; they showed that this critical velocity can be made arbitrarily small by letting the electrostatic force to approach the critical threshold in the absence of flow. (Maksimov and Tsymbalenko, 2002) recently reported on the observation of the Kelvin-Helmholtz instability of a crystal surface; in their experiement, a jet of liquid helium was produced by injecting electrons with a tungsten needle. However, there could be another explanation for their observation: the flow is inhomogeneous and may produce an inhomogeneous Bernoulli pressure, which could destabilize the surface. It would be interesting to reproduce their observations with a better control of all the relevant parameters.

A Kelvin-Helmholtz instability has been predicted for *facets* by (Andreev, 1994). He showed that in the presence of a superfluid flow parallel to the facet, the facet becomes unstable against the formation of pairs of steps aligned perpendicular to the superfluid velocity $v_{sf}$. As a result, the surface stiffness becomes finite in the direction of the superfluid flow, and the facet shape becomes cylindrical. The equilibrium density of steps was estimated as

$$n_s \sim \exp\left( -\frac{2\pi\beta}{\rho_L a v_{sf}^2} \right). \qquad (113)$$

For the c-facet on $^4$He crystals the exponent in Eq. (113) is of the order of unity if $v_{sf} \approx 4 \times 10^3$cm/s. this is large, so that the experimental observation of this type of Andreev's instability looks difficult.

Another type of hydrodynamical instability has been considered by (van Saarlos and Weeks, 1995) for rough surfaces. With usual fluids, it is well known that the standing capillary waves can be excited parametrically, by oscillating the fluid vertically; this is the "Faraday instability" (Faraday, 1831). Van Saarloos and Weeks suggested to excite standing crystallization waves at the horizontal liquid-solid interface by shaking the whole cell. At a given frequency, the instability threshold depends only on the growth coefficient $k$ and it is essentially the same for modes with different wave vectors $q$ (in the low-damping limit), thus providing an independent means to measure $k$. Moreover, the growth resistance and the surface stiffness being anisotropic, different patterns could be observed, not only the usual one which has triangular symmetry; van Saarlos proposed this experiment in order to obtain more information on both the surface properties of $^4$He crystals and the mechanisms of the pattern selection in the Faraday instability.

Recently (Nomura *et al.*, 2003) have studied the effect of an acoustic radiation pressure (Rayleigh, 1902) on the rough liquid-solid interface. When an acoustic wave was applied from the liquid side, it always induced melting of the crystal. When applied from the crystal side, melting was induced at high temperatures and crystallization was induced at temperatures below the inversion temperature, $T_i$, which varied in the interval from 0.6 to 0.8 K, depending on the surface orientation. The acoustic radiation pressure theory (Borgnis, 1953) explains reasonably well the experimental observations at low temperatures, but additional melting mechanisms are needed to explain the high temperature behavior, the origin of which is not known yet. Herefore again, this interesting phenomenon deserves further study.

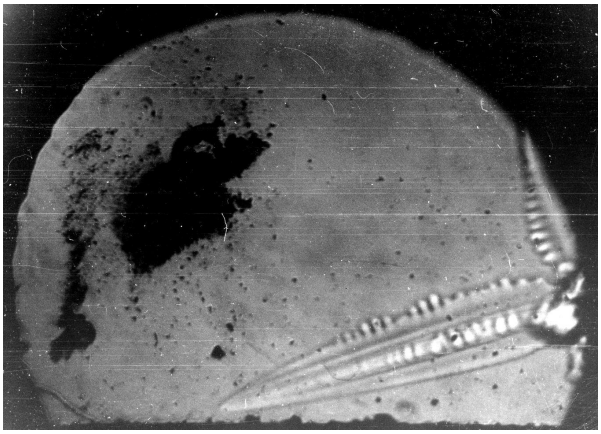

FIG. 63 . A $^3$He dendrite growing at 100 mK with a tip velocity of 30 $\mu$m/s. The cell width is 4 mm. Side branches appear at a distance of about 50 times the tip radius from this tip (Rolley *et al.*, 1994a).

### C. Dendrites

#### 1. Helium crystals in zero magnetic field

In a number of situations, the growth of helium crystals is governed by the diffusion of heat or mass in the two adjacent bulk phases. Under sufficiently strong departure from equilibrium, dendritic instabilities have been observed and analyzed. Franck and Jung (1986) and Rolley *et al.* (1994a) found some interesting differences between helium dendrites and more classical ones.

(Franck and Jung, 1986) studied the dendritic growth of pure $^4$He crystals at high pressure (210 to 4200 bar) and at high temperature (5.4 to 46 K). Under such conditions, liquid $^4$He is normal and solid $^4$He is a hcp crystal below 1120 bar (where the melting temperature is 15 K) and a fcc one above. Franck and Jung found that the growth velocity of crystals was larger than predicted and also that the side branches appeared much further away from the dendrite tip than in usual crystals. They tried to make some quantitative comparison with existing theories but had to estimate many unknown quantities.

Rolley *et al.* (1994a) studied the dendritic growth of $^3$He crystals between 80 and 120 mK. Thanks to many other experiments of the same group, most of the relevant physical quantities were known, including the anisotropy of the surface stiffness. They also found that the side branching instability was weak, so that these branches were often absent on dendrites with almost perfect parabolic shapes. On the fast growing shapes of crystals they found the side branches appearing a distance $\approx 50\rho_t$ away from the tip; $\rho_t$ being the tip curvature radius (see Fig. 63). This is ten times more than with usual crystals. They attributed this difference to the fact that the heat conductivity in the solid is much larger than in the liquid, an anomalous situation, but they asked also for further checks of their interpretation.

Rolley *et al.* (1986) noticed another interesting difference with usual crystals: the latent heat was released in the liquid under their experimental conditions and it had to go through the interface, whose thermal resistance $R_K$ was large, before being conducted through the solid whose thermal impedance was small. This allowed them to understand their measurement of the stability criterion of $^3$He dendrites, i.e., the selection of the dendrite tip velocity. In the calculation of this criterion, Rolley *et al.* (1994a) showed that the usual ratio of the heat conductivities on both sides of the liquid-solid interface had to be replaced by an expression involving the surface resistance $R_K$. Once this was done, they found agreement with their measurement on the product $v_t\rho_t^2$ ($v_t$ being the tip velocity).

#### 2. Melting process of highly magnetized solid $^3$He

The growth or melting of a solid is accompanied by mass and heat flows, which are due to the density and entropy differences between the two phases in contact. If the two phases have different magnetizations at equilibrium, there appears a magnetization flow. In the case of $^3$He, where the solid has a much larger susceptibility than the liquid, one can probe the magnetization flows on both sides of the interface as well as the magnetization transfer through the interface.

The melting of magnetized solid $^3$He has been considered by (Castaing and Nozières, 1979). They proposed that when the solid is melted on a time scale shorter than the spin-lattice relaxation time (about 1000 s at a few tens of mK), then a magnetization boundary layer builds up on the solid side of the interface. This boundary layer is simply due to the increased magnetization of the newly produced liquid, and that in turn enhances the magnetization in the solid near the interface. Later (Bonfait *et al.*, 1984) have suggested that, in analogy to the Mullins-Sekerka instability (Mullins and Sekerka, 1964), the buildup of this boundary layer would make the liquid-solid interface unstable and this suggestion was backed up by a calculation of (Puech *et al.*, 1986b).

The situation, as analyzed by Puech *et al.*, is sketched in Fig. 64(a) and that kind of picture has been used in several theoretical considerations (Kassner, 1996; Langer, 1980). The analysis of Puech *et al.* showed that when a planar interface propagates with a constant speed in the absence of magnetization gradients in the liquid, the interface would be unstable with a typical growth time for the most unstable modes of the order of 0.1 s.

Experimentally, the melting of highly polarized solid $^3$He has been studied by several groups (Bonfait *et al.*, 1984; Vermeulen *et al.*, 1987). The most recent experiments have been performed by the Leiden group who found with their new type of optical cryostat (see Fig. 7) that if the solid $^3$He was melted sufficiently rapidly in an 8.9 T field and at 9 mK, the instability of the interface occurred in several tens of seconds after melting was

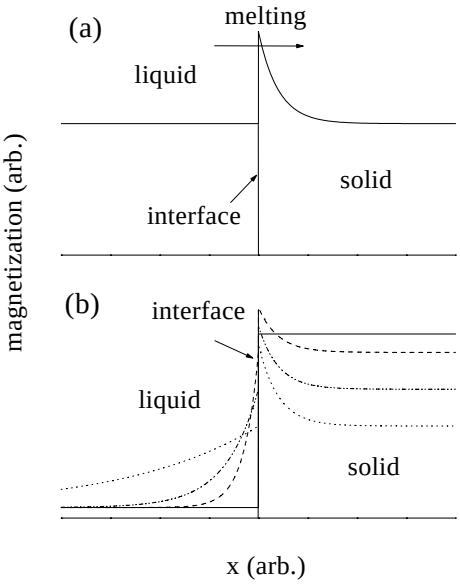


FIG. 64 . (a) Sketch of the magnetization profile of a planar interface melting with a constant speed, analyzed by Puech *et al.* (1986b). On the solid side, the magnetization profile falls off exponentially and there is no gradient on the liquid side. (b) Sketch of the buildup of the magnetization profiles as concluded by Akimoto *et al.* (2000) at time $t = 0$, when the melting is started (black line) and at three successive times during the initial melting phase. While the boundary layer with increased magnetization is building up in the solid, a stabilizing gradient is also building up in the liquid. The magnetization of the bulk solid (at right) decreases due to the increase in temperature during the rapid melting experiment. Both pictures are drawn in a frame moving with the liquid-solid interface. From Akimoto *et al.* (2000).

started. The solid formed many cellular dendrites, which were directed parallel to the magnetic field (see Fig. 65). No instability was observed during melting in low magnetic field nor with high initial temperature (about 100 mK) even in an 8.9 T field.

In their further rapid melting experiments, the Leiden group applied a small magnetic field gradient and they were able not only to image the liquid-solid interface but also to measure the magnetization profile perpendicular to the interface (Akimoto *et al.*, 2000). These measurements revealed the buildup of a magnetization gradient on both the liquid and the solid side of the interface during the first phase of the melting process [see Fig. 64(b)]. It was shown by Akimoto *et al.*, who extended the stability analysis of Puech *et al.*, that it is this gradient in the liquid which stabilizes the interface during the initial stage of melting. The interface becomes unstable only when the magnetization gradient on the liquid side is negligible, after what the instability develops in a short time, as predicted by theory. These results agreed also with numerical calculations performed by (Plomp *et al.*, 2001).

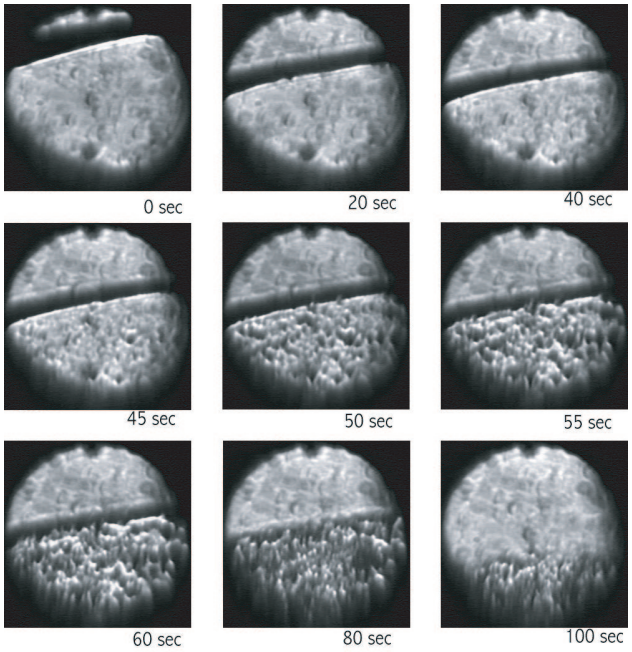


FIG. 65 . A sequence of images during rapid melting of solid $^3$He in an 8.9 T magnetic field. The instability occurs at about 45 s after the start of decompression of the cell: the cellular dendrites with a size of 50...100 $\mu$m appear in a vertical direction (Marchenkov *et al.*, 1999).

## VII. CONCLUSION: OPEN QUESTIONS

In conclusion, let us insist on a few open problems or unanswered questions which look interesting to us and deserve further study:

(1) Roughening in $^3$He. What is the roughening temperature of the (110) facets on $^3$He crystals? Is it possible that the coupling of the interface to the crystal lattice is weak at high temperature and strong at low temperature? How do the superfluid transition and the magnetic ordering transition affect surface properties like the step energies of facets and the growth rate of crystals?

(2) Roughening in $^4$He. New measurements on the step energy near $T_{R1}$ are necessary. If possible, independent measurements of the correlation length $\xi$ should allow to clarify some fundamental aspects of the renormalization group theories. One would also like to know if more than three roughening transitions can be observed in $^4$He.

(3) Crystallization waves in $^3$He. These waves are predicted to propagate below about 0.2 mK. To excite and detect waves at such low temperatures is an exciting challenge. Of particular interest is the magnetic field dependence of the kinetic energy of waves. In fact, the magnetic field dependence of the dynamics of rough surfaces in $^3$He is unexplored experimentally.

(4) Fast dynamics of facets at very low temperature in $^4$He. The mechanisms of several different fast growth modes have to be understood. Would it be possible that facets are so mobile at low temperature that the Kapitza

resistance becomes anomalous on facets as well, not only on rough surfaces? If so, could one observe non-linear crystallization waves on facets?

(5) Could one observe the competition between the crystal anisotropy and the stress anisotropy in the surface instability of stressed crystals? And could one study the crystallization waves near the instability threshold?

This list cannot be complete. It only gives some feeling of the rich variety of problems which can be addressed when studying the surface of helium crystals. Some of them are of general interest, some others are particular to helium and often surprising. Clearly, there is a lot to see at the surface of these crystals, not only what has been the matter of this review, but probably a lot more. Keesom would certainly have admitted it with great pleasure.


## Acknowledgments

Sébastien Balibar and Alexander Parshin are grateful to Prof. Mikko Paalanen and all members of the Low Temperature Laboratory (Helsinki) for their hospitality during the writing of this review. The authors acknowledge support from the EEC program ULTI III.


## Notations and Symbols

| | |
|---|---|
| $a$ | lattice constant |
| $A, B, C$ | Onsager matrixc coefficients |
| $()_{C,L}$ | indices for crystal and liquid |
| $c_C, c_L$ | sound velocity in the crystal and in the liquid |
| $c_l, c_t$ | longitudinal and transverse sound velocity in the crystal |
| $d$ | step height |
| $E$ | Young modulus |
| $k$ | surface mobility or growth coefficient |
| $k_B$ | Botzmann's constant |
| $k_s$ | step mobility |
| $m_I$ | interface inertia or mass per unit area |
| $m_k$ | kink mass |
| $q$ | wave vector |
| $R_K$ | Kapitza resistance |
| $T_R$ | roughening temperature |
| $t = (1 - T/T_R)$ | reduced temperature |
| $u$ | strain |
| $U$ | lattice potential per cell $L \times L$ |
| $v$ | velocity |
| $V$ | lattice potential per unit area |
| $w$ | step width |
| $Z = \rho c$ | acoustic impedance |
| $\alpha$ | surface tension or free energy per unit area |
| $\beta$ | step energy |
| $\gamma$ | surface stiffness |
| $\Delta$ | roton gap energy |
| $\delta$ | interaction energy between steps (per unit length) |
| $\delta_{el}$ | elastic interaction between steps |
| $\delta_S$ | entropic interaction between steps |
| $\delta\mu$ | difference in chemical potential |
| $\delta P$ | difference in pressure |
| $\delta T$ | difference in temperature |
| $\epsilon$ | kink energy |
| $\lambda$ | Onsager cross coefficient |
| $\mu$ | chemical potential (per unit mass) |
| $\nu$ | wave frequency |
| $\xi$ | correlation length |
| $\rho$ | density |
| $\sigma$ | stress |
| $\sigma_P$ | Poisson coefficient |
| $\theta, \phi$ | angles |
| $\Psi$ | velocity potential |
| $\omega$ | wave angular frequency |

## References


Akimoto, H., R. van Rooijen, R. Jochemsen, G. Frossati, and W. van Saarloos, 2000, Phys. Rev. Lett. **85**, 1894.

Akimoto, H., R. van Rooijen, A. Marchenkov, R. Jochemsen, and G. Frossati, 1998, Physica B **255**, 19.

Akutsu, Y., N. Akutsu, and T. Yamamoto, 1988, Phys. Rev. Lett. **61**, 424.

Alerhand, O. L., D. Vanderbilt, R. D. Meade, and J. D. Joannopulos, 1998, Phys. Rev. Lett. **61**, 1973.

Alles, H., V. Tsepelin, A. Babkin, R. Jochemsen, A. Y. Parshin, and I. Todoshchenko, 2001, J. Low Temp. Phys. **124**, 189.

Amrit, J., and J. Bossy, 1990, Physica **B 165-166**, 529.

Amrit, J., and J. Bossy, 1993, J. Low Temp. Phys. **92**, 415.

Amrit, J., P. Legros, and J. Poitrenaud, 1995a, J. Low Temp. Phys. **101**, 121.

Amrit, J., P. Legros, and J. Poitrenaud, 1995b, J. Low Temp. Phys. **101**, 971.

Andreev, A. F., 1981, Zh. Eksp. Teor. Fiz. **80**, 2042, [*Sov. Phys. JETP*, **53**, 1063 (1981)].

Andreev, A. F., 1982, *in Progress in Low Temperature Physics, Vol. 8, edited by D. F. Brewer* (Elsevier Science Publishers B.V., Amsterdam).

Andreev, A. F., 1990, Pis'ma Zh. Eksp. Teor. Fiz. **52**, 1204, [*JETP Lett.*, **52**, 619, (1990)].

Andreev, A. F., 1993, Pis'ma Zh. Eksp. Teor. Fiz. **58**, 740, [*JETP Lett.*, **58**, 715 (1993)].

Andreev, A. F., 1994, Zh. Eksp. Teor. Fiz. **106**, 1219, [*JETP*, **79**, 660 (1994)].

Andreev, A. F., 1995, Pis'ma Zh. Eksp. Teor. Fiz. **62**, 123, [*JETP Lett.*, **62**, 136, (1995)].

Andreev, A. F., 1996, Czech. J. Phys. **46 S6**, 3043.

Andreev, A. F., and V. G. Knizhnik, 1982, Zh. Eksp. Teor. Fiz. **83**, 416, [*Sov. Phys. JETP*, **56**, 226 (1982)].

Andreev, A. F., and Y. A. Kosevich, 1981, Zh. Eksp. Teor. Fiz. **81**, 1435, [*Sov. Phys. JETP*, **54**, 761 (1981)].

Andreev, A. F., and I. M. Lifshitz, 1969, Zh. Eksp. Teor. Fiz. **56**, 2057, [*Sov. Phys. JETP*, **29**, 1107 (1969)].

Andreev, A. F., and L. A. Melnikovsky, 2001, Zh. Eksp. Teor. Fiz. **120**, 1457, [*JETP*, **93**, 1261, (2001)].

Andreev, A. F., and A. Y. Parshin, 1978, Zh. Eksp. Teor. Fiz. **75**, 1511, [*Sov. Phys. JETP*, **48**, 763 (1978)].

Andreeva, O. A., and K. O. Keshishev, 1987, Pis'ma Zh. Eksp. Teor. Fiz. **46**, 160, [*JETP Lett.*, **46**, 200 (1987)].

Andreeva, O. A., and K. O. Keshishev, 1990, Pis'ma Zh. Eksp. Teor. Fiz. **52**, 799, [*JETP Lett.*, **52**, 164 (1990)].

Andreeva, O. A., and K. O. Keshishev, 1991, Physica Scripta T **39**, 352.

Andreeva, O. A., K. O. Keshishev, and S. Y. Osip'yan, 1989, Pis'ma Zh. Eksp. Teor. Fiz. **49**, 661, [*JETP Lett.*, **49**, 759 (1989)].

Armour, A. D., R. M. Bowley, and P. Nozières, 1998, J. Low Temp. Phys. **110**, 127.

Asaro, I., and W. A. Tiller, 1972, Metall. Trans. **3**, 1789.

Avron, J. E., L. S. Balfour, C. G. Kuper, J. Landau, S. G. Lipson, and L. S. Schulman, 1980, Phys. Rev. Lett. **45**, 814.

Avron, J. E., and R. K. P. Zia, 1988, Phys. Rev. B **37**, 6611.

Babkin, A. V., H. Alles, P. J. Hakonen, A. Y. Parshin, J. P. Ruutu, and J. P. Saramäki, 1995, Phys. Rev. Lett. **75**, 3324.

Babkin, A. V., K. O. Keshishev, D. B. Kopeliovich, and A. Y. Parshin, 1984, Pis'ma Zh. Eksp. Teor. Fiz. **39**, 519, [*JETP Lett.*, **39**, 633 (1984)].

Babkin, A. V., D. B. Kopeliovich, and A. Y. Parshin, 1985, Zh. Eksp. Teor. Fiz. **89**, 2288, [*Sov. Phys. JETP*, **62**, 1322 (1985)].

Balibar, S., 2002, J. Low Temp. Phys. **129**, 363.

Balibar, S., and J. P. Bouchaud, 1992, Phys. Rev. Lett. **69**, 862.

Balibar, S., and B. Castaing, 1980, J. Phys. Lett. (Paris) **41**, L329.

Balibar, S., B. Castaing, and C. Laroche, 1980, J. Phys. Lett. (Paris) **41**, L283.

Balibar, S., X. Chavanne, and F. Caupin, 2003, Physica B **329-333**, 380.

Balibar, S., D. O. Edwards, and C. Laroche, 1979, Phys. Rev. Lett. **42**, 782.

Balibar, S., D. O. Edwards, and W. F. Saam, 1991a, J. Low Temp. Phys. **82**, 119.

Balibar, S., F. Gallet, F. Graner, and C. Guthmann, 1991b, Physica B **169**, 209.

Balibar, S., C. Guthmann, and E. Rolley, 1993, J. Phys. I (France) **3**, 1475.

Balibar, S., T. Mizusaki, and S. Sasaki, 2000, J. Low Temp. Phys. **120**, 293.

Balibar, S., and P. Nozières, 1994, Sol. State Comm. **92**, 19.

Bartelt, N. C., T. L. Einstein, and E. Williams, 1990, Surf. Sci. Lett. **240**, 591.

van Beijeren, H., 1975, Comm. Math. Phys. **40**, 1.

van Beijeren, H., 1977, Phys. Rev. Lett. **38**, 993.

Bodensohn, J., K. Nicolai, and P. Leiderer, 1986, Z. Phys. B - Condensed Matter **64**, 55.

Boldarev, S. T., and V. P. Peshkov, 1973, Pis'ma Zh. Eksp. Teor. Fiz. **17**, 416, [*JETP Lett.*, **17**, 297 (1973)].

Bol'shov, L. A., V. L. Pokrovski, and G. V. Umin, 1984, Pis'ma Zh. Eksp. Teor. Fiz. **39**, 145, [*JETP Lett.*, **39**, 173 (1984)].

Bonfait, G., L. Puech, A. Greenberg, G. Eska, B. Castaing, and D. Thoulouze, 1984, Phys. Rev. Lett. **53**, 1092.

Borgnis, F. E., 1953, Rev. Mod. Phys. **25**, 653.

Bowley, R. M., and A. D. Armour, 1997, J. Low Temp. Phys. **107**, 225.

Bowley, R. M., and D. O. Edwards, 1983, J. Phys. (Paris) **44**, 723.

Burmistrov, S. N., and L. B. Dubovskii, 1993, Europhys. Lett. **24**, 749.

Burton, W. K., and N. Cabrera, 1949, Disc. Faraday Soc. **5**, 33.

Burton, W. K., N. Cabrera, and F. C. Frank, 1951, Phil. Trans. Roy. Soc. London **243A**, 299.

Carmi, Y., S. G. Lipson, and E. Polturak, 1985, Phys. Rev. Lett. **54**, 2042.

Carmi, Y., S. G. Lipson, and E. Polturak, 1987, Phys. Rev. B **36**, 1894.

Carmi, Y., E. Polturak, and S. G. Lipson, 1989, Phys. Rev. Lett. **62**, 1364.

Castaing, B., 1984, J. Phys. Lett. (Paris) **45**, L233.

Castaing, B., S. Balibar, and C. Laroche, 1980, J. Phys. (Paris) **41**, 897.

Castaing, B., A. S. Greenberg, and M. Papoular, 1982, J. Low Temp. Phys. **47**, 191.

Castaing, B., and P. Nozières, 1979, J. Phys. (Paris) **40**, 257.

Castaing, B., and P. Nozières, 1980, J. Phys. (Paris) **41**, 701.

Chavanne, X., S. Balibar, and F. Caupin, 2001, Phys. Rev. Lett. **86**, 5506.

Chernov, A. A., 1984, *Modern Crystallography, Vol. 3, Crystal Growth* (Springer, Berlin).
Chui, S. T., and J. Weeks, 1976, Phys. Rev. B **14**, 4978.
Chui, S. T., and J. Weeks, 1978, Phys. Rev. Lett. **40**, 733.
Conrad, E. H., and T. Engel, 1994, Surf. Sci. **299**, 391.
Cuthbertson, C., and M. Cuthbertson, 1932, Proc. R. Soc. London A **135**, 40.
Dash, G., 1982, Phys. Rev. **B 25**, 508.
Donnelly, R., and C. Barenghi, 1998, J. Phys. Chem. Ref. Data **27**, 1217.
Eckstein, Y., J. Landau, S. G. Lipson, and Z. Olami, 1980, Phys. Rev. Lett. **45**, 1805.
Edwards, D. O., and S. Balibar, 1989, Phys. Rev. B **39**, 4083.
Edwards, D. O., S. Mukherjee, and M. S. Pettersen, 1990, Phys. Rev. Lett. **64**, 902.
Edwards, D. O., M. S. Pettersen, and H. Baddar, 1991, *in Excitations in Two-Dimensional and Three-Dimensional Quantum Fluids, edited by A. F .G. Wyatt and H. J. Lauter* (Plenum press, New York).
Edwards, M., 1958, Can. J. Phys. **36**, 884.
Esaki, L., 1992, Physica Scripta T **42**, 102.
Faraday, M., 1831, Phil. Trans. Roy. Soc. London **121**, 319.
Feng, Y. P., 1991, [Ph.D. thesis, Stanford University].
Feng, Y. P., P. Schiffer, D. D. Osheroff, and M. C. Cross, 1993, J. Low Temp. Phys. **90**, 475.
Fisher, D. S., and J. D. Weeks, 1983, Phys. Rev. Lett. **50**, 1077.
Fradkin, E., 1983, Phys. Rev. B **28**, 5338.
Franck, J. P., and J. Jung, 1986, J. Low Temp. Phys. **64**, 165.
Gallet, F., 1986, [Ph.D. thesis, Paris].
Gallet, F., S. Balibar, and E. Rolley, 1987, J. Phys. (Paris) **48**, 369.
Gallet, F., P. E. Wolf, and S. Balibar, 1984, Phys. Rev. Lett. **52**, 2253.
Giorgini, S., and R. M. Bowley, 1995, J. Phys. I (Paris) **5**, 815.
Golub, A. A., and S. V. Svatko, 1980, Fiz. Nizk. Temp. **6**, 957, [*Sov. J. Low Temp. Phys.* **6**, 465 (1980)].
Graf, M. J., R. M. Bowley, and H. J. Maris, 1984, Phys. Rev. Lett. **53**, 1176.
Graf, M. J., R. M. Bowley, and H. J. Maris, 1985, J. Low Temp. Phys. **58**, 209.
Graf, M. J., and H. J. Maris, 1987, Phys. Rev. B **35**, 3142.
Graner, F., S. Balibar, and E. Rolley, 1989, J. Low Temp. Phys. **75**, 69.
Graner, F., R. M. Bowley, and P. Nozières, 1990, J. Low Temp. Phys. **80**, 113.
Gridin, V., J. Adler, Y. Eckstein, and E. Polturak, 1984, Phys. Rev. Lett. **53**, 802.
Grinfeld, M. Y., 1986, Sov. Phys. Doklady **31**, 831.
Grinfeld, M. Y., 1993, J. Non Lin. Sci. **3**, 35.
Gruber, E. E., and W. W. Mullins, 1967, J. Phys. Chem. Solids **28**, 875.
Guthmann, C., S. Balibar, E. Chevalier, E. Rolley, and J. Sutra-Fourcade, 1994, Rev. Sci. Instrum. **65**, 273.
Hakonen, P. J., H. Alles, A. V. Babkin, and J. P. Ruutu, 1995, J. Low Temp. Phys. **101**, 41.
Harris-Lowe, R., and K. Smee, 1970, Phys. Rev. A **2**, 158.
Hazareesing, A., and J. P. Bouchaud, 2000, Eur. Phys. J. B **14**, 713.
Helfrich, W., 1978, Z. Naturforsch. **33a**, 305.
Herring, C., 1953, *in Structure and Prorperties of Solid Surfaces, edited by R. Gomer and C. S. Smith* (University of Chicago).
Huber, T. E., and H. J. Maris, 1981, Phys. Rev. Lett. **47**, 1907.
Huber, T. E., and H. J. Maris, 1982, J. Low Temp. Phys. **48**, 463.
Huse, D., 1984, Phys. Rev. B **30**, 1371.
Iordanskii, S. V., and S. E. Korshunov, 1983, Pis'ma Zh. Eksp. Teor. Fiz. **38**, 542, [*JETP Lett.*, **38**, 655 (1983)].
Iordanskii, S. V., and S. E. Korshunov, 1984, Zh. Eksp. Teor. Fiz. **87**, 927, [*Sov. Phys. JETP*, **60**, 528 (1984)].
Jayaprakash, C., C. Rottman, and W. F. Saam, 1984, Phys. Rev. B **30**, 6549.
Jayaprakash, C., and W. F. Saam, 1984, Phys. Rev. B **30**, 3916.
Jayaprakash, C., W. F. Saam, and S. Teitel, 1983, Phys. Rev. Lett. **50**, 2017.
Jochemsen, R., 2002, private communication, unpublished.
Kagan, M. Y., 1986, Zh. Eksp. Teor. Fiz. **63**, 288, [*Sov. Phys. JETP*, **90**, 498 (1986)].
Kardar, M., G. Parisi, and Y. C. Zhang, 1986, Phys. Rev. Lett. **56**, 889.
Kassner, K., 1996, *Pattern Formation in Diffusion-Limited Crystal Growth* (World Scientific, Singapore).
Kawaguchi, Y., T. Ueno, Y. Kinoshita, Y. Sasaki, and T. Mizusaki, 2002, J. Low Temp. Phys. **126**, 27.
Keesom, W. H., 1926, CL **184b**, 17.
Keshishev, K. O., and O. A. Andreeva, 1991, *in Excitations in Two-Dimensional and Three-Dimensional Quantum Fluids, edited by A. F. G. Wyatt and H. J. Lauter* (Plenum press, New York).
Keshishev, K. O., A. Y. Parshin, and A. V. Babkin, 1979, Pis'ma Zh. Eksp. Teor. Fiz. **30**, 63, [*JETP Lett.*, **30**, 56 (1980)].
Keshishev, K. O., A. Y. Parshin, and A. V. Babkin, 1981, Zh. Eksp. Teor. Fiz. **80**, 716, [*Sov. Phys. JETP*, **53**, 362 (1981)].
Keshishev, K. O., A. Y. Parshin, and A. I. Shal'nikov, 1982, *Surface Phenomena in Quantum Crystals, in Soviet Scientific Reviews, edited by I. M. Khalatnikov, Section A: Physics Reviews, Vol. 4* (Harwood Academic, New York).
Korshunov, S. E., and A. V. Smirnov, 1982, Zh. Eksp. Teor. Fiz. **83**, 2128, [*JETP*, **56**, 1234 (1982)].
Kosevich, A. M., and Y. A. Kosevich, 1981, Fiz. Nizk. Temp. **7**, 809, [*Sov. J. Low Temp. Phys.*, **7**, 394 (1981)].
Landau, J., S. G. Lipson, L. M. Määttänen, L. S. Balfour, and D. O. Edwards, 1980, Phys. Rev. Lett. **45**, 31.
Landau, L. D., 1965, *The Equilibrium Form of Crystals, in Collected Papers* (Pergamon, Oxford).
Langer, J. S., 1980, Rev. Mod. Phys. **52**, 1.
Lapujoulade, J., 1994, Surf. Sci. Rep. **20**, 191.
Leamy, H. J., G. H. Gilmer, and K. A. Jackson, 1975, *in Surface Physics of Materials, edited by J. B. Blakeley* (Academic, New York).
Leiderer, P., 1995, Z. Phys. B:Condensed Matter **98**, 303.
Leiderer, P., H. Poisel, and M. Wanner, 1977, J. Low Temp. Phys. **28**, 167.
Maksimov, L. A., and V. L. Tsymbalenko, 2002, Zh. Eksp. Teor. Fiz. **122**, 530, [*JETP*, **95**, 455 (2002)].
Manninen, A. J., J. P. Pekola, G. M. Kira, J. P. Ruutu, A. V. Babkin, H. Alles, and O. V. Lounasmaa, 1992, Phys. Rev. Lett. **69**, 2392.
Marchenko, V. I., 1981a, Pis'ma Zh. Eksp. Teor. Fiz. **33**, 397, [*Sov. Phys. JETP Lett.*, **33**, 381].
Marchenko, V. I., 1981b, Zh. Eksp. Teor. Fiz. **80**, 2010, [*JETP*, **53**, 1045 (1981)].

Marchenko, V. I., and A. Y. Parshin, 1980a, Zh. Eksp. Teor. Fiz. **79**, 257, [*JETP*, **52**, 129 (1980)].
Marchenko, V. I., and A. Y. Parshin, 1980b, Pis'ma Zh. Eksp. Teor. Fiz. **31**, 767, [*JETP Lett.*, **31**, 724 (1980)].
Marchenkov, A., H. Akimoto, R. van Rooijen, R. Jochemsen, and G. Frossati, 1999, Phys. Rev. Lett. **83**, 4598.
Maris, H. J., and T. E. Huber, 1982, J. Low Temp. Phys. **48**, 99.
McKenna, M. J., T. P. Brosius, and J. D. Maynard, 1992, Phys. Rev. Lett. **69**, 3346.
Mochrie, S. G. J., 1987, Phys. Rev. Lett. **59**, 304.
Mullins, W. W., and R. F. Sekerka, 1964, J. Appl. Phys. **35**, 444.
Nightingale, P., W. F. Saam, and M. Schick, 1984, Phys. Rev. B **30**, 3830.
Nomura, R., H. H. Hensley, T. Matsushita, and T. Mizusaki, 1994, J. Low Temp. Phys. **94**, 377.
Nomura, R., Y. Suzuki, S. Kimura, and Y. Okuda, 2003, Phys. Rev. Lett. **90**, 075301.
Nozières, P., 1992, *Shape and Growth of Crystals, in Solids Far from Equilibrium, edited by C. Godrèche* (Cambridge University).
Nozières, P., and F. Gallet, 1987, J. Phys. (Paris) **48**, 353.
Nozières, P., F. Pistolesi, and S. Balibar, 2001, Eur. Phys. J. B **24**, 387.
Nozières, P., and M. Uwaha, 1987, J. Phys. (Paris) **48**, 389.
Osheroff, D., R. Richardson, and D. M. Lee, 1972, Phys. Rev. Lett. **28**, 885.
Osheroff, D. D., Y. P. Feng, and P. Shiffer, 1991, Physica B **169**, 204.
Osheroff, D. D., and R. C. Richardson, 1985, Phys. Rev. Lett. **54**, 1178.
Osheroff, D. D., and C. Yu, 1980, Phys. Lett. A **77**, 458.
Parshin, A. Y., 1985, *Crystallization Waves in He-4, in Low Temperature Physics, edited by A. S. Borovik-Romanov* (MIR, Moscow).
Parshin, A. Y., 1998, J. Low Temp. Phys. **110**, 133.
Parshin, A. Y., J. J. Saenz, and N. Garcia, 1988, J. Phys. C : Sol. State Phys. **21**, L305.
Parshin, A. Y., and V. L. Tsymbalenko, 2003, Pis'ma Zh. Eksp. Teor. Fiz. **77**, 372, [*JETP Lett.*, **77**, 321 (2003)].
Pierre, L., H. Guignes, and C. Lhuillier, 1985, J. Chem. Phys. **82**, 496.
Pipman, J., S. G. Lipson, J. Landau, and N. Bochner, 1978, J. Low Temp. Phys. **31**, 119.
Plomp, E. R., R. van Rooijen, H. Akimoto, G. Frossati, R. Jochemsen, and W. van Saarloos, 2001, J. Low Temp. Phys. **124**, 169.
Poitrenaud, J., M. Boiteux, and J. Joffrin, 1989, Europhys. Lett. **14**, 673.
Poitrenaud, J., and P. Legros, 1989, Europhys. Lett. **8**, 651.
Puech, L., G. Bonfait, and B. Castaing, 1986a, J. Low Temp. Phys. **62**, 315.
Puech, L., G. Bonfait, and B. Castaing, 1986b, J. Phys. (Paris) **47**, 723.
Puech, L., and B. Castaing, 1982, J. Phys. Lett. (Paris) **43**, L601.
Puech, L., B. Hebral, D. Thoulouze, and B. Castaing, 1982, J. Phys. Lett. (Paris) **43**, L809.
Puech, L., B. Hebral, D. Thoulouze, and B. Castaing, 1983, J. Phys. Lett. (Paris) **44**, L159.
Ramesh, S., and J. D. Maynard, 1982, Phys. Rev. Lett. **49**, 47.
Ramesh, S., Q. Zhang, G. Torzo, and J. D. Maynard, 1984, Phys. Rev. Lett. **52**, 2375.
Rayleigh, L., 1902, Phil. Mag. **3**, 338.
Rolley, E., S. Balibar, and F. Gallet, 1986, Europhys. Lett. **2**, 247.
Rolley, E., S. Balibar, F. Gallet, F. Graner, and C. Guthmann, 1989, Europhys. Lett. **8**, 523.
Rolley, E., S. Balibar, and F. Graner, 1994a, Phys. Rev. E **49**, 1500.
Rolley, E., S. Balibar, C. Guthmann, and P. Nozières, 1995a, Physica B **210**, 397.
Rolley, E., E. Chevalier, C. Guthmann, and S. Balibar, 1994b, Phys. Rev. Lett. **72**, 872.
Rolley, E., C. Guthmann, E. Chevalier, and S. Balibar, 1995b, J. Low Temp. Phys. **99**, 851.
van Rooijen, R., A. Marchenkov, H. Akimoto, O. Andreeva, P. van de Haar, R. Jochemsen, and G. Frossati, 2001, J. Low Temp. Phys. **124**, 497.
Rottman, C., M. Wortis, J. C. Heyraud, and J. J. Metois, 1984, Phys. Rev. Lett. **52**, 1009.
Ruutu, J. P., P. J. Hakonen, A. V. Babkin, A. Y. Parshin, J. S. Penttilä, J. P. Saramäki, and G. Tvalashvili, 1996, Phys. Rev. Lett. **76**, 4187.
Ruutu, J. P., P. J. Hakonen, A. V. Babkin, A. Y. Parshin, and G. Tvalashvili, 1998, J. Low Temp. Phys. **112**, 117.
Saam, W. F., 1973, Phys. Rev. A **8**, 1918.
van Saarlos, W., and J. D. Weeks, 1995, Phys. Rev. Lett. **74**, 290.
Saramäki, J. P., A. V. Babkin, P. J. Hakonen, R. M. Luusalo, and A. Y. Parshin, 1998, J. Low Temp. Phys. **110**, 141.
Savignac, D., J. Bodensohn, and P. Leiderer, 1983, *Ions at the 4He Solid-Superfluid Interface, in 75th Jubilee Conference on Helium-4* (World Scientific, Singapore).
Savignac, D., and P. Leiderer, 1982, Phys. Rev. Lett. **69**, 1869.
Shal'nikov, A. I., 1961, Zh. Eksp. Teor. Fiz. **41**, 1059, [*Sov. Phys. JETP*, **14**, 755(1962)].
Shal'nikov, A. I., 1964, Zh. Eksp. Teor. Fiz. **47**, 1727, [*Sov. Phys. JETP*, **20**, 1161 (1965)].
Straty, G. C., and E. D. Adams, 1969, Rev. Sci. Instrum. **40**, 1393.
Susuki, M., M. Thiel, and P. Leiderer, 1997, J. Low Temp. Phys. **109**, 357.
Suttleworth, R., 1950, Proc. Phys. Soc. London Sec. A **63**, 444.
Sydoriak, S. G., R. L. Mills, and E. R. Grilly, 1960, Phys. Rev. Lett. **4**, 495.
Thiel, M., A. Willibald, P. Evers, A. Levchenko, P. Leiderer, and S. Balibar, 1992, Europhys. Lett. **26**, 707.
Thuneberg, E. V., 1997, J. Low Temp. Phys. **106**, 575.
Todoshchenko, I. A., H. Alles, H. J. Junes, and A. Y. Parshin, 2004, unpublished.
Todoshchenko, I. A., H. Alles, H. J. Junes, A. Y. Parshin, and V. Tsepelin, 2003, Physica B **329-333**, 386.
Toner, J., and D. P. DiVincenzo, 1990, Phys. Rev. B **41**, 632.
Torii, R., and S. Balibar, 1992, J. Low Temp. Phys. **89**, 391.
Treiner, J., 1993, J. Low Temp. Phys. **92**, 1.
Tsepelin, V., H. Alles, A. Babkin, J. P. H. Härme, R. Jochemsen, A. Y. Parshin, and G. Tvalashvili, 2001, Phys. Rev. Lett. **86**, 1042.
Tsepelin, V., H. Alles, A. Babkin, R. Jochemsen, A. Parshin, and I. A. Todoshchenko, 2002a, Phys. Rev. Lett. **88**, 045302.
Tsepelin, V., H. Alles, A. Babkin, R. Jochemsen, A. Y. Parshin, and I. A. Todoshchenko, 2002b, J. Low Temp.

Phys. **129**, 489.
Tsepelin, V., J. P. Saramäki, A. V. Babkin, P. J. Hakonen, J. J. Hyvönen, R. M. Luusalo, A. Y. Parshin, and G. Tvalashvili, 1999, Phys. Rev. Lett. **83**, 4804.
Tsymbalenko, V. L., 1995, Zh. Eksp. Teor. Fiz. **108**, 686, [*JETP*, **81**, 373 (1995)].
Tsymbalenko, V. L., 2000, J. Low Temp. Phys. **121**, 53.
Tsymbalenko, V. L., 2003, Pis'ma Zh. Eksp. Teor. Fiz. **77**, 288, [*JETP Lett.*, **77**, 243 (2003)].
Uwaha, M., 1983, J. Low Temp. Phys. **52**, 15.
Uwaha, M., 1989, J. Low Temp. Phys. **77**, 165.
Uwaha, M., 1990, J. Phys. (France) **51**, 2743.
Uwaha, M., and G. Baym, 1982, Phys. Rev. B **26**, 4928.
Uwaha, M., and P. Nozières, 1986, J. Phys. (Paris) **47**, 263.
Uwaha, M., and P. Nozières, 1987, J. Phys. (Paris) **48**, 407.
Vermeulen, G., S. A. Wiegers, C. C. Kranenburg, R. Jochemsen, and G. Frossati, 1987, Can. J. Phys. **65**, 1560.
Vollhardt, D., and P. Wölfle, 1990, *The Superfluid Phases of Helium 3* (Taylor and Francis, London).
Wagner, R., P. J. Ras, P. Remeijer, S. C. Steel, and G. Frossati, 1994, J. Low Temp. Phys. **95**, 715.
Wagner, R., S. C. Steel, O. A. Andreeva, R. Yochemsen, and G. Frossati, 1996, Phys. Rev. Lett. **76**, 263.
Wang, C. L., and G. Agnolet, 1992a, Phys. Rev. Lett. **69**, 2102.
Wang, C. L., and G. Agnolet, 1992b, J. Low Temp. Phys. **89**, 759.
Wang, C. L., and G. Agnolet, 1994, Physica **B 194-196**, 935.
Weeks, J. D., 1980, *The Roughening Transition, in Ordering in Strongly Fluctuating Condensed Matter Systems, edited by T. Riste* (Plenum New York and London).
Wellard, N. V., P. W. Alexander, H. E. Hall, and J. R. Hook, 1982, Physica B **109-110**, 2096.
Williams, E., and N. C. Bartelt, 1991, Science **251**, 393.
Wilson, K., 1971, Phys. Rev. B **4**, 3174.
Wolf, P. E., S. Balibar, and F. Gallet, 1983a, Phys. Rev. Lett. **51**, 1366.
Wolf, P. E., D. O. Edwards, and S. Balibar, 1983b, JLTP **51**, 489.
Wolf, P. E., F. Gallet, S. Balibar, E. Rolley, and P. Nozières, 1985, J. Phys. (Paris) **46**, 1987.
Wulff, G., 1901, Z. Krist. Mineral. **34**, 449.
Wyborn, G. M., and A. F. G. Wyatt, 1990, Phys. Rev. Lett. **65**, 345.